



AFFIDAVIT

I declare that I have authored this thesis independently, that I have not used other than the declared sources/resources, and that I have explicitly indicated all material which has been quoted either literally or by content from the sources used. The text document uploaded to TUGRAZonline is identical to the present master's thesis dissertation.

Date

Signature

Acknowledgement

First of all, I would like to express my gratitude to my supervisor Dagmar Zweytick for giving me the opportunity to write my thesis at the Institute of Molecular Biosciences. Moreover, I want to thank her for her support, her patience and her friendly ear. Her guidance always helped me during my research and writing process.

Secondly I am deeply grateful to Sabrina Riedl for helping me with all my work and her patience in teaching me different experimental implementations.

Additionally, I would like to thank Alexandra Zenz, Nermina Malanovic, Regina Leber and Karl Lohner for their good advice and answers to any question I had. Above all, I would like to thank the whole Biophysics group of the IMB for integrating me so friendly in their group.

Furthermore, David Feuersinger, Manfred Briendl, Marielies Reiter, Melanie Kienzl and Mirjam Pennauer who became very important friends during my university years deserve many thanks.

Last but not least, I would like to thank my family, especially my parents and my grandmother, for financial and emotional support throughout my studies as well as close friends from home.

Table of Contents

Abstract	1
Zusammenfassung	3
1. Theoretical Background	5
1.1 Challenges in cancer therapy – malignant melanoma	5
1.2 PS exposure of cancer cells – not only a phenomenon of apoptosis	6
1.3 Host defense peptides – promising weapons in antimicrobial and anticancer therapy	8
1.4 Cholesterol – effects on membranes and peptides	12
1.5 Aim of the study	13
2. Material and Methods	14
2.1 Lipids	14
2.2 Peptides	14
2.3 Model system studies	14
2.3.1 Liposome preparation	14
2.3.2 Differential scanning calorimetry (DSC)	15
2.3.3 Tryptophan quenching	16
2.3.4 Zeta potential and size	16
2.3.5 Giant unilamellar vesicles (GUVs)	17
2.4 <i>In vitro</i> studies	18
2.4.1 Cell lines and cultures	18
2.4.2 Fluorescence microscopy	19
– Cell culturing	19
– Fixation of cells	19
– Propidium iodide (PI)-uptake	19
– R-DIM-P-LF11-322 localization and peptide effects	20
– Cholesterol staining	20
– Mitochondrial staining	20
– Golgi staining	21
– Nuclear staining	21
2.4.3 Cholesterol depletion studies	21
3. Results	23
3.1 Impact of phosphatidylserine on peptide activity and interaction	23
3.1.1 Phosphatidylserine is exposed on the outer leaflet of cancer cell membranes	23
3.1.2 Model system studies	23

–	DSC – Changes of thermodynamic phase behavior of cancer cell mimicking liposomes by peptides	24
–	Zeta potential and size – Electrostatic and hydrophobic interactions of peptides with cancer cell mimicking liposomes	27
–	Giant unilamellar vesicles – Changes of lipid distribution of GUVs mimicking cancer membranes upon peptide addition	29
3.2	Impact of cholesterol on peptide activity and interaction	33
3.2.1	Cholesterol distribution in cancer and non-cancer membranes – Cholesterol is present in both types of plasma membranes	33
3.2.2	Model system studies	34
–	DSC – Different impact of cholesterol on peptide activity and interaction	34
–	Tryptophan quenching – Impact of cholesterol on penetration depth of peptides	39
–	Zeta potential and size – Different impact of cholesterol on electrostatic and hydrophobic interactions of peptides with cancer membrane mimics	42
–	Giant unilamellar vesicles – Impact of cholesterol on peptide induced lipid distribution of GUVs	45
3.2.3	<i>In vitro</i> studies – Cholesterol depletion and its effect on peptide activity	51
3.3	<i>In vitro</i> studies – Effect of peptides on morphology of cancer cell membranes of living cells.....	52
3.3.1	Effect of peptides on plasma membranes and cholesterol distribution.....	54
3.3.2	Effect of peptides on mitochondria	56
3.3.3	Effects of peptides on Golgi apparatus	58
3.4	Summary of Results	60
4.	Discussion	61
5.	References.....	69

Abstract

In 2011, Riedl et al. have shown that cancer cells expose the negatively charged lipid phosphatidylserine (PS) in the outer leaflet of the plasma membrane. On the contrary, healthy cells present only neutral lipids such as phosphatidylcholine (PC) or cholesterol in the outer leaflet. Therefore, PS is a promising target for cationic peptides in cancer therapy. Indeed, R-DIM-P-LF11-322 and DIM-LF11-318, both derived from the human host defense peptide lactoferricin, show antitumor activity against several human cancer types. However, while R-DIM-P-LF11-322 interacts specifically with cancer cells, the non-specific DIM-LF11-318 shows activity against non-cancer cells as well.

Within this work the different modes of action and specificity of the two peptides with lipids of cancer and/or healthy plasma membrane mimics were investigated. Of special concern was the role of PS, PC and cholesterol in the peptide interaction. In *in vitro* studies, on the one hand, malignant melanoma cells were studied for possible influence of cholesterol on the effectiveness and specificity of the peptides. On the other hand, the different impact of the peptides on the distribution of cholesterol in cancer cell membranes was of interest. Additionally, the effect of the peptides on organelles involved in uncontrolled necrotic or programmed apoptotic cell death as the plasma membrane or the mitochondria and the Golgi, respectively, was studied.

Calorimetric studies of cancer mimicking liposomes with different ratios of PS, PC and cholesterol revealed that R-DIM-P-LF11-322 specifically interacts with PS, however, cholesterol reduces the effectiveness of the peptide. The non-specific DIM-LF11-318 interacts preferentially with PS but also with PC, whereas cholesterol has no influence on the interaction of the non-specific peptide with the model systems. This was confirmed *in vitro* with cholesterol depleted malignant melanoma cells which showed increased sensitivity to R-DIM-P-LF11-322, whereas the activity of DIM-LF11-318 was unaffected. Neutralization of the negative zeta potential of cancer mimics confirmed the interaction of both peptides with the negatively charged PS and an even increased interaction of DIM-LF11-318, also in presence of PC and cholesterol. Microscopic studies of giant unilamellar vesicles and cancer cells revealed strong changes in the lateral distribution and domain formation of the lipids upon addition of peptides. This might lead to severe primary and secondary effects as membrane perturbation and changes in membrane permeability, fluidity or protein activity. Mitochondria of melanoma cells started to swell upon addition of R-DIM-P-LF11-322 which is a sign for ongoing apoptosis. In contrast, DIM-LF11-318 did not cause mitochondrial swelling. However, no impact of both peptides on the Golgi was shown.

In conclusion, it was shown that R-DIM-P-LF11-322 specifically interacts with PS exposed in the outer leaflet of cancer cell plasma membranes. It is less effective when cholesterol is present but still leads to specific death of the cancer cells. By contrast, the non-specific DIM-LF11-318 preferentially interacts with PS but can also interact with neutral lipids as PC. The non-specific peptide is unaffected by cholesterol. Cholesterol may prevent the formation of the membrane active secondary structure of R-DIM-P-LF11-322, whereas DIM-LF11-318 structure formation occurs quickly and non-lipid-specific, hence, non-affected by cholesterol. Furthermore, it was shown that DIM-LF11-318 rapidly kills melanoma cells by cell lysis presumably acting only on the plasma membrane with no intracellular target. As opposed to this R-DIM-P-LF11-322 after entering the cell localizes to the Golgi and might thereby lead to the release of apoptosis signals. The obtained data showed that both peptides kill melanoma cells, however, the mode and site of interaction are different which seems to be crucial in terms of specificity.

Zusammenfassung

2011 zeigten Riedl et al., dass an der Außenseite von Krebszellen das negativ geladene Lipid Phosphatidylserin (PS) exponiert wird. Im Gegensatz dazu besteht die Außenseite gesunder Zellen aus neutralen Lipiden, wie Phosphatidylcholin (PC) oder Cholesterol, weswegen PS ein vielversprechendes Target für kationische Peptide in der Krebstherapie darstellt. Tatsächlich zeigten die Peptide, R-DIM-P-LF11-322 und DIM-LF11-318, die sich vom humanen Lactoferricin ableiten, Aktivität gegen verschiedene humane Krebsarten. R-DIM-P-LF11-322 interagiert jedoch spezifisch mit Krebszellen, während DIM-LF11-318 auch gesunde Zellen angreift.

Im Zuge dieser Arbeit wurden die verschiedenen Wirkungsweisen sowie die Spezifität der zwei Peptide auf Lipide der Plasmamembranen von Krebszellen und gesunden Zellen untersucht. Der Einfluss von PS, PC und Cholesterol auf die Peptidinteraktion war von besonderem Interesse. In *in vitro* Studien mit malignen Melanomzellen wurde einerseits der potentielle Einfluss von Cholesterol auf die Effektivität und Spezifität der Peptide und andererseits der Einfluss der Peptide auf die Cholesterolverteilung in Krebszellmembranen untersucht. Außerdem wurden die Peptideffekte auf Organellen studiert, die - wie die Plasmamembran - am unkontrollierten nekrotischen Zelltod oder - wie Mitochondrien oder Golgi - am programmierten apoptotischen Zelltod beteiligt sind.

Kalorimetrische Studien an Liposomen, mit verschiedenen Verhältnissen an PS, PC und Cholesterol, die Krebszellen nachahmen, ergaben, dass R-DIM-P-LF11-322 nur mit PS interagiert. Cholesterol reduzierte die Effektivität des Peptids. Das unspezifische Peptid DIM-LF11-318 interagierte sowohl mit PS, als auch mit PC, wobei Cholesterol keinen Einfluss hatte. Dies wurde *in vitro* durch Untersuchung von malignen Melanomzellen, deren Cholesterol der Plasmamembran entleert wurde, bestätigt. Zellen, die weniger Cholesterol in der Plasmamembran hatten, zeigten eine höhere Sensitivität gegenüber R-DIM-P-LF11-322, aber es wurde keine Änderung der Aktivität von DIM-LF11-318 beobachtet. Auch die Neutralisation des negativen Zeta-Potentials der Krebsmodellsysteme bestätigte, dass beide Peptide präferentiell mit PS interagieren, wobei auch hier der Effekt von DIM-LF11-318 verstärkt war, auch in der Gegenwart von PC und Cholesterol. Mikroskopische Analysen von Großen Unilamellaren Vesikeln (GUVs) sowie Krebszellen zeigten, dass es in Gegenwart von Peptiden zu starken Veränderungen der lateralen Verteilung der Lipide kommt. Daraus resultierende Domänen könnten zu gravierenden primären und sekundären Effekten, wie Membranperturbation oder Veränderungen in der Membranpermeabilität, -fluidität oder Proteinaktivität führen. In Gegenwart von R-DIM-P-LF11-322 schwellen Mitochondrien an,

was ein Zeichen für Apoptose darstellt. Es konnte jedoch kein Einfluss von beiden Peptiden auf den Golgi beobachtet werden.

Zusammenfassend wurde gezeigt, dass R-DIM-P-LF11-322 spezifisch mit PS, das von Krebszellen exponiert wird, interagiert. Es ist weniger aktiv wenn Cholesterol präsent ist, führt jedoch immer noch zu einem spezifischen Zelltod der Krebszellen. Das unspezifische DIM-LF11-318 hingegen interagiert zwar präferentiell mit PS, aber auch mit neutralen Lipiden wie PC, wobei es durch Cholesterol unbeeinflusst ist. Der Grund dafür könnte sein, dass Cholesterol die Ausbildung der membranaktiven Sekundärstruktur des spezifischen R-DIM-P-LF11-322 verhindert, wohingegen die Strukturausbildung von DIM-LF11-318 sehr schnell und lipid-unspezifisch verläuft und daher von Cholesterol unbeeinflusst bleibt. DIM-LF11-318 tötet Melanomzellen sehr schnell durch Lyse der Plasmamembran ohne intrazelluläres Target. Hingegen lokalisiert R-DIM-P-LF11-322 nach Eintritt in die Zelle im Golgi und führt dort vermutlich zur Freisetzung von Apoptose-Signalen. Die Ergebnisse zeigten, dass beide Peptide Melanomzellen töten, wobei Art und Ort der Interaktion unterschiedlich und kritisch für die Spezifität sind.

1. Theoretical Background

1.1 Challenges in cancer therapy – malignant melanoma

Cancer is one leading cause of death with 8.2 million related deaths in 2012 (<http://www.who.int/mediacentre/factsheets/fs297/en/>). Despite enormous progress in medicine over the last decades there are still many types of cancer that exhibit poor treatability or require therapies provoking side effects. One form of cancer with poor prognosis is malignant melanoma with a median survival rate of only six months.

In general, melanoma arises from melanocytes, pigmented cells which produce melanin and are mainly found in the skin but also in mucosal surfaces or uveal tract [1] (<http://www.ncbi.nlm.nih.gov/books/NBK66034/>). Each year there are about 2 to 3 million new cases of skin cancer where melanoma represents 5% thereof. However, it is the most dangerous form of skin cancer by causing 80% of skin cancer related deaths and is the cancer with the strongest increase of incidences at present [2]. If early detected, 80% of the melanoma cases can be cured simply by surgical removal. But as mentioned before, with increasing malignancy when spreading to lymph nodes or other organs the healing prospects are very poor. There are many complex molecular aberrations which may lead to melanoma. In 50 – 70% of malignant melanoma the oncogene BRAF is mutated, a factor that leads to constitutive ERK (Extracellular-signal Regulated Kinase) signaling and therefore results in excessive proliferation and survival of cells [3,4]. Furthermore, in 40% of all malignant melanoma cells the tumor suppressor APAF1 (Apoptotic Protease Activating Factor 1) is silenced [4,5]. APAF1 is a central part of the intrinsic pathway of the programmed cell death by establishing the apoptosome and further binding of caspase-9, which leads to activation of caspase-3 through caspase-9, resulting in apoptosis [6]. Therefore APAF1 silencing is responsible for defective apoptosis in melanoma.

Malignant melanoma shows only weak chemosensitivity, thus treatment with methylating agents as dacarbazine (DTIC) exhibits a response of only 15% [7]. Until 2011, the only FDA approved agents for treatment of metastatic melanoma were cytostatic DTIC and immunotherapeutic Interleukin-2 (IL-2). Although not FDA approved for melanoma treatment the oral analogue of DTIC the cytostatic temozolomide (FDA approved for glioblastoma treatment) is applied due to its more favorable toxicity profile. In the last five years, there was some progress regarding immunotherapy and signal transduction inhibitors as therapy for malignant melanoma. In 2011, the FDA approved the human monoclonal antibody ipilimumab. It is an anti-CTLA4-antibody which blocks the down regulation of T-cell

response by binding to the receptor CTLA4 and therefore increasing the immune response against cancer cells. Although it was celebrated as a successful breakthrough in melanoma therapy, ipilimumab can only prolong lifespan to 10.1 months. In combination with DTIC the overall survival is 11.2 months. Another human monoclonal antibody nivolumab was approved by the FDA in 2014. This antibody blocks the programmed cell death protein 1 (PD-1) of T-cells and therefore ligands of this receptor which would lead to down regulation of T-cell response cannot bind to the T-cells. Two BRAF targeting inhibitors and therefore signal transduction inhibitors of the RAS/RAF/MEK/ERK pathway are vemurafenib (FDA approved in 2011) and dabrafenib (FDA approval in 2013). The problem of BRAF kinase inhibitors is the development of resistances within 6 or 7 months [8,9].

Still, there is no 100% cure of malignant melanoma even though there is hope for achieving increased lifespan prolongation by using combinations of mentioned therapies depending on the genetic aberrations of the malignant melanoma. Nevertheless, these drugs are very toxic, leading to severe side effects and are mainly dependent on mutations in the occurring cancer. Additionally they bear the risk for lack of response or even formation of resistance upon therapy. Therefore, there is a need for new targets on or in cancer cells especially with poor treatability for selective treatment.

1.2 PS exposure of cancer cells – not only a phenomenon of apoptosis

The phospholipid bilayer of plasma membranes of eukaryotic cells is very complex and exhibits an asymmetric distribution of phospholipids. Normally the outer leaflet consists of neutral phospholipids like phosphatidylcholine (PC) and sphingomyelin (SM). On the contrary, the inner leaflet is negatively charged due to the presence of phosphatidylserine (PS) besides existence of phosphatidylethanolamine (PE) [10]. This asymmetry is important for the cell and is therefore maintained by energy (ATP) dependent mechanisms. Two ATP-dependent enzymes collaborate to transport the lipids against their concentration gradients. On the one hand, there is a minor specific floppase which transports the neutral phospholipids (PC and SM) as well as the aminophospholipids (PS and PE) unidirectionally to the outer leaflet. On the other hand, there is a more specific flippase which immediately transports the aminophospholipids PS and PE from the outer leaflet inwards to the inner leaflet. At high intracellular Ca^{2+} concentrations a non-specific ATP-independent phospholipid translocase (“scramblase”) is activated which transports the phospholipids randomly between the two monolayers which results in a collapse of the phospholipid asymmetry of the bilayer. This ensues in PS exposure in blood platelets when activated for coagulation. Further on,

scramblases are also reported to generate PS exposure of apoptotic cells, which is required for detection by phagocytes carrying a PS recognition receptor to eliminate these cells condemned to death. Interestingly, also at normal intracellular Ca^{2+} levels PS is exposed by apoptotic cells which seemingly demands also other trigger mechanisms for activation of the scramblase [11,12].

In this respect it is of great interest that Utsugi et al. [13] reported in 1991 that also tumorigenic cells express higher levels of PS than non-neoplastic cells (keratinocytes). PS exposure during malignant transformation was also reported by Zwaal et al. [14], Ran et al. [15,16] and others. 20 years later, Riedl et al. [17] were able to show that not only tumor cell lines but also primary cultures and metastases of tumor cells expose the negatively charged phospholipid PS (see Figure 1). Oxidative stress, acidity, thrombin, and inflammatory cytokines are reported to induce exposure of anionic phospholipids and are therefore discussed to cause the loss of asymmetry during malignant transformation [16].

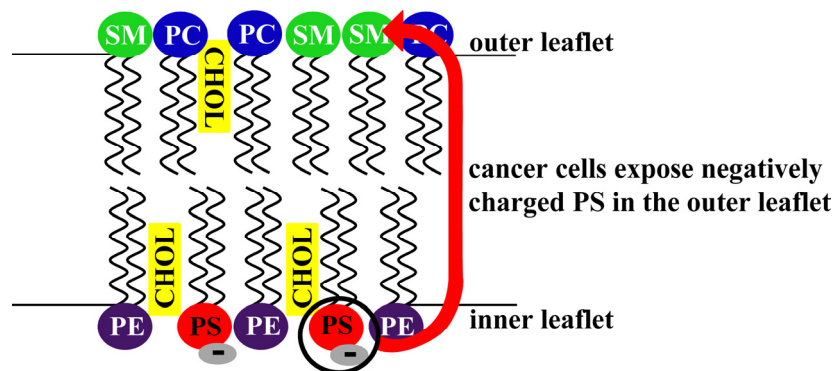


Figure 1: Exposure of the negatively charged lipid phosphatidylserine in the outer leaflet of cancer cells. The outer leaflet of the plasma membrane comprises neutral phospholipids like sphingomyelin (SM) or phosphatidylcholine (PC), while the inner leaflet consists of phosphatidylethanolamine (PE) and the negatively charged phosphatidylserine (PS). In both monolayers cholesterol (CHOL) is present. In cancer cells the asymmetry gets lost and PS is also present in the outer leaflet. This may be an Achilles' heel of cancer.

Although exposing PS which actually should lead to recognition by macrophages, surprisingly cancer cells prevent detection by macrophages and induction of apoptosis in further consequence. E.g., lung and colon cancer cells release molecules that can bind to FasL, a death activator on T-cells, preventing their death or, as mentioned, melanoma inhibit the expression of a gene encoding APAF1, the apoptotic protease activating factor-1 [5,18]. Nevertheless, the exposure of the negatively charged PS by cancer cells might be an Achilles' heel of cancer providing a potential target for cationic molecules which can discriminate between neutral surfaces of non-cancer and negatively charged surfaces of cancer membranes.

1.3 Host defense peptides – promising weapons in antimicrobial and anticancer therapy

One strategy on which the innate immune system relies as defense against microorganisms is the use of antimicrobial peptides (AMPs) as a part of the first line defense. AMPs are wide spread in nature, especially in the plant and animal kingdoms [19,20]. So far, the Antimicrobial Peptide Database [21–23] comprises ~ 2650 AMPs from six kingdoms. Due to its immense diversity it is hard to classify them. A broad classification can be made on basis of their secondary structure [19]. There are four groups: the α -helical and β -sheet structures which are mainly found in nature and additionally some evolve an extended or loop structure (see Figure 2) [20,24]. However, the fundamental structural principal for at least AMPs of animals and plants is an amphipathic design due to spatial distribution of hydrophobic and cationic amino acids. AMPs typically exhibit a positive net charge and are composed of about 12 to 55 amino acids [19,20].

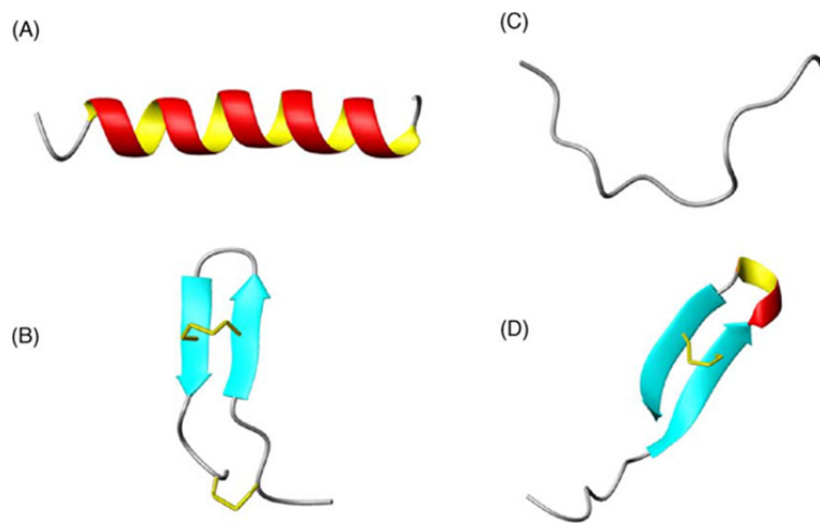


Figure 2: Antimicrobial peptide classification by secondary structure. There are mainly four classes: peptides which exhibit an α -helical structure like magainin 2 [25] (A), a β -sheet structure like tachyplesin [26] (B), an extended structure like indolicidin [27] (C) or a loop structure like thanatin [28] (D). Yellow indicates disulfide bonds. Figure was taken from Powers and Hancock [24].

Those cationic peptides are discussed to preferentially interact with negatively charged phospholipids via electrostatic interaction [29]. Several non-receptor mediated mechanisms of killing are discussed, whereby it depends on the type of peptide, the type of lipids as well as the peptide concentration [30–33].

The most often discussed models for the mode of action are the “carpet model” [34] and the formation of toroidal pores [35]. Peptides that are described to act via the carpet model lay

down in a carpet like manner on the membrane surface. At a peptide threshold concentration membrane permeabilization occurs [34]. At high concentration detergent-like actions can be induced by formation of bicelles, perforated sheets or micelles [18] (see Figure 3). In the toroidal pore model peptides line up with the head groups of the lipids of the membrane and form a pore, filled with water. Strong effects/perturbation can also occur due to phase separation of the lipids induced by peptides. Additionally, it was seen that peptides can even led to formation of hexagonal or cubic phases in bacterial membranes, resulting in formation of membrane blebs or protrusions or membrane lyses [36,37] (for schematic illustration taken from Riedl et al. [18] see Figure 3).

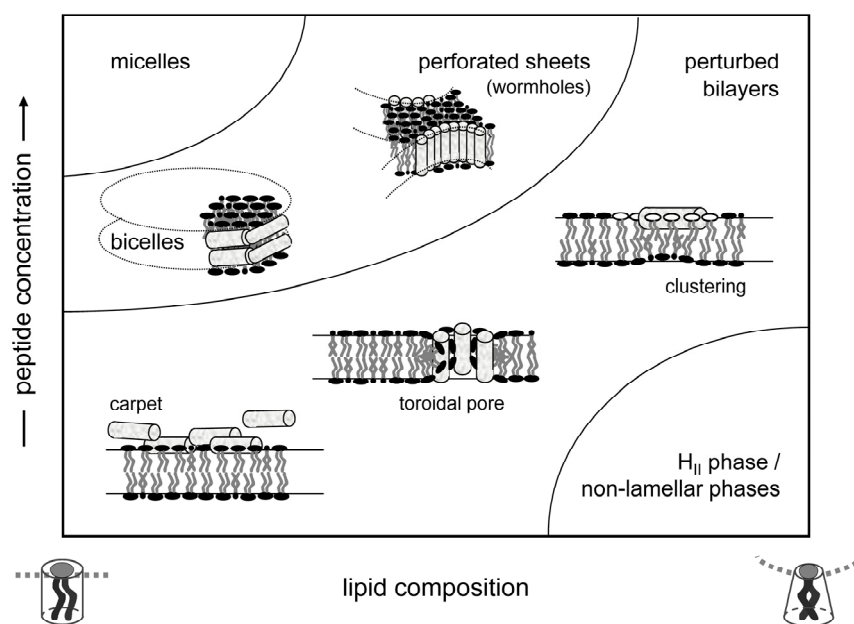


Figure 3: Different modes of action of host defense peptides. Depending on peptide type and concentration as well as lipid composition, host defense peptides develop different mechanisms of killing like the “carpet model” or by formation of toroidal pores. Figure was taken from Riedl et al. [18].

In addition to the antimicrobial effects, more and more studies report of anticancer activity exhibited by some AMPs. APD lists 188 anticancer/antitumor peptides so far, as for example magainin from the African claw frog *Xenopus laevis*, tachyplesin from the horseshoe crab or human as well as bovine lactoferricin [21–23]. As in bacteria, lipids as phosphatidylglycerol, cardiolipin or lipopolysaccharides are targeted, in this case also electrostatic interactions seem to play a key role in targeting the cancer cells due to the fact that cancer cells expose the negatively charged PS on the outside of the plasma membrane while healthy cells are usually neutral [18,38]. Further differences between cancer and non-cancer cells that may lead membrane active peptides to interact specifically with cancer cells were described by Riedl et al. 2011 [18]. For example cancer cell surfaces have an increased level of negatively charged

sialic acid in glycolipids and proteins. Moreover, the surface area is increased by microvilli and cancer cells also exhibit altered membrane fluidity. Two main mechanisms of killing of cancer cells by membrane active peptides may occur. One is the disruption and lysis of the plasma membrane - the necrosis of the cells; the other mechanism is reported to require entrance through the plasma membrane and induction of mitochondrial membrane lysis leading to apoptosis or apoptosis using the death receptor pathway [39]. As mentioned in 1.1, according to the world cancer report, cancer is one of the leading causes of mortality and despite huge progress in medicine (applying methods like surgery, chemotherapy, radiation) many cancers have a poor treatability or therapy connected with many side effects [18]. Thus, there is an urgent need for new anticancer therapeutics. Hence, anticancer peptides are promising new weapons in this field at least as a combination therapy to conventional chemotherapeutics.

One prominent human host defense peptide is lactoferricin (LFcin, Figure 4 (E)) which exhibits besides antimicrobial, antiviral and immunomodulatory also antitumor activity. Upon cleavage of the signal sequence and pepsin digestion of the ~ 80 kDa glycoprotein lactoferrin (LF) the active peptide LFcin arises corresponding to amino acids 1 to 49 of LF. As most of the AMPs also LFcin constitutes an amphipathic structure with hydrophobic and positively charged faces. Furthermore, the first interaction partners are negatively charged phospholipids. It was shown to kill Gram-positive and -negative bacteria not by severely damaging the membrane but rather by acting on unknown intracellular targets. Furthermore, it exhibits immunomodulatory effects (anti-inflammatory) not only by binding the bacterial endotoxin LPS [40].

Ensuing from this knowledge Zweytick et al. [41] reported in 2006 that variants of a peptide comprising the membrane active region between amino acid 21 – 31 of LFcin, the so called peptide LF11 (QWQRNIRKVR-NH₂), exhibited increased antimicrobial activities. The peptides were improved in their activity against several Gram-positive and -negative bacterial strains over three generations. Important properties of the potent antibacterial peptide derivatives were deletion of non-charged polar residues and strengthening of the hydrophobic N-terminal part upon addition of a bulky hydrophobic amino acid or N-acylation [36]. These peptides showed correlation of bacterial activity with perturbation of bacterial model liposomes composed of the negatively charged lipids phosphatidylglycerol or cardiolipin. Amongst the potent non-acylated peptides designed in this study were, for instance, LF11-322 (PFWRIRIRR-NH₂, +5 net charge) or LF11-318 (FWQRRIRRWRR-NH₂, +7 net charge). Due to the fact that also cancer cells expose a negatively charged lipid phosphatidylserine

(PS), Riedl et al. [17] tested if LF11-322 and other antibacterially active LF11-derivatives also revealed specific killing efficiency against cancer cells but anti-cancer activity of the short peptides was low [42]. Yang et al. [43] unveiled that for potent antitumor activity a minimum positive net charge (at least + 7) and hydrophobicity is important. To reach this minimum net charge di-peptides were designed by addition of the same or its retro sequence. R-DIM-P-LF11-322, which is LF11-322 linked to its retro sequence via a proline residue, turned out to fulfill all important parameters: a minimum length, a high positive net charge, a high affinity to the target PS and an adequate hydrophobicity (PFWRIRIRR-P-RRIRIRWFP-NH₂, + 9 net charge) [42]. A 10-fold increased toxicity to malignant melanoma cells A375 was shown for R-DIM-P-LF11-322 compared to its parent peptide LFcin.

LC₅₀ values determined by PI uptake revealed that R-DIM-P-LF11-322 exhibits potent activity against cancer cell lines like A375 with a lethal concentration of 10 μM needed for killing 50% of the tumor cells while 6.5 times more peptide was needed to kill healthy cells (NHDF, normal human dermal fibroblasts) (see Table 1). On the contrary, the di-peptide of the antibacterially active peptide LF11-318, DIM-LF11-318 revealed a highly antitumor-active but non-selective peptide (FWQRRIRRWRR-FWQRRIRRWRR-NH₂, + 13 net charge) with a LC₅₀ of 4 μM for A375 and 2 μM for NHDF (Table 1) [44].

Table 1: LC₅₀ values determined by PI uptake (8 hours) for R-DIM-P-LF11-322 and DIM-LF11-318 for malignant melanoma cells (A375) and normal human dermal fibroblasts (NHDF). Data was taken from Riedl et al. [44].

	LC ₅₀ (PI)	
	A375	NHDF
R-DIM-P-LF11-322	9.5 ± 0.3 μM	65.1 ± 2.5 μM
DIM-LF11-318	3.8 ± 0.5 μM	2.2 ± 0.9 μM

As shown by Riedl et al. [44], the online program PEP-FOLD [45–48] for *in silico* secondary structure prediction revealed a conformation of two β-strands for R-DIM-P-LF11-322 and an α-helical structure without a loop for DIM-LF11-318 (see Figure 4). This was experimentally confirmed by circular dichroism studies. These studies revealed that the in solution mainly unstructured R-DIM-P-LF11-322 exhibits a significant increase in β-sheet conformation in presence of the cancer mimicking micelles composed of sodium dodecyl sulfate (SDS). It remains unstructured in presence of dodecylphosphocholine (DPC) mimicking non-cancer membranes. This reveals a structure dependent cancer selective toxicity. DIM-LF11-318 changes its conformation significantly to an α-helical structure in presence of cancer and non-cancer mimics though being unstructured in solution, whereas R-DIM-P-LF11-322 only

changes its structure in presence of the cancer mimic, namely to a β -sheet [44]. Riedl et al. [44] performed this analysis with further peptides and showed that peptides with non-looped α -helical structures exhibit non-specific toxicity for cancer and non-cancer cells, whereas loop structures could be correlated to highly cancer specific peptides. Furthermore, specificity seems to be also related to the killing mechanism. Specific peptides were shown to kill cancer cells slowly through induction of apoptosis in a concentration dependent manner, whereas non-specific peptides killed cancer cells fast via necrosis.

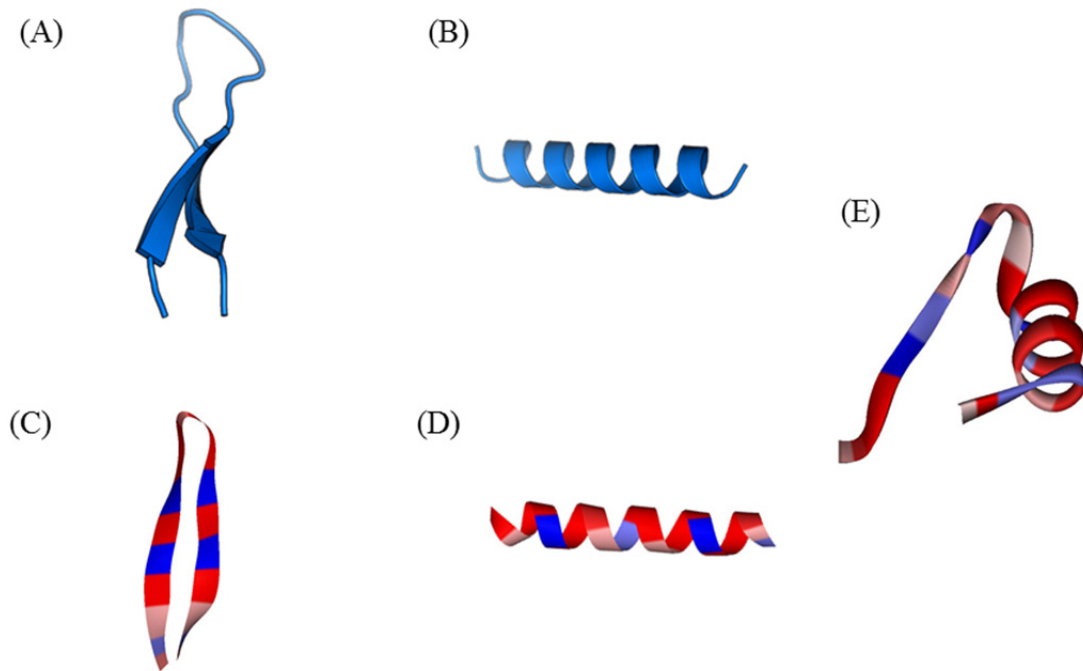


Figure 4: Predicted structures for two anticancer peptide derivatives (R-DIM-P-LF11-322 and DIM-LF11-318) as well as for the parent peptide hLFcin. The specific R-DIM-P-LF11-322 ((A), (C)) was predicted to form a β -sheet structure while the non-specific DIM-LF11-318 ((B),(D)) was predicted to exhibit an α -helical structure. (C) and (D) represent the hydrophobic (blue) and cationic (red) regions of the peptides. (E) represents the human parent peptide lactoferricin (hLFcin) with a helical and a β -sheet part, separated by a loop. Predictions were performed using PEP-FOLD [45–48]. Predicted structure for hLFcin (E) is consistent with literature [40].

1.4 Cholesterol – effects on membranes and peptides

The plasma membrane of eukaryotic cells contains besides phospholipids also up to one molecule cholesterol per phospholipid [49]. In the bilayer the polar hydroxyl group of the rigid sterol molecule arranges in the region of the polar head groups, while the four-ring system interacts with the hydrocarbon chains of the phospholipids thereby increasing the order of the neighboring lipids. Through this interaction the fluid bilayer gets less deformable, more rigid and therefore the permeability of the bilayer is decreased. Cholesterol is reported to preferentially interact with sphingolipids in so called rafts [50,51].

Matsuzaki et al. [35] reported that cholesterol depletion of erythrocytes led to increased

sensitivity against the AMP magainin, suggesting that cholesterol may have a protective role against AMPs. Interestingly, they revealed that the lytic effect of the non-specific melittin was independent of the cholesterol content, whereas they had no explanation for these phenomena at this point. Another group published that the effect of pardaxin is also reduced when model systems contain cholesterol [52]. Furthermore, McHenry et al. [53] published in 2012 that membrane disruption of AMP is prevented by cholesterol in non-raft model systems. Since phase separation naturally occurs in eukaryotic cells, McHenry et al. tried to investigate the effect of cholesterol on AMPs when present in heterogeneous systems with phase separation. They found that upon incorporation of cholesterol into raft-like domains cholesterol cannot inhibit the disruption of the membrane through AMPs. They claimed that raft formation may lead to less cholesterol in non-raft domains. These parts would lose their stiffness and therefore would be an easy target for AMPs [53,54]. Li et al. [55] stated that some cancer types like breast or prostate cancer have elevated levels of cholesterol-rich lipid rafts, whereas the rest of the membrane contains less cholesterol.

Another theory claims that hydrogen bonds formed between the hydroxyl-group of cholesterol and residues of the peptides may prevent formation of the secondary structure of the peptides needed for the proper interaction with the acidic phospholipid bilayer [29]. This can be one explanation for cholesterol effects seen by Matsuzaki et al. [35]. Melittin has a well-defined structure already in aqueous solution while magainin needs to form its membrane active structure in presence of the (target) membrane. The latter can be affected by the presence of cholesterol.

1.5 Aim of the study

Based on studies of Zweytick and Riedl et al. the aim of this thesis was to analyze differences in the mode of action and specificity of two human lactoferricin derivatives, namely the specific R-DIM-P-LF11-322 and the non-specific DIM-LF11-318 on malignant melanoma cells. The main focus lay on effects of the lipids PS, PC and cholesterol on the peptide interaction with its target membrane. Thereto lipid model systems mimicking cancer cells with different ratios of PS, PC and cholesterol in absence and presence of either R-DIM-P-LF11-322 or DIM-LF11-318 were analyzed with different biophysical methods. Furthermore, the peptide effects *in vitro* on malignant melanoma cells in absence of plasma membrane cholesterol as well as morphological changes of certain cell organelles were determined. This should help to further optimize the peptides with the purpose to design a new, specific and potent therapy against malignant melanoma.

2. Material and Methods

2.1 Lipids

The lipids 1,2-dipalmitoyl-*sn*-glycero-3-phosphocholine (DPPC), 1,2-dipalmitoyl-*sn*-glycero-3-phospho-L-serine (sodium salt) (DPPS), 1-palmitoyl-2-oleoyl-*sn*-glycero-3-phosphocholine (POPC), 1-palmitoyl-2-oleoyl-*sn*-glycero-3-phospho-L-serine (sodium salt) (POPS) and fluorescently labeled 1,2-dioleoyl-*sn*-glycero-3-phosphoethanolamine-N-(lissamine rhodamine B sulfonyl) (ammonium salt) (RhoDOPE) were purchased from Avanti Polar Lipids, Inc. (Alabaster, AL, USA). Cholesterol was purchased at Sigma-Aldrich Co. LLC (Deisenhofen, Germany). Lipids were used without any further purification. Stock solutions of DPPC and POPC were prepared in a mixture of chloroform and methanol of 2:1 (v/v). Stock solutions of DPPS and POPS were prepared in a mixture of chloroform and methanol of 9:1 (v/v). Cholesterol and RhoDOPE were dissolved in pure chloroform. Stock solutions were stored at $-20\text{ }^{\circ}\text{C}$.

2.2 Peptides

The C-terminally amidated peptides R-DIM-P-LF11-322 (PFWRIRIRR-P-RRIRIRWFP-NH₂, M = 2677.4 g/mol), DIM-LF11-318 (FWQRRIRRWRR-FWQRRIRRWRR-NH₂, M = 3413.1 g/mol) and the fluorescently labeled peptide (5-6)-FAM-R-DIM-P-LF11-322 ((5-6)-FAM-PFWRIRIRR-P-RRIRIRWFP-NH₂, M = 3035.7 g/mol) were purchased from NeoMPS, Inc. (San Diego, CA, USA). A purity of higher than 96% for all peptides had been determined by RP-HPLC. Stock solutions of R-DIM-P-LF11-322 and DIM-LF11-318 were prepared in acetic acid (0.1% v/v) at a concentration of about 3 mg/ml and for better solubility treated with ultrasonication. The peptide concentrations of the non-labeled peptides were determined via measurement of UV-absorbance of tryptophan at 280 nm (using NanoDrop ND 1000 (Peqlab, VWR International, Inc. Erlangen, Germany)). The fluorescently labeled peptide was solved in Dulbecco's Phosphate Buffered Saline (DPBS, Gibco[®], Life Technologies, USA) at a concentration of about 3 mg/ml. Again ultrasonication was used for better solubility. All peptide solutions were stored at $4\text{ }^{\circ}\text{C}$.

2.3 Model system studies

2.3.1 Liposome preparation

For preparation of lipid films of single component and lipid mixtures containing DPPC, DPPS and/or cholesterol at certain molar ratios the respective amounts of lipids were mixed in

Pyrex[®] culture tubes to reach a total amount of 1 mg. The solvent of the lipids was removed under a stream of nitrogen on a heating block at 30 °C for half an hour. Afterwards the lipid films were evaporated overnight to remove the remaining solvent. The lipid films were stored at 4 °C.

To prepare liposomes the lipid films (1 mg of lipids) were hydrated in 1 ml of phosphate buffered saline (PBS) (20 mM NaPi, 130 mM NaCl, pH 7.4) at a temperature well above (~ 10 – 15 °C) the gel to liquid phase transition of the respective lipid or lipid mixture via intermittent strong vortexing. The hydrating procedure was performed in the absence or presence of the respective peptides with a molar ratio of lipid to peptide of 25:1 in a sand bath placed in a heating incubator for improved heat transfer. DPPC was hydrated at 50 °C for two hours, while vortexing every 15 minutes for one minute. DPPS was hydrated at 65 °C for 1.5 hours while vortexing every 15 minutes for one minute. For preparation of lipid mixtures for zeta potential/size measurements, tryptophan quenching as well as for differential scanning calorimetry (DSC) measurements a preparation method called freeze and thaw was used. Hydration of all mixtures was performed at 65 °C for two hours by vortexing accompanied by one freeze and thaw cycle every 15 minutes. Thereby vortexing for one minute occurred before freezing and during thawing at each cycle. All mixtures for DSC measurements were also hydrated without the freeze and thaw method. The liposomes were stored at room temperature (RT).

For the hydration of liposomes for the zeta potential and size measurement studies, the peptides were not added during the preparation procedure. For these experiments after the preparation liposomes were extruded ten times through a 200 nm Whatman[®] Nuclepore[™] Track-Etched Membrane (Sigma Aldrich Co. LLC), using a Mini-Extruder of Avanti Polar Lipids, Inc. Peptides were added afterwards (see 2.3.4)

2.3.2 Differential scanning calorimetry (DSC)

DSC measurements were performed with a differential scanning calorimeter (VP-DSC) from MicroCal, Inc. (Northhampton, MA, USA). The heating scans were performed with a scan rate of 30 °C/h with pre-scan thermostating for 30 minutes. The cooling scans were performed with the same scan rate with one minute pre-scan thermostating. Every measurement included two heating and two cooling scans. DPPC measurements were performed between 20 °C and 50 °C, DPPS measurements between 25 °C and 65 °C. For the mixtures the first two cycles occurred between 25 °C and 65 °C and the second two cycles occurred between 25 °C and 70 °C. For analyses of the characteristics of the respective thermotropic phase behaviors the

MicroCal Origin Software (VP-DSC version) was used. Briefly the peak areas were integrated after normalization to the phospholipid concentration and baseline adjustment for calculation of the enthalpies of the pre-transition and the main transition, ΔH_{pre} and ΔH_m , respectively. The phase transition temperatures of the pre- and the main transition (T_{pre} and T_m) were determined as the maxima of the peaks. The $T_{1/2}$ (half-width) was defined as peak width at half height [56]. Deconvolution was used for analyses of data of overlapping phase transitions.

2.3.3 Tryptophan quenching

Spectra of tryptophan fluorescence were measured at RT with a Cary Eclipse fluorescence spectrophotometer of Varian (Salt Lake City, UT, USA). The excitation wavelength was set 280 nm and the slit-width was 5 nm for the excitation as well as for the emission monochromators. The wavelength scans were recorded between 300 nm and 410 nm. The quenching of the tryptophan of the peptides was determined in absence (15 μ g peptide in 1 ml PBS only) and presence of phospholipid liposomes (DSC samples diluted 1:10 in PBS; lipid to peptide ratio 25:1) with 0 M, 0.1 M, 0.4 M and 0.7 M acrylamide [57–59]. For data analyzing the Stern-Volmer equation (Equation 1) was used:

$$\frac{F_0}{F} = 1 + K_{SV} * [Q]$$

Equation 1: Stern-Volmer Eq.

F_0 and F represent the intensity of the fluorescence emission in absence and presence of the Quencher (Q) acryl amide. K_{SV} represents the Stern-Volmer quenching constant, a quantitative measure for the accessibility of tryptophan to acrylamide [57].

2.3.4 Zeta potential and size

A Zetasizer Nano ZSP (Malvern Instruments, Herrenberg, Germany) was used for determination of the zeta potential (surface potential) of liposomal mimics of cancer and non-cancer membranes in absence or presence of peptides, by measuring the electrophoretic mobility applying the Henry equation. For the calculation the Smoluchowski approximation was used which is suitable for aqueous solutions. Furthermore the size of the particles was measured.

Freshly extruded liposomes (see 2.3.1) (lipid mixtures, freeze and thaw; single component, non freeze and thaw) were diluted with HEPES cesium chloride buffer (10 mM HEPES, 2 mM CsCl, pH 7.1) to a final lipid concentration of 0.05 mg/ml. For measurements in presence of

peptides, peptides were added to 1 ml of the liposome suspension at a 25:1 lipid to peptide ratio. For measurements in presence of Ca^{2+} , its concentration was 1 mM. After dilution and optional addition of peptides or CaCl_2 the liposomes were incubated for five minutes at 65 °C. After vortexing and one minute of cooling at RT, the samples were transferred in a measurement cuvette (disposable folded capillary cell DTS1070; Malvern). Three measurements were performed at 25 °C (120 seconds equilibration time) with 10 – 30 runs and a 60 seconds delay between the three determinations. The attenuation as well as the voltage selection was automatic. The analysis mode was auto-mode. Size was measured at 25 °C after each zeta potential measurement. 173 ° backscatter was used as angle for detection. Analysis method was a multi parameter analysis and the analysis model was on normal resolution. When the Pdi (polydispersity index) was lower than 0.5 the z-average (mean value of the size; calculated from the signal intensity of light scattering measurement) was used for comparison of sizes. When the Pdi was above 0.5 the number mean values were used being of better validity.

2.3.5 Giant unilamellar vesicles (GUVs)

For preparation of GUVs the electroformation method was used [60]. First a lipid and dye mixture was prepared. Therefore to 100 μl of 2 mg/ml respective lipid mixtures (with different molar ratios) 1 μl of 2 mg/ml Rhodope was added. The mixed solution was applied on the conductive sides of two clean indium tin oxide (ITO) glasses via circular movements to produce a thin lipid film by slowly spreading three spots of 2 μl of the mixture for two times on each glass, always waiting until the solvent was evaporated per spot. With a Teflon frame in between the two glasses were closed via paper clips with the conductive sides facing each other (see Figure 5).

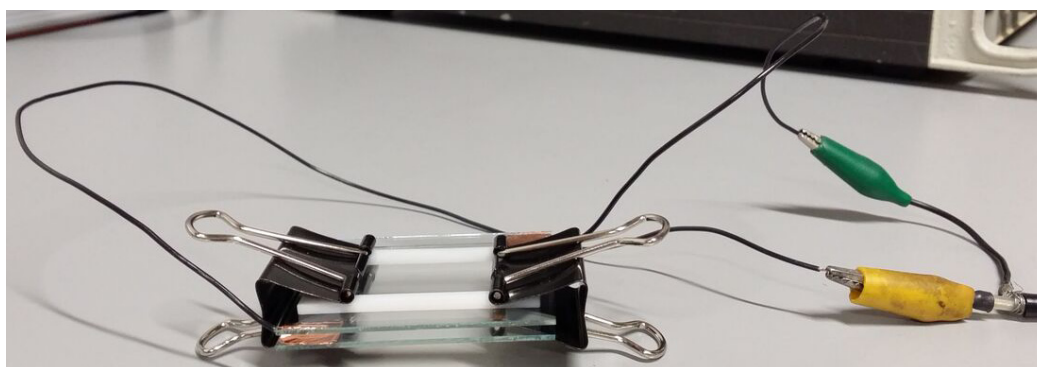


Figure 5: Setup for preparation of giant unilamellar vesicles (GUVs). The respective lipid + dye solution was spread on the conductive sides of two ITO-glasses. The glasses were closed with paper clips using a Teflon frame in between. A cord was fixed with a copper band for easier connection to the function generator. Small holes in the frame allowed filling of the chamber with the aqueous solution.

Then the glasses were connected to a WaveTek synthesized function generator 288 (Fluke LLC., Brunn am Gebirge, Lower Austria, Austria) with AC field adjustment, sine function, 10 Hz, 1 V, VPP for ten minutes. Afterwards, the chamber was disconnected to fill it with double distilled water followed by connection to the function generator again. The starting voltage of 1 V was increased by 0.5 V every 20 minutes until 2.5 V were reached. In case of neutral lipids 2.5 V were held for four hours, in case of charged lipids for only half an hour. In the final step the voltage was decreased from 2.5 V to 1.5 V and the frequency from 10 Hz to 5 Hz. After 15 minutes the GUVs suspension was transferred into a black Eppendorf tube ready for microscopic studies. The protocol was kindly provided by Karin A. Riske (Departamento de Biofísica, Universidade Federal de São Paulo, São Paulo, Brazil). To determine changes in lipid distribution of GUVs upon peptide addition, they were used freshly for microscopic inspection. 20 μ l of the GUVs solution were incubated with 1 μ l of respective peptide [3 mg/ml] in Ibidi μ -slides (18 wells) for 30-60 minutes. The mixtures DPPC/POPS/Cholesterol 1:1:0.25 and 1:1:0.5 had to be analyzed immediately after peptide addition due to fast destruction in presence of peptides. Microscopic inspection (see 2.4.2 for microscope description) occurred at excitation wavelength of 558 nm and an emission wavelength of 582 nm.

2.4 *In vitro* studies

2.4.1 Cell lines and cultures

The cell line of normal human dermal fibroblasts (NHDF) and the melanoma cell line A375 were purchased from PromoCell, Inc. (Heidelberg, Germany) and from ATCC (American Type Culture Collection, Manassas, VA, USA), respectively. Both cell lines were cultured in Dulbecco's Modified Eagle Medium with GlutaMAXTM, high glucose and phenol red (DMEM, Gibco[®]) supplemented with 10% fetal bovine serum (FBS, Gibco[®]). The atmosphere for cultivation was kept at 5% CO₂ at 37 °C. At 90% confluence of cells in the culture flasks (75 cm²) they were passaged after detachment with accutase (Gibco[®]) (incubation 2 – 3 minutes at 37 °C with 1.5 ml accutase solution, > 600 U/ml). For fluorescence microscopy studies cells were seeded on Ibidi μ -Slide 8 wells (Martinsried, Munich, Germany).

2.4.2 Fluorescence microscopy

Experiments were performed with a Leica DMI6000 B with IMC using a Leica DFC360 FX camera and AF 6000 software (Leica Microsystems, Vienna, Austria). Excitation and emission wavelengths used for respective stainings are listed in Table 2.

Table 2: Excitation and emission wavelengths used for visualization of respective stainings by fluorescence microscopy

Fluorescent Dye	Excitation Wavelength [nm]	Emission Wavelength [nm]
Filipin (staining of cholesterol)	352	454
NucBlue [®] (Höchst 33342) (staining of nucleus)	359	461
(5-6)- Carboxyfluorescein ((5-6)-FAM) (label of peptide)	495	519
Propidium Iodide (PI) (staining of DNA, membrane damage)	538	617
CellLight [®] Golgi-RFP BacMam 2.0 (staining of Golgi)	558	582
Rhodamine (RhoDOPE) (staining of fluid/disordered lipids)	558	582
MitoTracker [®] Deep Red (staining of mitochondria)	650	668

– Cell culturing

For microscopic experiments cells were seeded in Ibidi μ -Slide 8 wells (Martinsried, Munich, Germany) with a cell-density of $1 - 2 * 10^4$ per well. The cells were grown in 300 μ l DMEM + 10% FBS for two to three days to a confluent layer ($\sim 10^5$ cells/well).

– Fixation of cells

For fixation of cells media was removed and cells were washed gently with 300 μ l DPBS. Afterwards 300 μ l 1% (w/v) paraformaldehyde solution was added and cells were incubated for 10 minutes at RT in the wells. After fixation cells were washed twice with DPBS and staining of cholesterol, mitochondria and/or Golgi followed.

– Propidium iodide (PI)-uptake

PI staining was used in cell culture experiments to determine the toxicity of the peptides indicated by induction of membrane damage and cell death. 2 μ l of a 50 μ g/ μ l PI-solution (in DPBS) (Biosource, Camarillo, CA, USA) were added to each well. For microscopic

inspection the excitation wavelength for PI was set 538 nm, the emission wavelength was set 617 nm.

PI staining was used for staining of the DNA (nucleus) together with cholesterol staining and depletion, as well as for peptide localization experiments.

– R-DIM-P-LF11-322 localization and peptide effects

For R-DIM-P-LF11-322 localization studies an N-terminal (5-6)-Carboxyfluorescein (5-6-FAM)-label was used. 3 µl of a (5-6)-FAM-R-DIM-P-LF11-322 peptide stock (~ 3 mg/ml) were added to each well with confluent A375 melanoma cells (Ibidi µ-Slide 8 wells) and incubated at 37 °C for certain time periods (two and four hours). Afterwards cells were gently washed two times with DPBS and fixation followed. After fixation cells were washed twice with DPBS. Then 300 µl DPBS were added to each well and PI staining was performed. For microscopic inspection of peptide localization an excitation wavelength of 495 nm and an emission wavelength of 519 nm were set.

Peptide localization was also performed with cholesterol, mitochondria and/or Golgi apparatus co-staining.

– Cholesterol staining

Filipin complex (Sigma-Aldrich Co. LLC) was used for cholesterol staining of cell membranes of NHDF and A375 melanoma. Filipin was solved in DMSO at a concentration of 25 mg/ml. Stocks were stored in dark glass vials (filled to the top), oxygen was removed and vial was closed immediately to prevent oxidation (storage at – 20 °C). At 90% confluence cells were fixed. After two gentle washing steps with DPBS cells were stained with 300 µl of filipin (0.05 mg/ml in DPBS) for at least 10 minutes at 37 °C. After staining and after the cells were gently washed twice PI staining was performed. For visualization via fluorescence microscopy an excitation wavelength of 352 nm and an emission wavelength of 454 nm were set.

For experiments in presence of peptides (labeled and unlabeled), peptide was added to confluent cells and incubated for a certain time (0 min, 30 min, 60 min and 120 min), then the fixation, cholesterol and PI staining of DNA followed. Filipin staining was also used for cholesterol depletion control experiments (see 2.4.3).

– Mitochondrial staining

The MitoTracker[®] Deep Red of Invitrogen (Molecular Probes Inc., Eugene, OR, USA) was used for staining of mitochondria in A375 melanoma cells. The stock solution (1 mM in

DMSO) was diluted 1:20000 in DPBS. At 90% confluence cells were fixed. Then the cells were washed two times before 300 µl of the diluted MitoTracker[®] were transferred into each well. An incubation step of 15 minutes at 37 °C followed. After removal of the staining solution and two gentle washing steps, cells were ready for microscopic inspection (excitation wavelength 650 nm, emission wavelength 668 nm).

For experiments in presence of peptides (labeled and unlabeled), peptide incubation was the first step. After certain incubation times (0 min, 30 min, 60 min and 120 min), fixation, mitochondrial and cholesterol staining were performed.

– Golgi staining

For staining of the Golgi apparatus (Golgi) the CellLight[®] Golgi-RFP BacMam 2.0 (Molecular Probes Inc.) reagent and the BacMam enhancer (Molecular Probes) were used. 300 µl of the enhancer (1:1000 dilution with DMEM + 10% FBS) were added to the confluent cells and incubated for 1.5 hours at 37 °C. Subsequently the cells were washed two times with DPBS, 300 µl fresh medium were added and 12 µl of the pure cell light reagent were transferred into each well. At least 16 hours of incubation at 37 °C were required for proper integration. Afterwards, the cells were washed twice with DPBS. For fluorescence microscopy analyses an excitation wavelength of 558 nm and an emission wavelength of 582 nm were set. For further studies in presence of peptides, peptides were added after Golgi staining for certain incubation times (0 min, 30 min, 60 min and 120 min), fixation and cholesterol staining or nuclear staining followed.

– Nuclear staining

NucBlue[®] Live ReadyProbes[®] Reagent (Life Technologies) was used for co-staining of nucleus with mitochondria or Golgi. One drop of the ready to use kit (~ 5 µl) was transferred in each well and incubated for 5 minutes before microscopic analyses were performed. The excitation wavelength was 359 nm and the emission wavelength was 461 nm.

2.4.3 Cholesterol depletion studies

For preliminary tests cells grown in Ibidi µ-Slide 8 wells were washed gently with DPBS. Then 300 µl DPBS + 10% FBS were added to each well, followed by 0.04 mM, 1 mM and 5 mM of the cholesterol depletion agent methyl-β-cyclodextrin (MβCD). After 30 min incubation at 37 °C, cells were gently washed twice with DPBS. Afterwards, on the one hand, cells were fixed, followed by filipin and PI staining. On the other hand, prior to fixation, filipin and PI staining, cells were incubated for two hours with DPBS + 10% FBS, to exclude

that intracellular cholesterol is transported to the plasma membrane within these two hours. Visualization by fluorescence microscopy was equal to that described under 2.4.2 (cholesterol staining). 5 mM were shown to be sufficient for depletion of plasma membrane cholesterol. For the cholesterol depletion experiments, cells were grown in three 175 cm² culture flasks to 90% confluence. 20 ml DPBS supplemented with 10% FBS were added to the first flask - control cells, no cholesterol depletion. Cells in the second flask were incubated with 5 mM and in the third with 10 mM M β CD in DPBS supplemented with 10% FBS during shaking of the flasks at 100 rpm at 37 °C. Afterwards the media was removed and cells were washed with 10 ml DPBS, detached with 3 ml accutase, suspended in 2 ml DMEM without phenol red supplemented with 10% FBS and seeded in wells of a dark 96 well plate with a density of 10⁵ cells per well (10⁵ cells per 100 μ l + 2 μ l PI). Subsequently respective peptides at concentrations of 0 μ M, 10 μ M, 20 μ M or 40 μ M were added and the PI uptake was measured at different time points (0, 1, 2 and 4 hours) using the GloMax[®] Multi+ Detection System (Promega, Madison, WI, USA). The excitation wavelength was 536 nm and the emission wavelength 617 nm. For the 100% value (P₁₀₀) 2 μ l Triton (10% v/v) were added after the time series and after two minutes of incubation the PI fluorescence in each well was measured. For peptide cytotoxicity calculation the percentage of PI positive cells was measured in presence of the peptides (P_x) and of PI positive cells in media without any peptide (P₀) (see Equation 2).

$$\% \text{PI} - \text{uptake} = \frac{100 * (P_x - P_0)}{(P_{100} - P_0)}$$

Equation 2: Equation for PI uptake calculation

3. Results

The two peptides used in the studies reveal different specificities. While R-DIM-P-LF11-322 only harms cancer cells, DIM-LF11-318 kills both cancer and healthy cells, the studies by Riedl et al. [44] revealed correlation with secondary structure and different permeabilization of membranes. To unveil further potential reasons for the differences in specificity the following experiments with model systems as well as *in vitro* studies were performed.

3.1 Impact of phosphatidylserine on peptide activity and interaction

3.1.1 Phosphatidylserine is exposed on the outer leaflet of cancer cell membranes

Cancer cells specifically expose the negatively charged lipid phosphatidylserine (PS) in the outer leaflet of the plasma membrane (see Figure 1, Page 7, for schematic illustration) [13,17]. One method for illustrating PS exposure of cancer membranes is the specific binding of a fluorescently labeled Annexin V (Alexa Fluor 488 (green)) to PS exposed on the surface of intact plasma membranes of cancer cells (Figure 6, right, melanoma cell line SBcl-2), whereas non-cancer cells do not expose PS and therefore do not bind Annexin V (Figure 6, left, melanocytes). PS exposure due to apoptosis could be excluded because of absence of cleavage of caspase-3.

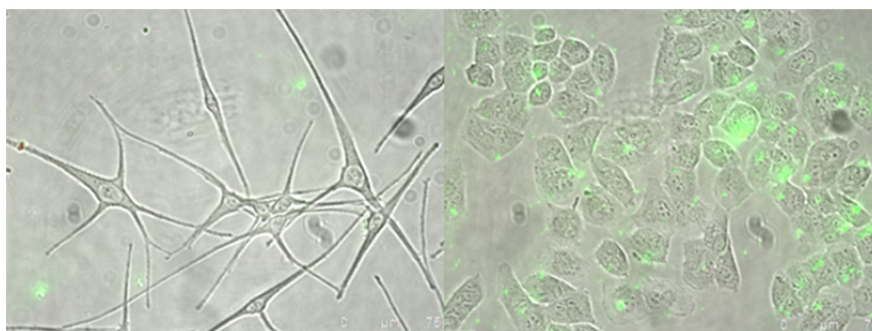


Figure 6: Alexa Fluor 488 Annexin V staining of melanocytes and melanoma cells (SBcl-2). Overlay of bright field and fluorescence pictures of melanocytes (left) and SBcl-2 (right). Green indicates specific binding of Annexin V only to PS exposed by SBcl-2 melanoma cells (right). Images taken from Riedl et al. [17].

Therefore in the following section the impact of the negatively charged PS as a target for the cationic peptides, the cancer-specific R-DIM-P-LF11-322 and the non-specific DIM-LF11-318 were studied.

3.1.2 Model system studies

In the following model studies all liposomes composed of either single PS or mixtures containing PS and PC were used as cancer mimics, whereas liposomes composed of single PC were used as non-cancer “healthy” mimics.

- DSC – Changes of thermodynamic phase behavior of cancer cell mimicking liposomes by peptides

To study a potential interaction of the peptides with the membrane lipids PS and/or PC, changes in the thermodynamic phase behavior of respective liposomes mimicking plasma membranes of cancer (DPPS, DPPC/DPPS 1:1 and 3:1, molar ratios) and non-cancer cells (DPPC) in presence of R-DIM-P-LF11-322 and DIM-LF11-318 (lipid to peptide molar ratio 25:1) were measured using DSC. Changes of the calorimetric enthalpy ΔH_{cal} , the phase transition temperature T_m and the half width of the phase transition ($T_{1/2}$) indicate potential perturbation of the respective mimics by the peptides (see Figure 7 and Table 3). Consistently with literature DPPC showed two phase transitions [41]. A pre-transition at 35.6 °C with a pre-transition enthalpy ΔH_{pre} of 1.5 kcal/mol corresponding to the transition from the tilted gel phase ($L_{\beta'}$) to the rippled gel phase ($P_{\beta'}$) and a main phase transition corresponding to the transition from the lamellar gel (L_{β}) to the liquid crystalline (L_{α}) phase at 41.7 °C with a transition enthalpy of 9.5 kcal/mol and a high cooperativity $T_{1/2}$ of 0.12 °C was seen. The thermotropic phase behavior of the healthy mimic DPPC did not change when R-DIM-P-LF11-322 was added which indicated that there is no interaction. Interestingly the peptide DIM-LF11-318 which shows high activity with non-cancer cells *in vitro* did not cause membrane perturbation of the DPPC liposomes either.

However, severe membrane perturbation by the peptides was shown for the cancer mimic DPPS. Upon incubation with R-DIM-P-LF11-322 the transition split into two peaks, which might represent peptide enriched and peptide poor DPPS domains. The peptide affected lipid domains comprised 80% of the liposome, the phase transition temperature was strongly decreased by 5.1 °C and the half width was increased to nearly double, together indicating a strong perturbation of the cancer mimic DPPS by R-DIM-P-LF11-322. Lipid domains which were not affected showed a phase transition at a temperature near that of DPPS in absence of peptide ($T_m = 52.6$ °C). The overall enthalpy of the two domains yielded a 20% reduction compared to the absence of peptide. A decrease in ΔH_m of almost 50% was reached when DIM-LF11-318 was added to DPPS liposomes. With only 5.3 kcal/mol needed for the phase transition in comparison to 9.9 kcal/mol needed for DPPS liposomes, this indicated a severe membrane destabilization ($T_{1/2} = 3.24$ °C; $T_m = 52.8$ °C).

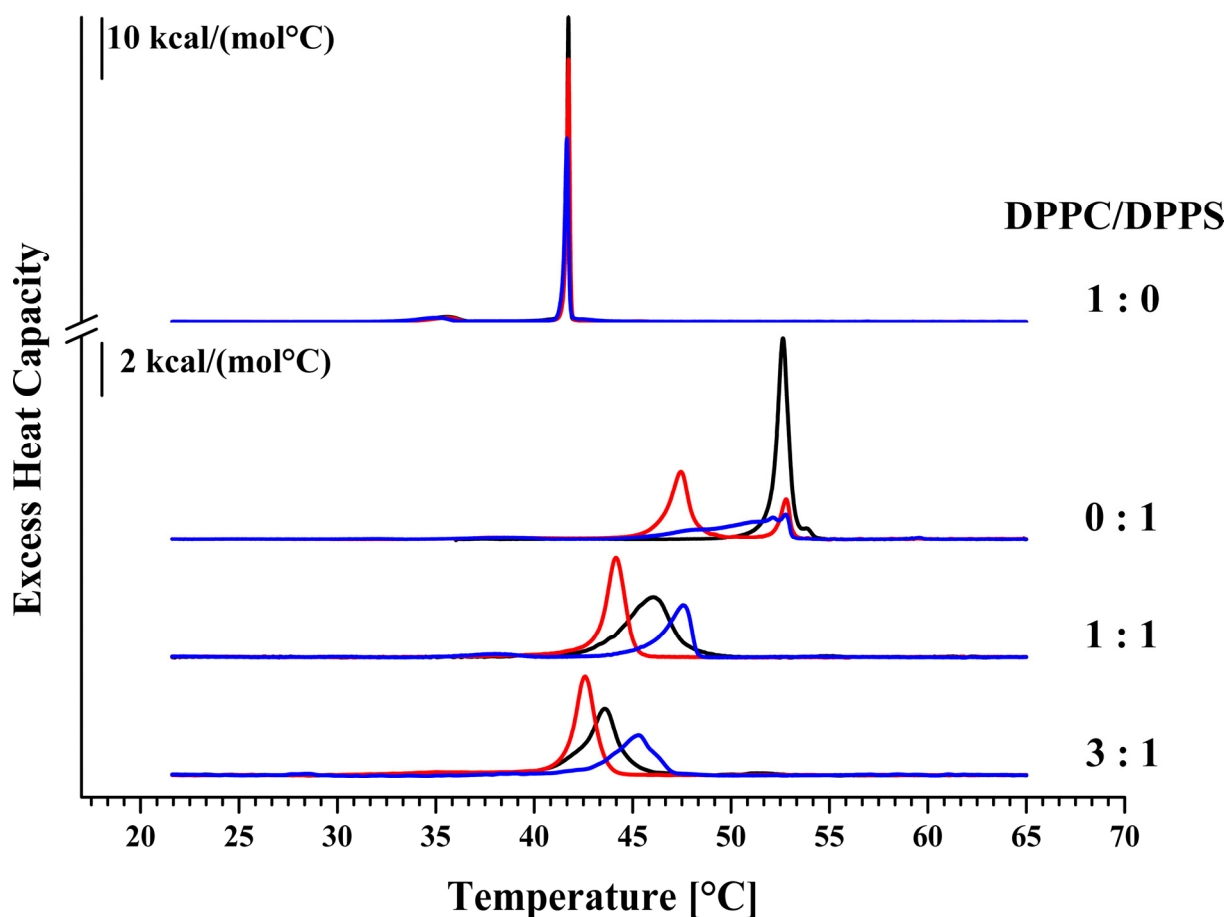


Figure 7: DSC thermograms of liposomes composed of DPPC and/or DPPS in absence and presence of R-DIM-P-LF11-322 or DIM-LF11-318. Liposomes of pure DPPC (1:0), pure DPPS (0:1) or DPPC/DPPS 1:1 and 3:1 (molar ratios; freeze and thaw) were used to determine the effect of the two LF11 derivatives on the respective lipid systems (lipid to peptide molar ratio 25:1). Black represents thermograms in absence of peptide; red in presence of R-DIM-P-LF11-322 and blue in presence of DIM-LF11-318. For clarity, the DSC curves were displayed on the ordinate by an arbitrary increment. For analyzed data see Table 3.

Furthermore, cancer cell mimicking liposomes containing DPPC/DPPS 1:1 and 3:1 molar ratios which were prepared using freeze and thaw to yield homogenous distribution of lipids, were studied. The 1:1 mixture showed one broad main phase transition at 46.1 °C. Addition of R-DIM-P-LF11-322 and DIM-LF11-318 resulted in a decrease of the main transition enthalpy though to different extent. In presence of R-DIM-P-LF11-322 the enthalpy was reduced by 20% (10.6 kcal/mol to 8.2 kcal/mol). Furthermore a severe temperature shift to lower temperature by 1.9 °C occurred. This shift indicates that the peptide preferentially perturbs the higher chain melting DPPS proportion of the mixture leaving DPPC enriched liposomes unaffected in the gel phase. This was also confirmed by an increase in cooperativity by more than 50%. Addition of DIM-LF11-318 resulted in an even stronger enthalpy reduction by 50% (from 10.6 kcal/mol to 5.2 kcal/mol) and a temperature shift to higher temperatures by 1.5 °C which indicates a strong perturbation of the lipid mixture and due to the shift of the T_m near the higher chain melting DPPS a presumable higher perturbation of the proportion of

DPPC. Addition of DIM-LF11-318 also resulted in a more highly cooperative phase transition indicated by a narrower $T_{1/2}$ of 1.43 °C and a small transition at 38 °C with a ΔH_m of 0.5 kcal/mol occurred (not listed in Table 3). This peak may represent kind of a pre-transition generated by a peptide induced chain tilt, for clarification X-ray analyses have to be performed. At increased DPPC ratios (DPPC/DPPS 3:1) there was no significant change in enthalpy in presence of R-DIM-P-LF11-322 (8.7 kcal/mol to 8.3 kcal/mol), however, the decrease of the T_m by 1 °C still indicates a strong interaction of the peptide with reduced proportion of 25 mol% DPPS. DIM-LF11-318 again had a stronger effect and led to a reduction of the phase transition enthalpy by 30%, indicating perturbation of the non-specific peptides with both lipids, DPPS (25 mol%) and DPPC (75 mol%). Again an increase of the main transition temperature by 1.8 °C (to 45.4 °C) confirmed the possible perturbation of DPPS and DPPC liposomes by the peptide. Addition of R-DIM-P-LF11-322 again led to a more homogenous phase transition at decreased temperatures ($T_{1/2} = 1.51$ °C in absence and 1.05 °C in presence of R-DIM-P-LF11-322), confirming specific interaction with DPPS. On contrary, addition of DIM-LF11-318 resulted in an increase of $T_{1/2}$ by 0.7 °C, indicating an interaction with both components of the mixture by the non-specific peptide.

Table 3: Thermodynamic parameters of DPPC, DPPS and DPPC/DPPS 1:1 and 3:1 (molar ratios; freeze and thaw) liposomes in absence and presence of R-DIM-P-LF11-322 or DIM-LF11-318. For thermograms see Figure 7.

	ΔH_{pre} [kcal/mol]	T_{pre} [°C]	ΔH_m [kcal/mol]	T_m [°C]	$T_{1/2}$ [°C]
DPPC	1.5	35.6	9.5	41.7	0.12
+ R-DIM-P-LF11-322	1.3	35.6	9.6	41.7	0.17
+ DIM-LF11-318	1.5	35.1	8.7	41.7	0.21
DPPS			9.9	52.6	0.64
+ R-DIM-P-LF11-322			7.5 (5.9/1.6)	47.5/52.8	1.07/0.54
+ DIM-LF11-318			5.3	52.8	3.24
DPPC/DPPS (1:1)			10.6	46.1	2.59
+ R-DIM-P-LF11-322			8.2	44.2	1.07
+ DIM-LF11-318			5.2	47.6	1.43
DPPC/DPPS (3:1)			8.7	43.6	1.51
+ R-DIM-P-LF11-322			8.3	42.6	1.05
+ DIM-LF11-318			5.9	45.4	2.23

- Zeta potential and size – Electrostatic and hydrophobic interactions of peptides with cancer cell mimicking liposomes

Another way to clarify potential differences in the interactions between the studied peptides and the lipid model systems are zeta potential measurements. The zeta potential is defined as difference in charge between a particle and its surrounding. If a charged peptide interacts with the model system, a change in the zeta potential of the model system should occur. The measurements were performed with DPPC, DPPS and DPPC/DPPS (1:1; molar ratio) liposomes in presence and absence of R-DIM-P-LF11-322, DIM-LF11-318 (lipid to peptide ratio 25:1) or CaCl_2 [1 mM], respectively (see Figure 8). Ca^{2+} was added as a reference for electrostatic interactions. Further it has to be mentioned that for these experiments liposomes were prepared and extruded afterwards to exhibit comparable sizes. Peptides were added just briefly before measurements to follow and simulate the first steps of interaction of the peptides with plasma membranes of cancer and non-cancer cells.

While DPPC liposomes, mimicking healthy cells, exhibited a neutral zeta potential (0 mV), cancer cell mimicking DPPS liposomes as well as 1:1 mixtures of both lipids showed a negative zeta potential of about - 50 mV. These data are in accordance with zeta potentials shown for non-cancer cells and cancer cells [44]. Addition of R-DIM-P-LF11-322, DIM-LF11-318 or CaCl_2 did not lead to any significant changes of the zeta potential of the DPPC liposomes, indicating absence of any (electrostatic or hydrophobic) interaction. On the contrary, addition of R-DIM-P-LF11-322 to DPPS liposomes strongly shifted the zeta potential from - 54 mV to 0 mV, so the specific peptide was able to completely neutralize the negatively charged surface. This indicates an electrostatic interaction between the positive charges of the peptides and the negative charges of the liposomes. Addition of DIM-LF11-318 led to a stronger shift of the zeta potential to even positive values (+ 15 mV) supposing beyond the electrostatic probably also hydrophobic interactions. Similar effects were seen when R-DIM-P-LF11-322, DIM-LF11-318 or CaCl_2 were added to DPPC/DPPS 1:1 liposomes. The presence of R-DIM-P-LF11-322 induced again neutralization of the negative surface potential. The presence of DIM-LF11-318 induced more positive values up to + 18 mV. All exact zeta potential values are listed in Table 4.

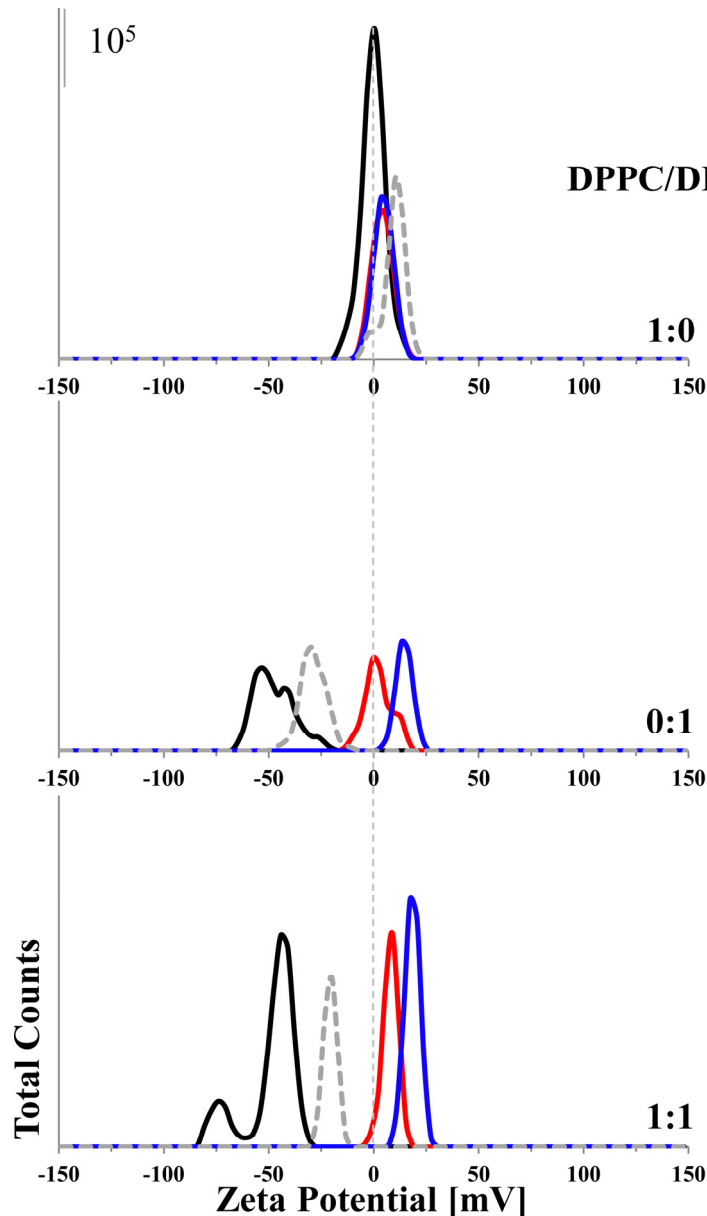


Figure 8: Zeta potential of different liposomes in presence and absence of R-DIM-P-LF11-322, DIM-LF11-318 or CaCl_2 . The zeta potentials of pure DPPC and DPPS liposomes as well as of DPPC/DPPS 1:1 (molar ratio) liposomes were determined in absence (black) and presence of R-DIM-P-LF11-322 (red), DIM-LF11-318 (blue) (lipid to peptide ratio 25:1) or CaCl_2 [1 mM] (dashed gray). While there is no change in zeta potential of DPPC liposomes in presence of peptides/calcium, those supplements reduce the negative zeta potential of liposomes when DPPS is present. This indicates an interaction of the peptides/calcium with the negatively charged lipid. For analyzed data see Table 4.

Furthermore, dynamic light scattering measurements were performed to determine changes in the size of the liposomes in presence of peptides. The values for the size measurements as well as those of the Pdi are listed in Table 4.

There was no significant change of DPPC liposome size when peptides were added. No change of zeta potential correlated with no change of size and polydispersity. In contrast, addition of R-DIM-P-LF11-322 or DIM-LF11-318 to DPPS or to DPPC/DPPS (1:1) liposomes did not only lead to changes in the surface potential but also to a significant increase of size. This indicated possible aggregation of the liposomes as a consequence of the

peptide interaction. Interestingly DIM-LF11-318 even induced two differently sized populations. Addition of Ca^{+2} did not cause any change of size. So the single change of the zeta potential does not naturally lead to an increase in size. However, the amount of Ca^{2+} was shown to be not sufficient to completely neutralize the negative surface charge of the DPPS containing liposomes, which might affect aggregation. In general a correlation between the changes of the zeta potential and increase of the size could be seen.

Table 4: Zeta potential and size values of DPPC, DPPS or DPPC/DPPS (1:1, molar ratio) liposomes in absence and presence of R-DIM-P-LF11-322, DIM-LF11-318 or CaCl_2 . (See Figure 8)

	Zeta potential [mV]	Size (z - average)*/ Number mean* [nm]	Polydispersity Index (Pdi)
DPPC	0	180	0.22
+ R-DIM-P-LF11-322	+ 4	210	0.27
+ DIM-LF11-318	+ 5	160	0.13
+ CaCl_2 (1 mM)	+ 10	170	0.13
DPPS	- 54	130	0.11
+ R-DIM-P-LF11-322	+ 2	250	0.52
+ DIM-LF11-318	+ 15	300	0.51
+ CaCl_2 (1 mM)	- 29	160	0.16
DPPC/DPPS (1:1)	- 49	70	0.56
+ R-DIM-P-LF11-322	+ 8	840	0.38
+ DIM-LF11-318	+ 18	200/640	0.28/n.d.
+ CaCl_2 (1 mM)	- 21	90	0.71

* z-average was taken when polydispersity index (Pdi) was below 0.5; number mean was taken when Pdi was above 0.5
n.d. not determined

- Giant unilamellar vesicles – Changes of lipid distribution of GUVs mimicking cancer membranes upon peptide addition

Giant unilamellar vesicles (GUVs) generated by electroformation are a perfect tool to visualize changes in model bilayers. The red dye RhoDOPE was used to stain lipids in the disordered or fluid phase. Figure 9 shows the fluorescence and bright field picture of a freshly prepared GUV (70 μm) composed of POPC/DPPS 3:1 (molar ratio). The fluorescence dye was mainly spread homogenously indicating a homogenous distribution of (the fluid) POPC over the GUV. Some macroscopic linear (brighter) domains were seen, referring to lipids in the fluid phase.

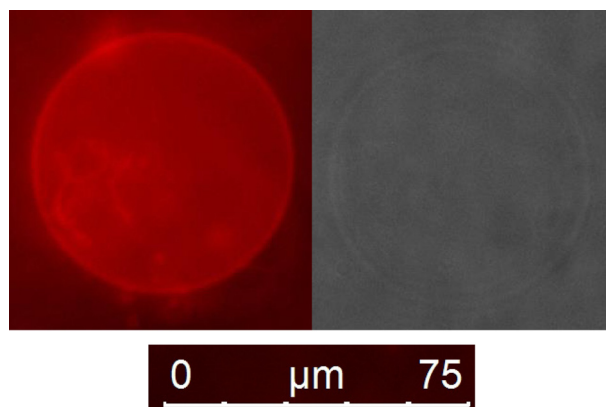


Figure 9: Giant unilamellar vesicle. GUVs composed of 3:1 (molar ratio) POPC/DPPS + Rhodamine-DOPE were prepared by electroformation, followed by visualization in fluorescence channel (left) and bright field (right).

To study formation or disappearance and changes in distribution of the bright (fluid/disordered) domains on the liposomes upon peptide addition, GUVs with POPC/DPPS 1:1 and 3:1 (molar ratios) were generated. Subsequently the lipid systems mimicking cancer cells were incubated with R-DIM-P-LF11-322 or DIM-LF11-318 for one hour and visualized under the microscope. The results for the 1:1 mixture in absence and presence of R-DIM-P-LF11-322 or DIM-LF11-318 can be seen in Figure 10. The first row shows 1:1 GUVs without peptide exhibiting an average size of $\sim 20 \mu\text{m}$. Linear (mainly) and circular domains indicate a macroscopic phase separation of gel phase DPPS and fluid phase POPC. However, upon addition of R-DIM-P-LF11-322 and DIM-LF11-318 the phase separation seems reduced and the linear domains disappear (Figure 10, second and third row, respectively), leaving only a few small circular bright domains on the GUVs. In the presence of the non-specific DIM-LF11-318 this effect seemed to be partially stronger, with larger remaining bright spots. So far, we do not have a simple explanation for the seemingly strong decrease of the bright fluid areas upon addition of peptides. In presence of both peptides the number of GUVs was decreased, indicating peptide induced destruction. The size of the GUVs was not significantly altered in presence of the peptides.

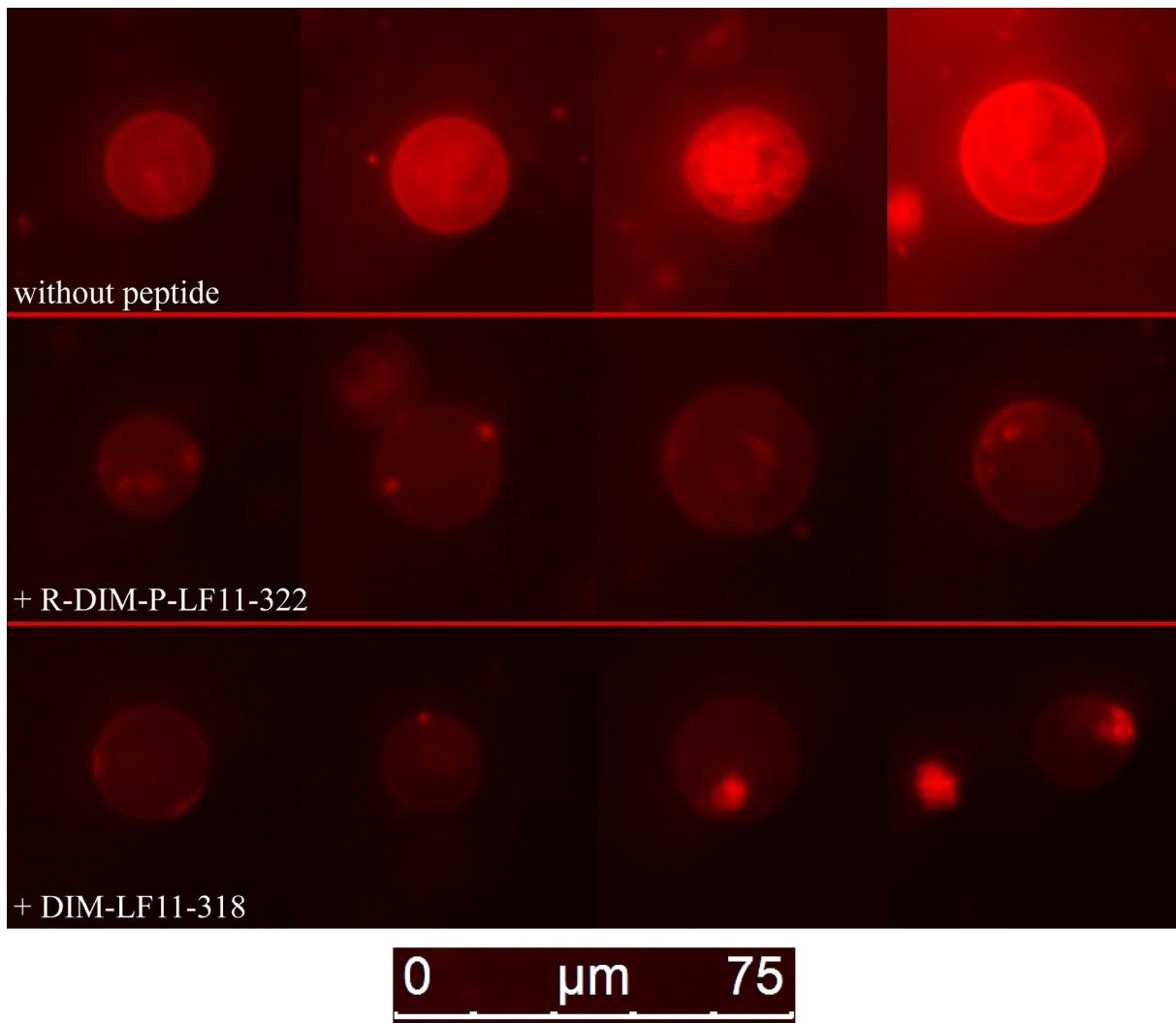


Figure 10: Giant unilamellar vesicles composed of 1:1 POPC/DPPS in absence and presence of R-DIM-P-LF11-322 and DIM-LF11-318. GUVs composed of 1:1 POPC/DPPS (molar ratio) + Rhodamine-DOPE were generated using electroformation. Visualization followed without peptide (1st row), in presence of R-DIM-P-LF11-322 (2nd row) or DIM-LF11-318 (3rd row) (50 μ M; 30 minutes incubation). Bright areas show domains of fluid lipids. Brightness and contrast were equally enhanced.

In Figure 11 studies with increased levels of PC (3:1 POPC/DPPS) are shown. Again the first row shows GUVs without any peptide, the second in presence of R-DIM-P-LF11-322 and the third in presence of DIM-LF11-318. With a higher amount of POPC the GUVs seemed to be larger than the one of the 1:1 mixture with an average size of $\sim 40 \mu\text{m}$. Again there were mainly linear bright and partially circular domains (last picture, first row) visible which disappeared upon peptide addition. However, in contrary to the mixture 1:1, more bright (fluid) domains remained. Bright spots were seen in presence of R-DIM-P-LF11-322 (second row, Figure 11). Sometimes in presence of both peptides also fusion of liposomes occurred (last picture, second and third row) and the number of GUVs in presence of both membrane active peptides decreased indicating a destructive effect. Especially at the contact regions of the fused GUVs brightness was amplified, indicating increased lateral diffusion of fluid lipids

to these areas. The fusion may have been also due to connection or crosslinking by the peptides, therefore bright domains may also be peptide interaction positions. Furthermore, studies were performed using POPS being fluid at RT in 1:1 and 3:1 (molar ratios) mixtures (DPPC/POPS). Data are not shown here due to the fact that the staining was very weak, probably due to repulsion between the negatively charged lipid POPS and the negatively charged Rhodamine.

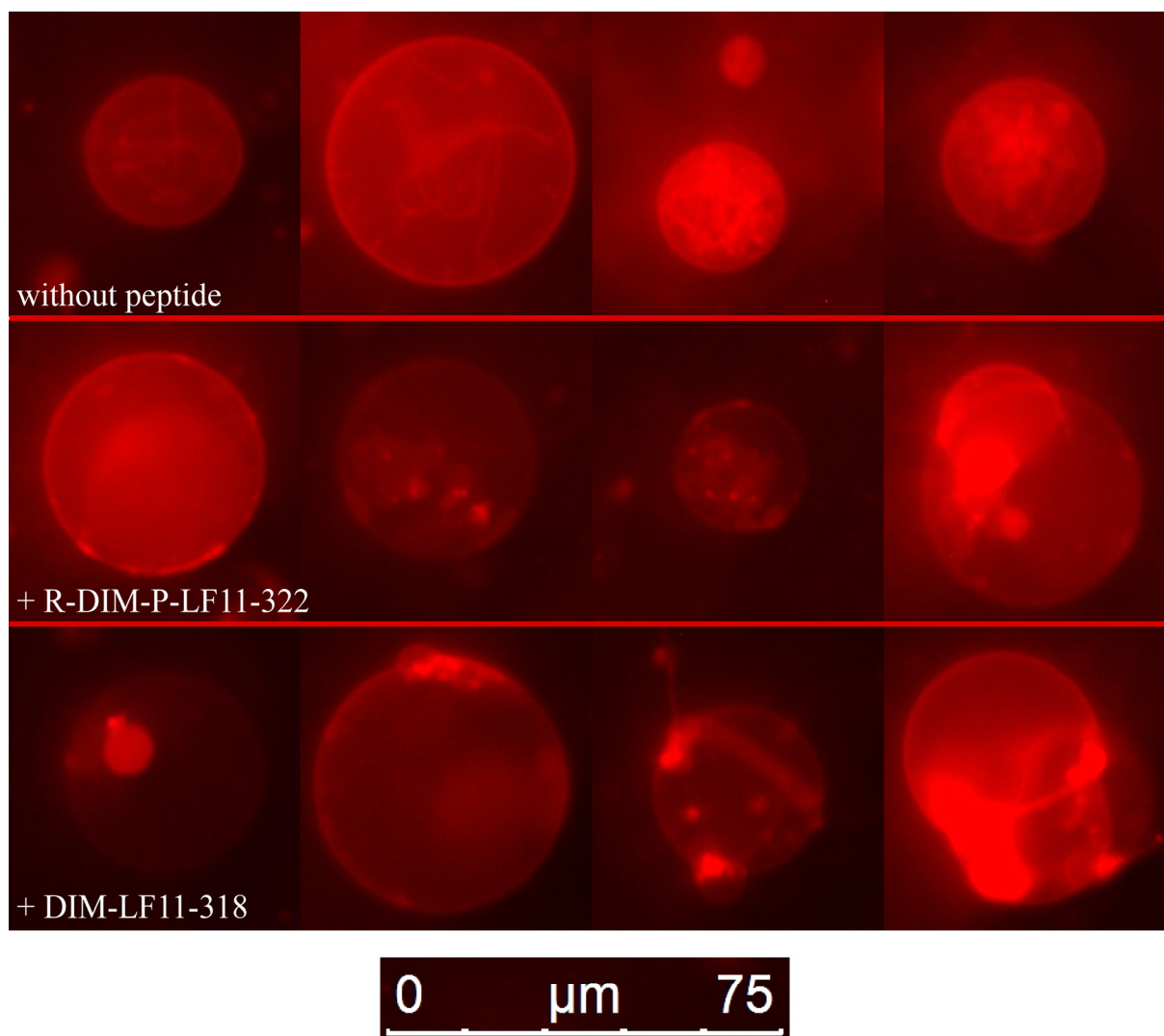


Figure 11: Giant unilamellar vesicles composed of 3:1 POPC/DPPS in absence and presence of R-DIM-P-LF11-322 and DIM-LF11-318. GUVs composed of 3:1 POPC/DPPS (molar ratio) + Rhodamine-DOPE were generated by electroformation. Visualization without peptide (1st row), in presence of R-DIM-P-LF11-322 (2nd row) or DIM-LF11-318 (3rd row) (50 µM; 30 minutes incubation) are presented. Bright areas show domains of fluid lipids. Brightness and contrast were equally enhanced.

3.2 Impact of cholesterol on peptide activity and interaction

3.2.1 Cholesterol distribution in cancer and non-cancer membranes – Cholesterol is present in both types of plasma membranes

The plasma membrane of a cell is very complex. Besides proteins, diverse phospholipids and glycolipids it contains also cholesterol, which controls the permeability of the bilayer and acts as stabilizer and decreasing its fluidity [50]. The plasma membrane comprises the highest amount of cholesterol followed by endosomes, the Golgi apparatus and mitochondria [61]. Indeed staining of cholesterol of normal human dermal fibroblasts NHDF with the dye filipin (blue) revealed cholesterol located to the plasma membrane and surrounding the nucleus (red, PI) with fine dots (blue) approaching the plasma membrane (see Figure 12, upper row), which resembles mitochondria and probably endosomes. Stronger staining of the plasma membrane was achieved for NHDF which were not fixed (data not shown). In contrast, the melanoma cells A375 showed a strong staining of plasma membrane cholesterol (see Figure 12, lower row). Furthermore, the melanoma cells showed strong intracellular cholesterol contents different to that of NHDF, mainly one large spot located at one side of the nucleus was seen, a staining being typical for the Golgi [62]. A confirmation is given in 3.3 by filipin co-staining with a Golgi marker in A375 (see Figure 23).

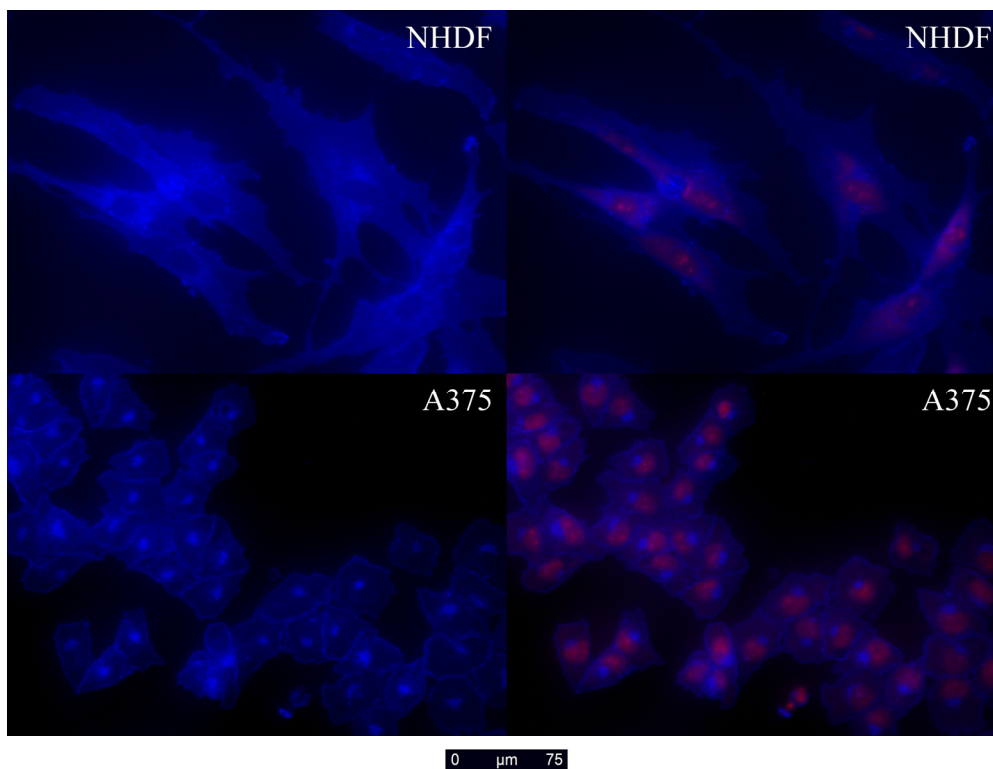


Figure 12: Distribution of cholesterol in membranes of NHDF and A375. Normal human dermal fibroblasts (NHDF; upper row) and melanoma cells (A375; lower row) were fixed. Cholesterol was stained with filipin (blue) and nucleus with PI (red). Overlay on the right side.

As elevated in 1.4, cholesterol is also reported to have impact on the membrane interaction of peptides. Matsuzaki et al. [35] reported that the presence of cholesterol reduced the effects of magainin on membranes. In the following section a possible difference in the effect of cholesterol on the cancer specific R-DIM-P-LF11-322 and the non-specific DIM-LF11-318 was studied.

3.2.2 Model system studies

- DSC – Different impact of cholesterol on peptide activity and interaction

To elevate potential changes in the interaction of peptides with membranes when cholesterol is present cancer mimicking liposomes containing DPPC and DPPS without cholesterol (1:1:0 molar ratio) and stepwise increasing amounts of cholesterol like 1:1:0.25, 1:1:0.5, 1:1:0.75 (molar ratios) were studied in absence and presence of R-DIM-P-LF11-322 or DIM-LF11-318 (lipid to peptide ratio 25:1). This time the mixtures were prepared again by freeze and thaw to yield liposomes with homogeneously distributed lipids (Figure 13, Table 5). A second set of experiments however included the preparation of the same mixtures without freeze and thaw to yield inhomogeneous lipid distribution and thereby formation of lipid domains, to study a possible impact of domains on the peptide activity (Figure 14, Table 5). As already described under 3.1.2 (DSC) the 1:1:0 mixture prepared with freeze and thaw showed one phase

transition with a ΔH_m of 10.6 kcal/mol, at a T_m of 46.1 °C and a half width of 2.59 °C. Addition of both peptides resulted in a decrease of the main transition enthalpy, R-DIM-P-LF11-322 by 20%, DIM-LF11-318 by 50%. A more homogenous phase transition was induced by both peptides indicated by a $T_{1/2}$ reduction of 1.5 °C when R-DIM-P-LF11-322 and 1.2 °C when DIM-LF11-318 was added. While there was a shift to a lower transition temperature by 1.9 °C when R-DIM-P-LF11-322 was present, addition of DIM-LF11-318 led to an increase of T_m by 1.5 °C. This indicates a main interaction of R-DIM-P-LF11-322 with the cancer specific marker DPPS leaving DPPC which is present in cancer and non-cancer membranes unaffected. DIM-LF11-318 seemed to interact with both lipids DPPC and DPPS and causing a shift to a higher T_m .

In the thermograms of the mixtures in absence of peptide in (Figure 13) it can be seen that with increasing levels of cholesterol the phase transition got decreased which is conform with literature reporting that cholesterol increases the fluidity of lipids in the gel phase [63]. The 1:1:0.25 mixture showed one phase transition at 44.8 °C with a $T_{1/2}$ of 2.87 °C. The phase transition decreased by 15% (from 7.7 kcal/mol to 6.6 kcal/mol) when R-DIM-P-LF11-322 was added, while the phase transition temperature remained almost the same. Compared to the effect of R-DIM-P-LF11-322 on 1:1:0 liposomes (25% reduction), the peptide seemed to exhibit a weaker effect when cholesterol was present. There was an increase of the cooperativity when R-DIM-P-LF11-322 was added. This was indicated by the decrease of the transition half width (from 2.87 °C to 1.4 °C). The effect of DIM-LF11-318 in the presence of 11 mol% cholesterol in contrast was highly increased to that in absence. There was a splitting into three broad phase transitions with a decrease of the phase transition enthalpy by 70% which indicated a strong destabilization of the gel phase of the mixture. Taking in account that PS only comprises 45 mol% of the mixture, DIM-LF11-318 is thereby proven to also perturb the DPPC proportion of the mixture. All analyzed parameters are listed in Table 5 for a better overview. The three transitions occurred at a temperature of about 36.5 °C, 45.8 °C and 51.7 °C. An increase of the cholesterol content up to 20 mol% (1:1:0.5) further decreased the effect of R-DIM-P-LF11-322. Even though, a splitting into two domains - a peptide affected domain of only 30% with a T_m of 40.2 °C and a remaining peptide unaffected domain (70%) with a transition temperature of 46.0 °C, as in absence of peptide, occurred. In contrary, the effect of DIM-LF11-318 was further enhanced by the increase of cholesterol in 1.1:0.5 and 1:1:0.75, where no phase transition could be observed anymore. For determination of the parameters the peaks were deconvoluted.

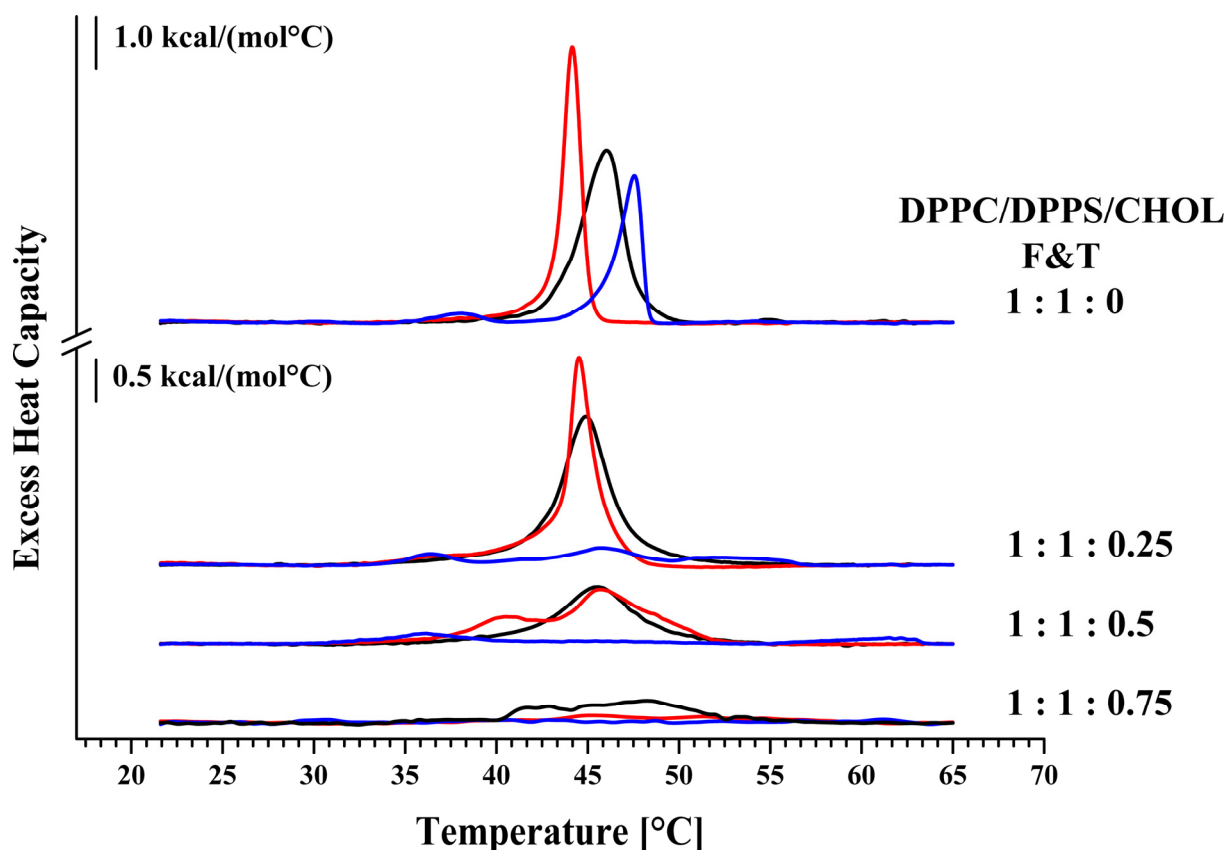


Figure 13: DSC thermograms in absence and presence of R-DIM-P-LF11-322 or DIM-LF11-318 of freeze and thaw preparations of DPPC/DPPS liposomes with increasing amounts of cholesterol. Liposomes containing DPPC/DPPS/Cholesterol in different molar ratios (1:1:0, 1:1:0.25, 1:1:0.5 and 1:1:0.75) were prepared using the freeze and thaw method. DSC was used to determine the influence of higher amounts of cholesterol on the phase behavior and on peptide effects. Black represents measurements without peptide; red corresponds to measurements in presence of R-DIM-P-LF11-322 and blue in presence of DIM-LF11-318. For clarity, the DSC curves were displayed on the ordinate by an arbitrary increment. For analyzed data see Table 5.

As elevated, all mixtures were also prepared without freeze and thaw approaching physiologically relevant cell mimics exhibiting domains. The inhomogeneous distribution without freeze and thaw preparation is demonstrated in Figure 14 by splitting of the phase transition of the 1:1:0 mixture in two peaks. Namely, one at lower temperature that can be assigned to a PC rich fraction (43.7 °C) and a second broader one at higher temperatures (45.6 °C) that can be assigned to several PS enriched fractions ($T_{1/2}$ 5.27 °C). Interestingly, the effect of R-DIM-P-LF11-322 was independent of homogeneity of the lipid distribution, exhibiting the same effect as with freeze and thaw. DIM-LF11-318 however exhibited a slightly increased effect in the presence of domains with a reduction of the enthalpy by about 80% instead of 50% in the homogenous mixture 1:1:0. Also of interest is that the homogenizing effect of the freeze and thaw preparation decreased with increasing amounts of cholesterol, 1:1:0.25 did not exhibit any visible phase separation in DPPC and DPPS enriched liposomes anymore. However, the cooperativity of the transition was still decreased ($T_{1/2}$ 2.9 to 4.2 °C, nearly doubling). The 1:1:0.5 and 1:1:0.75 mixtures prepared by freeze and thaw or

non freeze and thaw were comparable in their homogeneity.

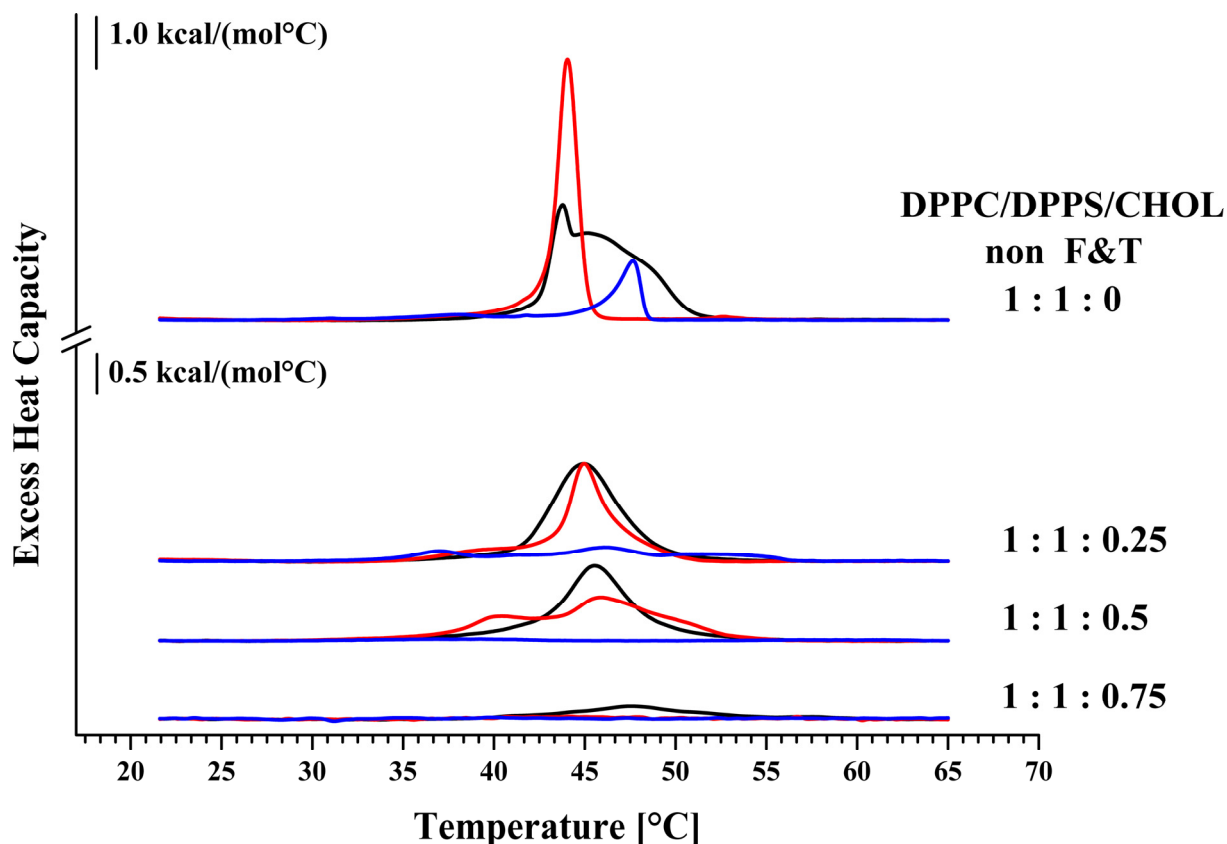


Figure 14: DSC thermograms in absence and presence of R-DIM-P-LF11-322 or DIM-LF11-318 of DPPC/DPPS liposomes with increasing amounts of cholesterol without using freeze and thaw for preparation. Liposomes containing DPPC/DPPS/Cholesterol in different molar ratios (1:1:0, 1:1:0.25, 1:1:0.5 and 1:1:0.75) were prepared without using freeze and thaw. DSC was used to determine the influence of higher amounts of cholesterol on the phase behavior and on peptide effects. Black represents measurements without peptide; red corresponds to measurements in presence of R-DIM-P-LF11-322 and blue in presence of DIM-LF11-318. For clarity, the DSC curves were displayed on the ordinate by an arbitrary increment. For analyzed data see Table 5.

Summing up, the effect of R-DIM-P-LF11-322 with increasing cholesterol ratios was comparable with both methods. This reveals independence of its effect on phase separated domains, but a decreasing effect of cholesterol on its capability of membrane perturbation was shown. On the contrary the effect of DIM-LF11-318 was even strengthened in its perturbation efficiency and furthermore exhibited a slightly increased effect in the presence of domains.

Table 5: Thermodynamic parameters of freeze and thaw (first row) and non freeze and thaw (second row) preparations of liposomes of DPPC/DPPS/Cholesterol 1:1:0, 1:1:0.25, 1:1:0.5 and 1:1:0.75 (molar ratios) in absence and presence of R-DIM-P-LF11-322 or DIM-LF11-318. Deconvolution was used for analyses of data of overlapping phase transitions. For thermograms see Figure 13 (freeze and thaw) and Figure 14 (non freeze and thaw).

	ΔH_m [kcal/mol]	T_m [°C]	$T_{1/2}$ [°C]
DPPC/DPPS/Cholesterol (1:1:0)			
<i>freeze and thaw</i>	10.6	46.1	2.59
<i>non freeze and thaw</i>	11.4 (0.6/10.8)	43.7/45.6	0.39/5.27
+R-DIM-P-LF11-322			
<i>freeze and thaw</i>	8.2	44.2	1.07
<i>non freeze and thaw</i>	8.7	44.0	1.20
+ DIM-LF11-318			
<i>freeze and thaw</i>	5.2	47.6	1.43
<i>non freeze and thaw</i>	2.3	47.7	1.46
DPPC/DPPS/Cholesterol (1:1:0.25)			
<i>freeze and thaw</i>	7.7	44.8	2.87
<i>non freeze and thaw</i>	6.2	44.9	4.20
+R-DIM-P-LF11-322			
<i>freeze and thaw</i>	6.6	44.5	1.40
<i>non freeze and thaw</i>	4.8	44.9	2.28
+ DIM-LF11-318			
<i>freeze and thaw</i>	2.0 (0.4/1.1/0.5)	36.5/45.8/51.7	3.05/4.35/5.97
<i>non freeze and thaw</i>	2.0 (0.5/1.0/0.5)	36.9/46.3/51.4	3.48/4.98/5.87
DPPC/DPPS/Cholesterol (1:1:0.5)			
<i>freeze and thaw</i>	4.2	45.5	4.57
<i>non freeze and thaw</i>	5.3	45.6	3.95
+R-DIM-P-LF11-322			
<i>freeze and thaw</i>	5 (1.3/3.7)	40.2/46.0	3.82/4.85
<i>non freeze and thaw</i>	4.9 (1.6/3.3)	40.1/46.6	5.09/5.31
+ DIM-LF11-318			
<i>freeze and thaw</i>	1.4 (0.7/0.3/0.4)	36.1/45.3/61.5	4.73/4.59/5.43
<i>non freeze and thaw</i>	0.3 (0.2/0.1)	39.3/56.9	8.12/3.42
DPPC/DPPS/Cholesterol (1:1:0.75)			
<i>freeze and thaw</i>	2.5	47.8	15.42
<i>non freeze and thaw</i>	1.4	47.3	6.31
+R-DIM-P-LF11-322			
<i>freeze and thaw</i>	1.2	~ 42.0	10.95
<i>non freeze and thaw</i>	0.3	40.8	4.37
+ DIM-LF11-318			
<i>freeze and thaw</i>	-	-	-
<i>non freeze and thaw</i>	-	-	-

– Tryptophan quenching – Impact of cholesterol on penetration depth of peptides

Depending on the polarity of the environment of the aromatic amino acid tryptophan, the emission wavelength, when excited with UV-light, changes. This alteration as well as fluorescence quenching by acryl amide can be used to study localization of tryptophan in different environments, as for example membranes. A decrease of the emission wavelength $\lambda_{em,max}$ of 355 nm (R-DIM-P-LF11-322) or 354 nm (DIM-LF11-318) in polar environment, called blue shift, in combination with a decrease of the Stern-Volmer constant K_{SV} as a consequence of less access to the quencher, indicates interaction and/or penetration of the peptide tryptophan molecules with/in the non-polar lipid membrane. The emission spectra of the two tryptophan molecules of R-DIM-P-LF11-322 and the four of DIM-LF11-318 were analyzed in PBS, in presence of non-cancer mimicking liposomes composed of DPPC or DPPC/DPPS/Cholesterol 5:0:1 (molar ratio), as well as in presence of cancer cell mimicking systems DPPC/DPPS/Cholesterol with molar ratios of 1:1:0, 1:1:0.25, 1:1:0.5, 1:1:0.75, 3:1:0 and 3:1:1 or pure DPPS liposomes (lipid to peptide ratio 25:1).

The emission spectrum of R-DIM-P-LF11-322 in PBS exhibited a maximum ($\lambda_{em,max}$) at 355 nm with a K_{SV} of about $23.8 M^{-1}$ indicating no peptide aggregation (see Figure 15). Also DIM-LF11-318, which showed an emission wavelength maximum at 354 nm and a K_{SV} of $23.5 M^{-1}$, does not seem to be aggregated in PBS (see Figure 16). Tryptophan emission of R-DIM-P-LF11-322 in presence of the healthy cell mimicking DPPC/DPPS/Cholesterol liposomes 5:0:1 or pure DPPC liposomes did not exhibit any significant wavelength shift, the K_{SV} just slightly decreased to a value of $14.8 M^{-1}$ (DPPC) and $14.0 M^{-1}$ (5:0:1).

Although harming healthy cells *in vitro* in presence of the healthy cell mimics there was no significant change of the $\lambda_{em,max}$ of DIM-LF11-318. Again the K_{SV} decreased to a value of $14.5 M^{-1}$ in presence of DPPC liposomes and to $14.3 M^{-1}$ in presence of 5:0:1 liposomes. All data of tryptophan spectra measurements are listed in Table 6.

In presence of all cancer mimics a blue shift (decrease) of the emission wavelength of the tryptophan molecules of R-DIM-P-LF11-322 by 13 to 22 nm occurred. This indicates that the tryptophan molecules reside in a less polar environment as compared to solution, hence interacting with these model membranes (see Figure 15 and Table 6). Also the K_{SV} decreased to 1/4 - 1/8 of the value of R-DIM-P-LF11-322 in PBS. Although 50% less DPPS is present in 1:1:0 liposomes the K_{SV} and the blue shift were almost the same as in presence of pure DPPS liposomes. The strongest blue shift as well as the lowest K_{SV} were seen in presence of 1:1:0.25 and 1:1:0.5 liposomes, while in presence of 1:1:0.75 the values were comparable with the ones in presence of 1:1:0 or pure DPPS liposomes. The results revealed that presence

of cholesterol did not lead to a significant difference. A higher amount of DPPC (3:1:0 and 3:1:1) led to a less massive blue shift of the tryptophan emission maximum of R-DIM-P-LF11-322 and to a less massive decrease of the K_{SV} but it still was significant.

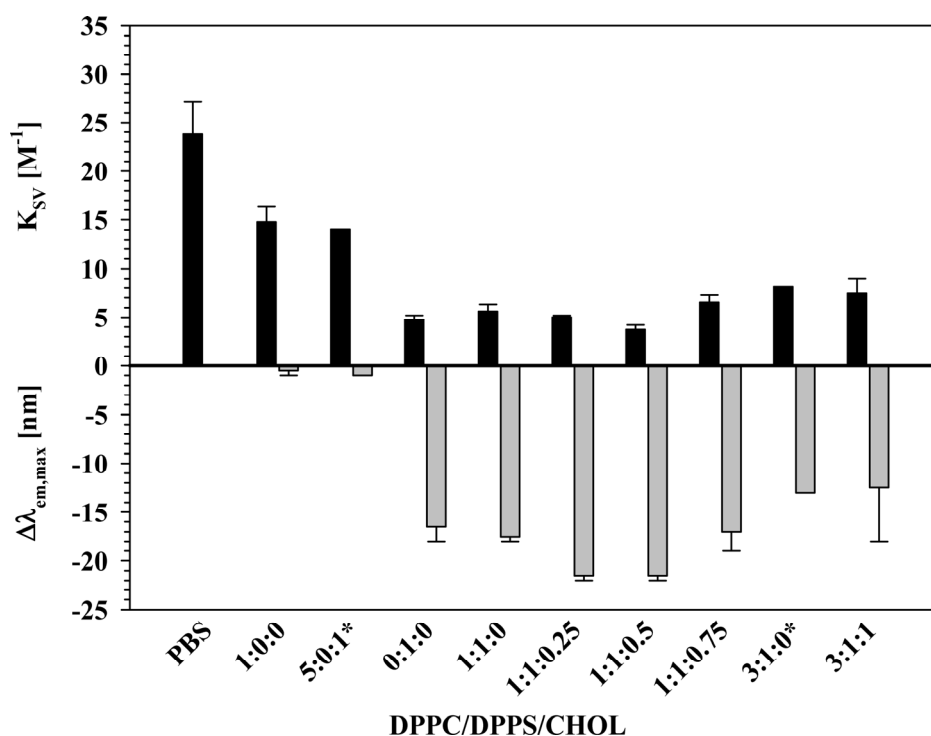


Figure 15: Tryptophan quenching of R-DIM-P-LF11-322 for determination of peptide solubility and membrane penetration depth. The Stern-Volmer quenching constants (K_{SV}) and the changes of the maximum of the emission spectra ($\Delta\lambda_{em,max}$, gray) of the peptide in PBS (355 nm) in comparison to different lipid environments (pure DPPC, pure DPPS, DPPC/DPPS/Cholesterol 1:1:0, 1:1:0.25, 1:1:0.5, 1:1:0.75, 3:1:0, 3:1:1 and 5:0:1 (molar ratios) liposomes) were determined with a lipid to peptide ratio 25:1. Acryl amide was used at different concentrations to determine the quenching constant by analyzing the emission spectrum (black). For analyzed data see Table 6. (* marks single determinations)

Also the emission spectrum of DIM-LF11-318 significantly changed in presence of cancer mimicking liposomes (see Figure 16). The strongest blue shift was seen in presence of pure DPPS ($\Delta\lambda_{em,max} = 13.5$ nm) indicating strongest interaction with pure DPPS. Also the K_{SV} was low. Less blue shift was seen in presence of 1:1:0 and 3:1:0 liposomes. A slightly stronger blue shift was shown in presence of 1:1:0.25 and 1:1:0.5 liposomes, while there was hardly any change in the emission maximum when 1:1:0.75 or 3:1:1 liposomes were present.

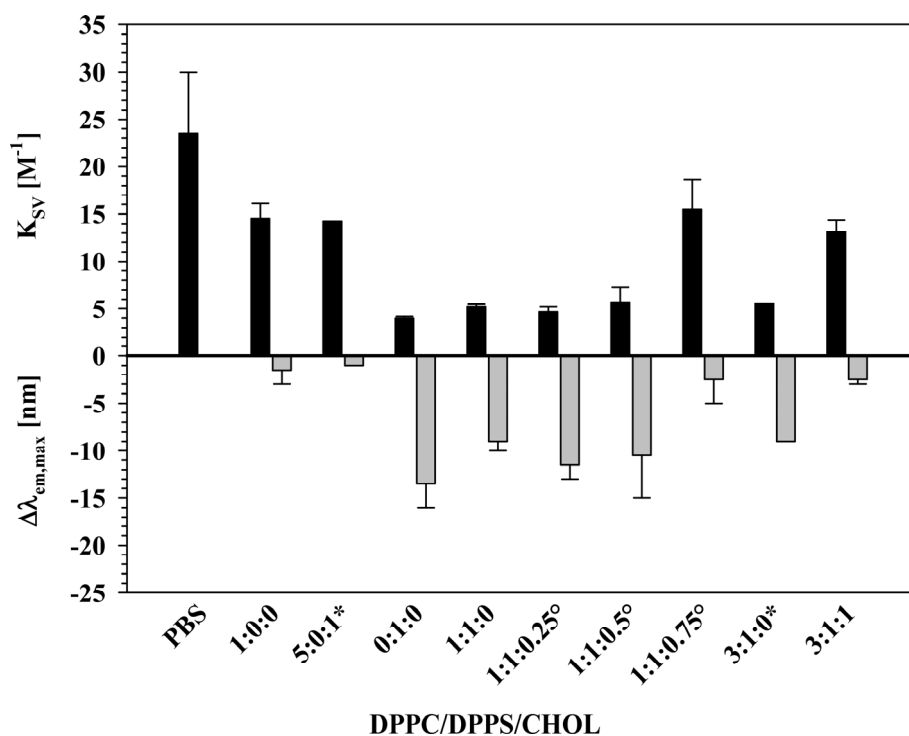


Figure 16: Tryptophan quenching of DIM-LF11-318 for determination of peptide solubility and membrane penetration depth. The Stern-Volmer quenching constants (K_{SV}) and the changes of the emission spectrum ($\Delta\lambda_{em,max}$, gray) of the peptide in PBS (354 nm) in comparison to different lipid environments (pure DPPC, pure DPPS, DPPC/DPPS/Cholesterol 1:1:0, 1:1:0.25, 1:1:0.5, 1:1:0.75, 3:1:0, 3:1:1 and 5:0:1 (molar ratios) liposomes) were determined with a lipid to peptide ratio 25:1. Acryl amide was used at different concentrations to determine the quenching constant by analyzing the emission spectrum (black). For analyzed data see Table 6. (* marks single determinations; ° marks emission spectra with more than one emission maximum)

However, the maxima of the emission wavelengths of the 1:1:0, 1:1:0.25, 1:1:0.5 and also 1:1:0.75 measurements in presence of DIM-LF11-318 were hard to determine, due to the fact that the emission spectra showed many peaks. This indicated that there were at least two different environments for the tryptophan molecules. Some were in solution, while some aggregated or located in the lipid membrane interface. Furthermore, in the DSC measurements strong perturbation and destruction of these mixtures had been observed in presence of DIM-LF11-318, which might also hinder a proper analysis.

Table 6: Mean values of Stern-Volmer quenching constants (K_{SV}) and changes of maxima of emission wavelengths ($\Delta\lambda_{em,max}$) of R-DIM-P-LF11-322 and DIM-LF11-318 in DPPC, DPPS, DPPC/DPPS/Cholesterol 1:1:0, 1:1:0.25, 1:1:0.5, 1:1:0.75, 3:1:0, 3:1:1 and 5:0:1 (molar ratios) membranes with a lipid to peptide molar ratio of 25:1 in comparison to values of the peptide in PBS. For graphical depiction of mean values with standard deviation see Figure 15 (R-DIM-P-LF11-322) and Figure 16 (DIM-LF11-318).

	R-DIM-P-LF11-322		DIM-LF11-318	
	$\Delta\lambda_{em,max}$ [nm]	K_{SV} [M^{-1}]	$\Delta\lambda_{em,max}$ [nm]	K_{SV} [M^{-1}]
PBS	(355)	23.8	(354)	23.5
<i>Non-cancer mimics</i>				
DPPC/DPPS/CHOL 1:0:0	-0.5	14.8	-1.5	14.5
DPPC/DPPS/CHOL 5:0:1	-1.0	14.1	-1.0	14.3
<i>Cancer mimics</i>				
DPPC/DPPS/CHOL 0:1:0	-16.5	4.8	-13.5	4.0
DPPC/DPPS/CHOL 1:1:0	-17.5	5.6	-9.0	5.2
DPPC/DPPS/CHOL 1:1:0.25	-21.5	5.0	-11.5	4.7
DPPC/DPPS/CHOL 1:1:0.5	-21.5	3.7	-10.5	5.7
DPPC/DPPS/CHOL 1:1:0.75	-17.0	6.6	-2.5	15.5
DPPC/DPPS/CHOL 3:1:0	-13.0	8.1	-9.0	5.6
DPPC/DPPS/CHOL 3:1:1	-12.5	7.4	-2.5	13.1

In summary, it was shown that both peptides penetrate into cancer mimicking membranes, but not in non-cancer membranes. A linear or significant impact of cholesterol on the membrane penetration could not be observed, probably due to destruction of liposomes and the fact that the peptides exhibit more than one tryptophan complicating the analyses of the measurements. Due to this, the fact that the membrane lysing peptide DIM-LF11-318 showed less blue shift than R-DIM-P-LF11-322 was not interpreted as less membrane interaction.

- Zeta potential and size – Different impact of cholesterol on electrostatic and hydrophobic interactions of peptides with cancer membrane mimics

To determine if cholesterol has an influence on peptide activity zeta potential measurements were performed. As described under 3.1.2 (zeta potential) a change in the zeta potential indicates an electrostatic probably also hydrophobic interaction between the positive charges of the peptides and the negative charges of the lipid DPPS. The measurements were now performed with increasing cholesterol ratios with DPPC/DPPS/Cholesterol molar ratios 1:1:0, 1:1:0.25 and 1:1:0.5 in presence and absence of R-DIM-P-LF11-322, DIM-LF11-318 (lipid to peptide ratio 25:1) or $CaCl_2$ [1 mM]. Ca^{2+} was added as a reference for electrostatic interactions. The results of the measurements are shown in Figure 17 and Table 7. The zeta potentials of the 1:1:0, 1:1:0.25 and the 1:1:0.5 liposomes without peptide were in the range of - 50 mV to -57 mV. In presence of R-DIM-P-LF11-322 the zeta potential of liposomes with increasing cholesterol shifted from + 8 mV (1:1:0) to - 6 mV (1:1:0.25) to - 13 mV

(1.1:0.5). This might indicate a decreasing electrostatic interaction of the cancer specific peptide with increasing ratios of cholesterol. In contrary, the zeta potential values of the different liposomes with increasing amounts of cholesterol in presence of DIM-LF11-318 remained unaffected in the range of + 20 mV (1:1:0 and 1.1:0.25) to + 16 mV (1:1:0.5), indicating that membrane interaction of DIM-LF11-318 does not seem to be affected by cholesterol. The results also confirm the interpretation in 3.1.2 (zeta potential) that the first interactions of R-DIM-P-LF11-322 with the target membrane are electrostatic and those of DIM-LF11-318 are electrostatic and hydrophobic. This might be a hint for the non-specific interaction with non-cancer membranes of the latter. The exact values are listed in Table 7. For completeness also the zeta potential values of DPPC and DPPS liposomes with or without respective supplement (described in 3.1.2 zeta potential) are listed.

As in 3.1.2 (zeta potential) dynamic light scattering measurements were performed to determine whether there was a change in the size of the liposomes when peptides or CaCl_2 were added or not. Addition of the peptides led to a drastic increase in the size of the particles, indicating that there was aggregation after peptide addition. Ca^{+2} addition did not lead to an increase in size. The particles showed the same size as in absence of any supplement. The size measurements were only suitable for rough size approximations, due to the fact that measurements of highly polydisperse (size) samples are not completely reliable. So it was not possible to conclude exact size differences of two types of liposomes with different lipid compositions. However, it was possible to deduce that there were changes upon peptide addition. In general, a correlation of changes in the zeta potential and increase of the size could be seen.

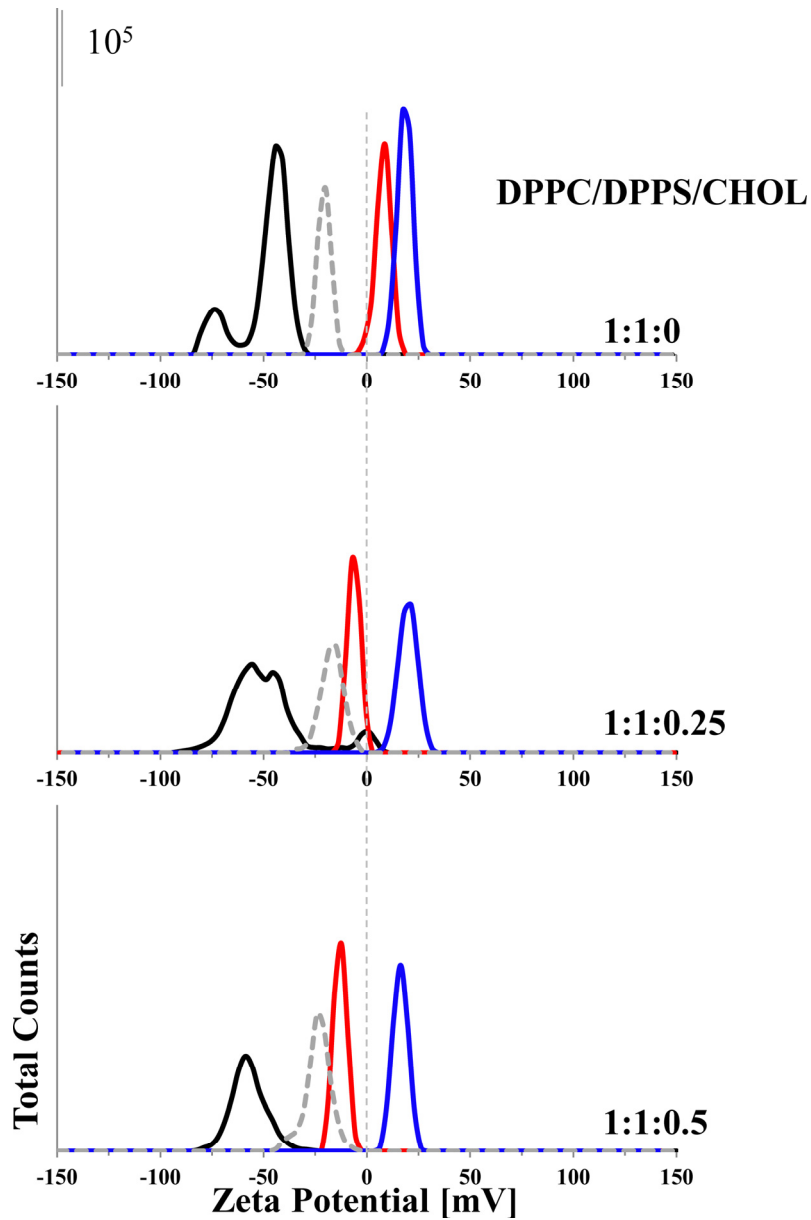


Figure 17: Zeta potential of liposomes with increasing amounts of cholesterol in presence and absence of R-DIM-P-LF11-322, DIM-LF11-318 or CaCl₂. The zeta potentials of DPPC/DPPS/Cholesterol liposomes containing different amounts of cholesterol ((1:1:0, 1:1:0.25 and 1:1:0.5) (molar ratios)) were determined in absence (black) and presence of R-DIM-P-LF11-322 (red), DIM-LF11-318 (blue) (lipid to peptide ratio 25:1) or CaCl₂ [1 mM] (dashed gray). Peptide or calcium addition reduced the negative zeta potential of the respective liposomes. This indicates an interaction of the peptides/calcium with the negatively charged liposome. In presence of cholesterol the effect of R-DIM-P-LF11-322 gets reduced, while DIM-LF11-318 remains unaffected. For analyzed data see Table 7.

Table 7: Zeta potential and size values of DPPC, DPPS or DPPC/DPPS/Cholesterol (1:1:0, 1:1:0.25 and 1:1:0.5; molar ratios) liposomes in absence and presence of R-DIM-P-LF11-322, DIM-LF11-318 or CaCl₂. (See also Figure 17) DPPC and DPPS values (gray) were listed for purpose of comparison and were discussed in 3.1.2 (zeta potential).

	Zeta potential [mV]	Size (z - average)/ Number mean* [nm]	Polydispersity Index (Pdi)
DPPC	- 0	180	0.22
+ R-DIM-P-LF11-322	+ 4	210	0.27
+ DIM-LF11-318	+ 5	160	0.13
+ CaCl ₂ (1 mM)	+ 10	170	0.13
DPPS	- 54	130	0.11
+ R-DIM-P-LF11-322	+ 2	250	0.52
+ DIM-LF11-318	+ 15	300	0.51
+ CaCl ₂ (1 mM)	- 29	160	0.16
DPPC/DPPS/Cholesterol (1:1:0)	- 49	70	0.56
+ R-DIM-P-LF11-322	+ 8	840	0.38
+ DIM-LF11-318	+ 18	200/640	0.28/n.d.
+ CaCl ₂ (1 mM)	- 21	90	0.71
DPPC/DPPS/Cholesterol (1:1:0.25)	- 49	100	0.09
+ R-DIM-P-LF11-322	- 6	860	0.54
+ DIM-LF11-318	+ 20	560	0.26
+ CaCl ₂ (1 mM)	- 17	110	0.20
DPPC/DPPS/Cholesterol (1:1:0.5)	- 57	130	0.08
+ R-DIM-P-LF11-322	- 13	790	0.61
+ DIM-LF11-318	+ 16	1200	0.47
+ CaCl ₂ (1 mM)	- 24	130	0.07

* z-average was taken when polydispersity index (Pdi) was below 0.5; number mean was taken when Pdi was above 0.5
n.d. not determined

- Giant unilamellar vesicles – Impact of cholesterol on peptide induced lipid distribution of GUVs

As described under 2.3.5 (GUVs) giant unilamellar vesicles were formed using the electroformation protocol. The red dye RhoDOPE was used to stain lipids in the disordered or fluid phase. For the determination of the potential influence of cholesterol on peptide effectivity different amounts of cholesterol were used in PC/PS mixtures. First mixtures composed of POPC/DPPS/Cholesterol (1:1:0.25, 1:1:0.5, 1:1:1 and 1:1:2; molar ratios) were studied.

Figure 18 shows fluorescence pictures of GUVs composed of POPC/DPPS/Cholesterol with increasing ratios of cholesterol in absence (first row) and presence of R-DIM-P-LF11-322 (second row) or DIM-LF11-318 (third row) with increasing ratios of cholesterol (30 min peptide incubation).

POPC/DPPS/Cholesterol (1:1:0.25) GUVs mimicking cancer cells exhibited an average size of ~ 30 μm (first column, first image). Some destroyed GUVs could be observed (not shown).

However, intact vesicles of this mixture showed phase separation with mainly circular liquid disordered or fluid domains as bright areas on their surface (see Figure 18). Upon peptide addition the number of GUVs decreased, probably due to destruction by the peptide. Furthermore, they got smaller. In presence of R-DIM-P-LF11-322 the GUVs showed an average size of $\sim 20 \mu\text{m}$ or $\sim 10 \mu\text{m}$. No distorted vesicles were seen which may be due to the fact that those were an easier target for R-DIM-P-LF11-322 and therefore have been destroyed already. When R-DIM-P-LF11-322 was added a few bright spots occurred (see Figure 18). This again indicated protrusion at these parts. After 30 minutes incubation in presence of DIM-LF11-318 the average size of the GUVs was $\sim 10 \mu\text{m}$. Just a small part of the GUVs showed liquid disordered domains. These results showed that both peptides interact with the cancer cell mimic and change the lipid distribution/fluidity.

A higher amount of cholesterol (1:1:0.5) led to GUVs which exhibited an average size of $40 \mu\text{m}$ or $20 \mu\text{m}$ (two main sizes). More linear domains were seen in this mixture. Again the addition of R-DIM-P-LF11-322 led to a decrease in size and disappearance of the linear domains. Interestingly, fused GUVs were seen suggesting that the peptide probably links the GUVs by binding to at least two. Furthermore, a few bright domains were seen. Addition of DIM-LF11-318 led to a decrease in size (average size $10 \mu\text{m}$). Linear domains disappeared, instead bright protrusions and sometimes also fusion of the GUVs appeared (not shown). The size of 1:1:1 GUVs was diverse. There were some with a size of about $60 \mu\text{m}$, others with $30 \mu\text{m}$ or $10 \mu\text{m}$. Linear domains were seen but mainly the GUVs were stained homogeneously. Upon peptide addition GUVs reached a maximal size of $30 \mu\text{m}$. Again linear domains disappeared and one bright cluster remained. In presence of both peptides hardly any GUV was seen, again indicating that the peptides interact with the mimic. In presence of DIM-LF11-318 sometimes aggregation occurred as well as in number varying bright domains.

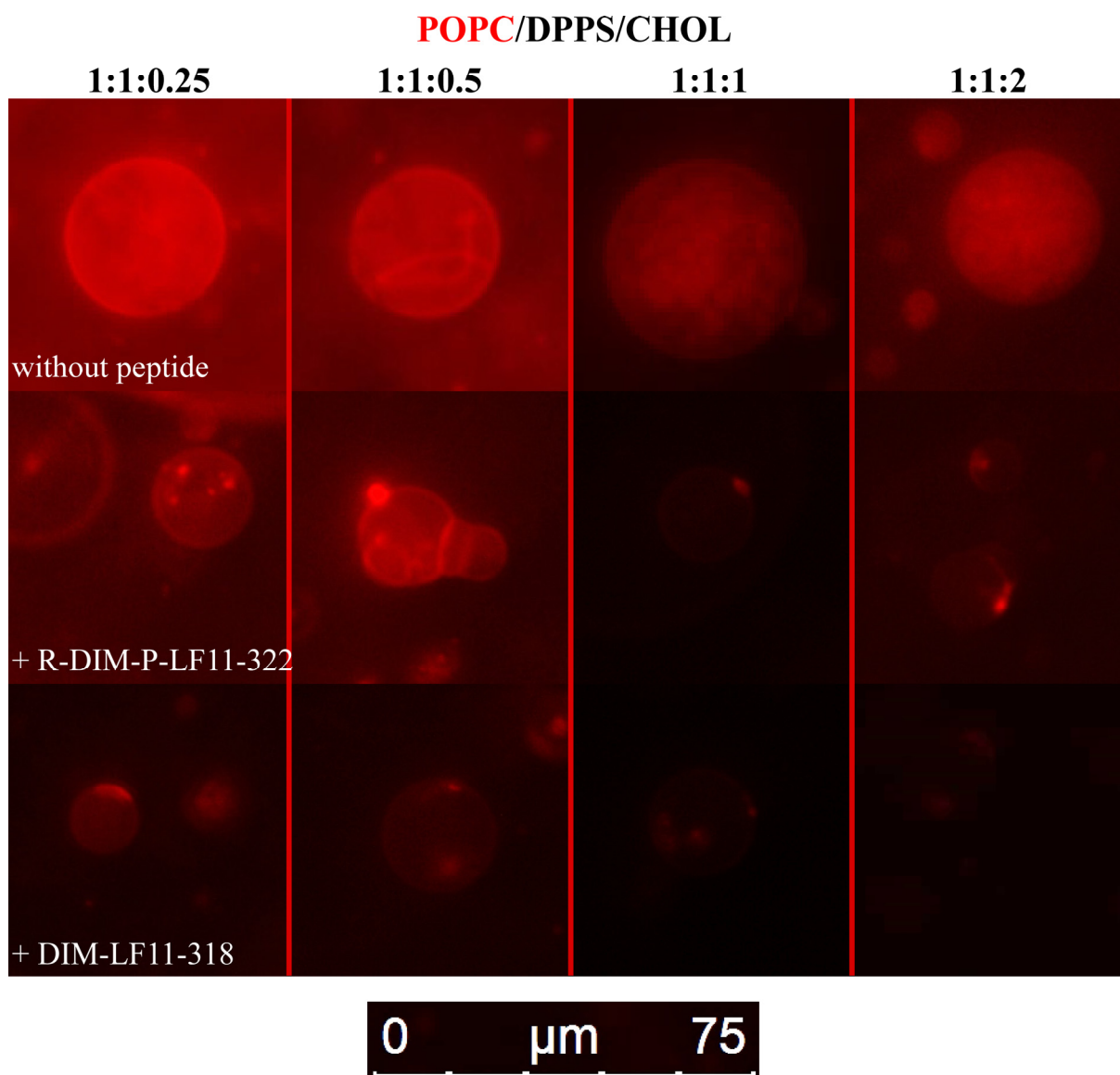


Figure 18: Giant unilamellar vesicles of POPC/DPPS/Cholesterol with increasing amounts of cholesterol in absence and presence of R-DIM-P-LF11-322 and DIM-LF11-318. GUVs consisting of POPC/DPPS/Cholesterol (1:1:0.25, 1:1:0.5, 1:1:1 and 1:1:2 molar ratios) + Rhodamine-DOPE were generated using electroformation. Visualization followed in absence of peptides (1st row), in presence of R-DIM-P-LF11-322 (2nd row) or DIM-LF11-318 (3rd row) (50 μM; 30 minutes). Bright areas show domains of fluid lipids. Brightness and contrast were equally enhanced.

Analyzed GUVs with the highest amount of cholesterol (1:1:2) could reach a size of 20 μm. No linear but rather punctual domains were seen. Addition of R-DIM-P-LF11-322 led to aggregation of the GUVs and bright spots developed. Also DIM-LF11-318 addition led to fusion and to the development of bright domains. Summarizing, different amounts of cholesterol led to different sizes and domain formation in GUVs without peptides. The 1:1:1 mixture resulted in largest GUVs, the 1:1:2 mixture was comparable with 1:1:0.25. Upon peptide addition instead of linear domains bright protrusions were seen, indicating that there was a change in lipid distribution. Furthermore, the average size was decreased in presence of both peptides as well as the staining intensity abated. With increasing amounts of cholesterol

no significant changes in the effectivity of peptides were seen except for fusion which occurred sometimes upon peptide addition when at least 20 mol% cholesterol (1:1:0.5) were present. Furthermore the intensity decreased.

Additionally, GUVs were generated with DPPC/POPS/Cholesterol 1:1:0.25, 1:1:0.5, 1:1:1 and 1:1:2 (molar ratios). The potential target for the peptides, PS, is now present in the fluid phase. Again GUVs were visualized in absence and presence of R-DIM-P-LF11-322 or DIM-LF11-318. GUVs of 1:1:0.25 and 1:1:0.5 needed to be analyzed immediately after peptide addition, due to the strong destruction capability of the peptides on these mixtures.

Fluorescence of GUVs of 1:1:0.25 or 1:1:0.5 was weak and therefore hardly detectable in absence of R-DIM-P-LF11-322 or DIM-LF11-318 (see Figure 19), but they were seen in bright field (Figure 20). 1:1:0.25 GUVs had an average size of 20 μm . Weak staining was probably due to repulsion between the negatively charged Rhodamine and the negatively charged POPS. It seemed like there was a homogenous distribution of fluid or disordered domains. It was the same for the 1:1:0.5 GUVs which reached a slightly higher average size (40 μm). Some of the 1:1:0.25 GUVs without any supplement had an oval shape instead of a spherical one. Upon addition of R-DIM-P-LF11-322 intensity of the domains of the GUVs was significantly increased. With an average size of 20 μm many strongly stained domains were seen. There were hardly any GUVs left and as mentioned before after 30 minutes no vesicles were found. Addition of DIM-LF11-318 also led to all over the vesicle distributed bright domains. Furthermore, some GUVs were fused to others (see Figure 19). Both peptides showed strong effects on the GUVs but the effect on the 1:1:0.5 mixture were even stronger. Only clumps were seen. Without any supplement the average size of the vesicles was 40 μm . Sometimes there were GUVs in one another but again the staining of the GUVs was very weak in absence of peptides.

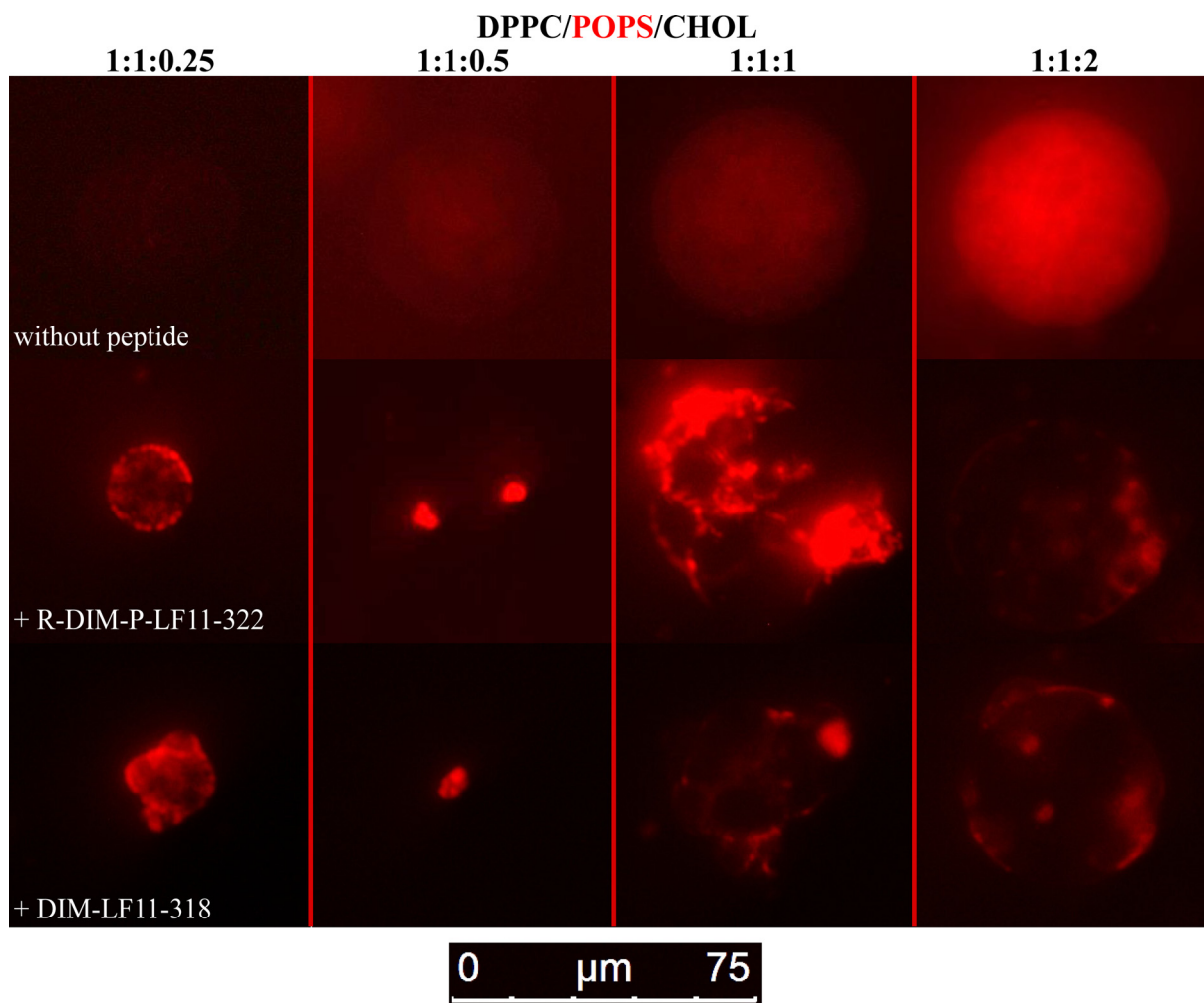


Figure 19: Giant unilamellar vesicles of DPPC/POPS/Cholesterol with increasing amounts of cholesterol in absence and presence of R-DIM-P-LF11-322 and DIM-LF11-318. GUVs consisting of DPPC/POPS/Cholesterol (1:1:0.25, 1:1:0.5, 1:1:1 and 1:1:2 molar ratios) + Rhodamine-DOPE were generated using electroformation. Visualization followed in absence of peptides (1st row), in presence of R-DIM-P-LF11-322 (2nd row) or DIM-LF11-318 (3rd row) (50 μM). Peptide incubation for 1:1:1 and 1:1:2 was 30 minutes, 1:1:0.25 and 1:1:0.5 were visualized immediately due to strong destruction. Bright areas show domains of fluid lipids. Brightness and contrast were equally enhanced for GUVs in presence of peptides. Without any peptide brightness was increased stronger.

The 1:1:1 GUVs exhibited the largest size. Most of them had an average size of 60 μm but there were even some with 100 μm. Again GUVs were seen with smaller GUVs trapped inside. In contrast to 1:1:0.25 and 1:1:0.5 peptide incubation was 30 minutes. The effect of the peptides on GUVs with high amounts of cholesterol (1:1:1 and 1:1:2) was not that strong. Upon R-DIM-P-LF11-322 or DIM-LF11-318 incubation GUVs started to fuse, suggesting cross linking via the peptides. Furthermore, very bright domains were seen all over the vesicles. These domains could be protrusions of the GUVs where many lipids are tightly packed (dark parts in bright field, see Figure 20). The GUVs with the highest amount of cholesterol tested (1:1:2) (Figure 19) showed linear domains, some circular ones. Again there were GUVs which had GUVs trapped inside. Vesicles containing DPPC/POPS/Cholesterol 1:1:2 showed with 5 to 50 μm a very broad size distribution. Addition of R-DIM-P-LF11-322

or DIM-LF11-318 led to changes in the domains. Fusion between the GUVs and again protrusion/punctual domains occurred.

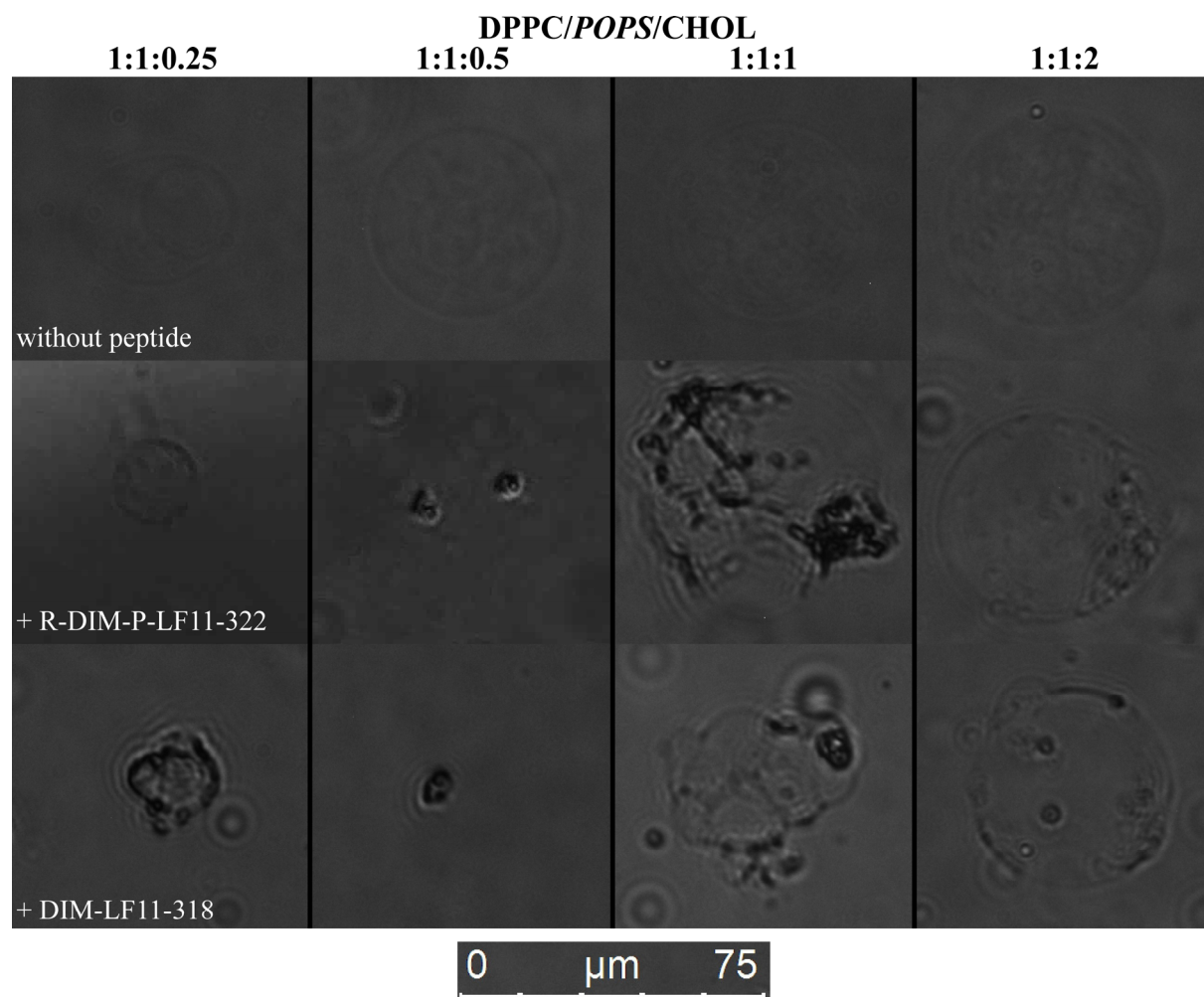


Figure 20: Giant unilamellar vesicles of DPPC/POPS/Cholesterol with increasing amounts of cholesterol in absence and presence of R-DIM-P-LF11-322 and DIM-LF11-318 in bright field. GUVs consisting of DPPC/POPS/Cholesterol (1:1:0.25, 1:1:0.5, 1:1:1 and 1:1:2 molar ratios) + Rhodamine-DOPE were generated using electroformation. Visualization followed in absence of peptides (1st row), in presence of R-DIM-P-LF11-322 (2nd row) or DIM-LF11-318 (3rd row) (50 μ M). Peptide incubation for 1:1:1 and 1:1:2 was 30 minutes, 1:1:0.25 and 1:1:0.5 were visualized immediately due to strong destruction. Bright areas show domains of fluid lipids. Brightness and contrast were equally enhanced for GUVs in presence of peptides. Without any peptide brightness was increased stronger.

Those experiments revealed that the peptides induce a very strong effect on 1:1:0.25 or 1:1:0.5 GUVs, since prompt visualization was needed to still see some GUVs. But in contrast to GUVs consisting of POPC/DPPS/Cholesterol where increasing amounts of cholesterol had no influence on peptide effectivity, at the 1:1:1 and 1:1:2 DPPC/POPS/Cholesterol GUVs the effectivity of both peptides decreased though still showed dramatic effects on the lipid and domain distribution. Again increasing amounts of cholesterol led to an increase in size of the GUVs. The vesicles were hardly seen in absence of peptides, but upon peptide addition there was phase separation which led to bright domains which were spread all over the GUVs, even though less phase separation was seen for 1:1:1 and 1:1:2 GUVs. Furthermore, fusion

occurred in all vesicles when peptides were present. Vesicles were significantly damaged by the peptides.

3.2.3 *In vitro* studies – Cholesterol depletion and its effect on peptide activity

Cholesterol was predicted to exert a protective role in membranes against damage by host defense antitumor peptides [35]. To study possible effects on the two peptides malignant melanoma cells A375 were treated with different amounts of the cholesterol depletion agent methyl-beta-cyclodextrin (M β CD) (0 mM, 5mM and 10 mM) to test the impact of absence of plasma membrane cholesterol on the peptide activity.

Untreated A375 showed a normal cholesterol distribution in the plasma membrane and staining of an intracellular organelle (presumably Golgi apparatus) (see Figure 21, left). It was assured in preliminary tests with different amounts of M β CD that already in presence of 5 mM M β CD plasma membrane cholesterol was successfully depleted (see Figure 21, right) only the inner cellular cholesterol remained. By detection of possible PI-uptake it was also ensured that the tested amounts of M β CD did not lead to cell death (data not shown). Furthermore, it was proved that even after two hours no intracellular cholesterol was transported to the plasma membrane (data not shown). Cytotoxicity studies in absence and presence of 5 mM and 10 mM M β CD with 20 μ M R-DIM-P-LF11-322 or DIM-LF11-318 were performed (Figure 22). There was no impact on killing efficiency of DIM-LF11-318 when cholesterol was depleted (Figure 22, left), after one hour 40% of the cells were killed in absence and presence of cholesterol. After two hours 70% and after four hours 90% of the cells were killed, independent of the amount of cholesterol present in the plasma membrane. This indicated that cholesterol did not have a protective role against the helically structured non-specific peptide. In contrast, the depletion of cholesterol did have a significant influence on the toxicity of R-DIM-P-LF11-322 on the melanoma cells (see Figure 22 right). While after one hour 4% of A375 without M β CD treatment (normal cholesterol) (Figure 22, black line) were killed, 31% of those treated with 5 mM M β CD (dark gray) and 36% of with 10 mM M β CD (light gray) treated cells were killed in the absence of plasma membrane cholesterol. After two hours 13% of the cells with the normal amount of cholesterol were killed, while 50% of with 5 mM and 70% of with 10 mM M β CD treated A375 were killed. After four hours depletion of cholesterol of 10 mM M β CD resulted in an increase of the killing efficiency from 26% to 85%.

All in all, activity of DIM-LF11-318 did not seem to be affected by plasma membrane cholesterol, while the activity of R-DIM-P-LF11-322 was reduced to about 1/3. This may

represent a protection mechanism of non-cancer cells against host defense peptides. Nevertheless, in presence of the target PS the toxicity of the cancer specific R-DIM-P-LF11-322 against cancer cells is still high enough to kill cancer cells while leaving non-cancer cells unharmed.

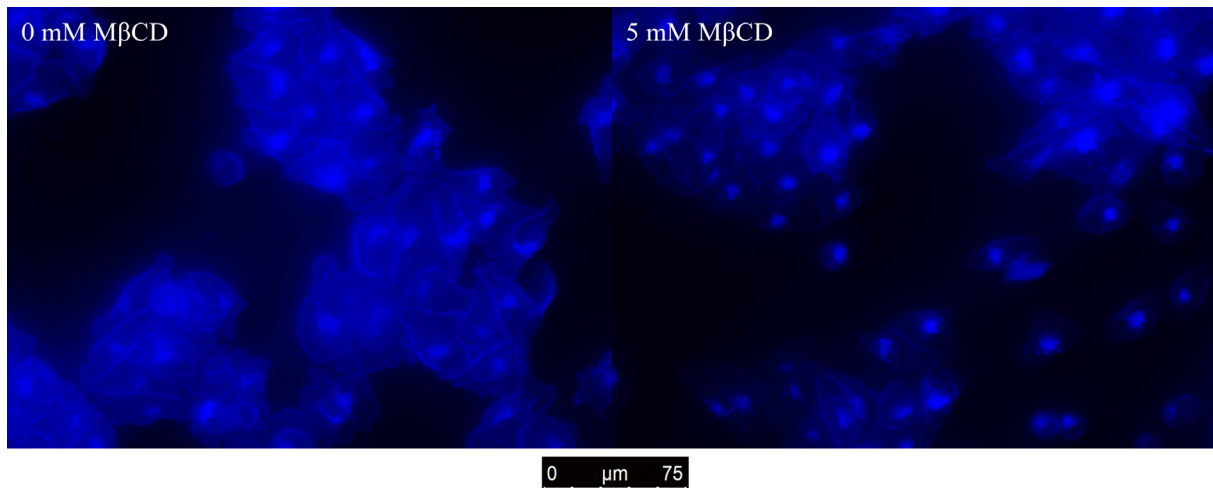


Figure 21: Depletion of plasma membrane cholesterol in membranes of A375 treated with MβCD. Melanoma cells (A375) were not treated with the cholesterol depletion agent MβCD (0 mM MβCD, left) or treated with 5 mM MβCD (5 mM MβCD, right). Cholesterol was stained with filipin (blue). 5 mM of the cholesterol depletion agent led to a strong decrease of cholesterol in the plasma membrane.

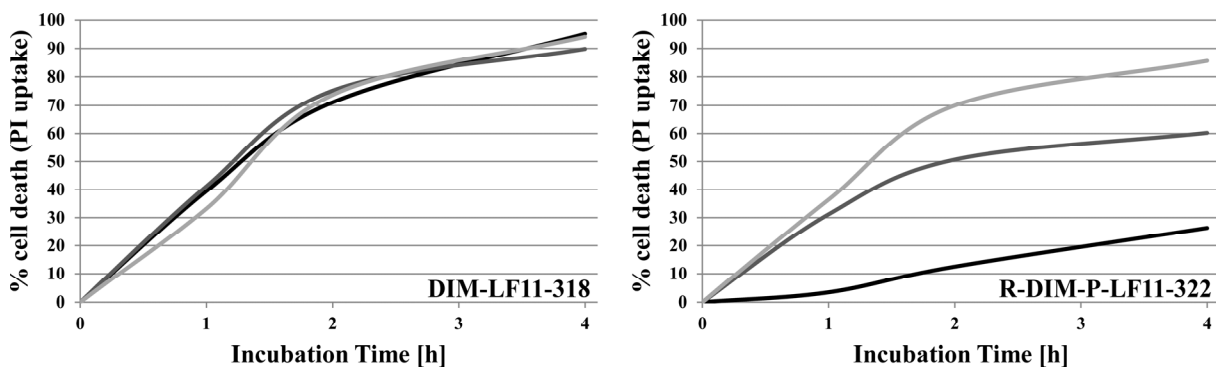


Figure 22: Influence of cholesterol depletion of plasma membrane on killing efficiency of peptides. A375 malignant melanoma cells were treated with different amounts of the cholesterol depletion agent MβCD before peptide incubation. Upon peptide incubation (20 μM DIM-LF11-318, left; 20 μM R-DIM-P-LF11-322, right) the PI uptake of cancer cells which is direct proportional to the percentage of killed cells was measured over four hours. Black represents the mortality curve of A375 without MβCD treatment. Dark gray represents cells treated with 5 mM and light gray with 10 mM MβCD.

3.3 *In vitro* studies – Effect of peptides on morphology of cancer cell membranes of living cells

As shown by Riedl et al. [44], the cancer specific R-DIM-P-LF11-322 triggers apoptosis whereas the non-specific DIM-LF11-318 induces necrosis in cancer cells. Apoptosis demands entrance into cells and interaction with intracellular targets as mitochondria or Golgi [64,65], necrosis mainly requires interaction with the plasma membrane. One way to visualize the interaction sites of a peptide is to track it with a fluorescence label. Figure 23 illustrates the

localization of the (5-6)-FAM labeled R-DIM-P-LF11-322 in A375 melanoma cells (green). It was shown that the peptide enters the cell and localizes in an area next to the nucleus (red) (Figure 23 bottom, left) indicated by arrows. This intracellular peptide localization resembled the intracellular localization of cholesterol (blue), reported already in 3.2.1. Co-staining with a Golgi marker further revealed that the intracellular cholesterol and the Golgi overlap indicated by arrows ((pink spots, overlay of Golgi and cholesterol). Only a few cells were Golgi stained, because the transfection of the plasmid which is required for the expression of the Golgi marking peptide is not that effective.

This leads to the assumption that the specific peptide R-DIM-P-LF11-322 localizes to the Golgi. This hypothesis was also confirmed by Riedl et al. (unpublished data). Fluorescently labeled DIM-LF11-318 was not available, therefore localization studies were only performed with R-DIM-P-LF11-322.

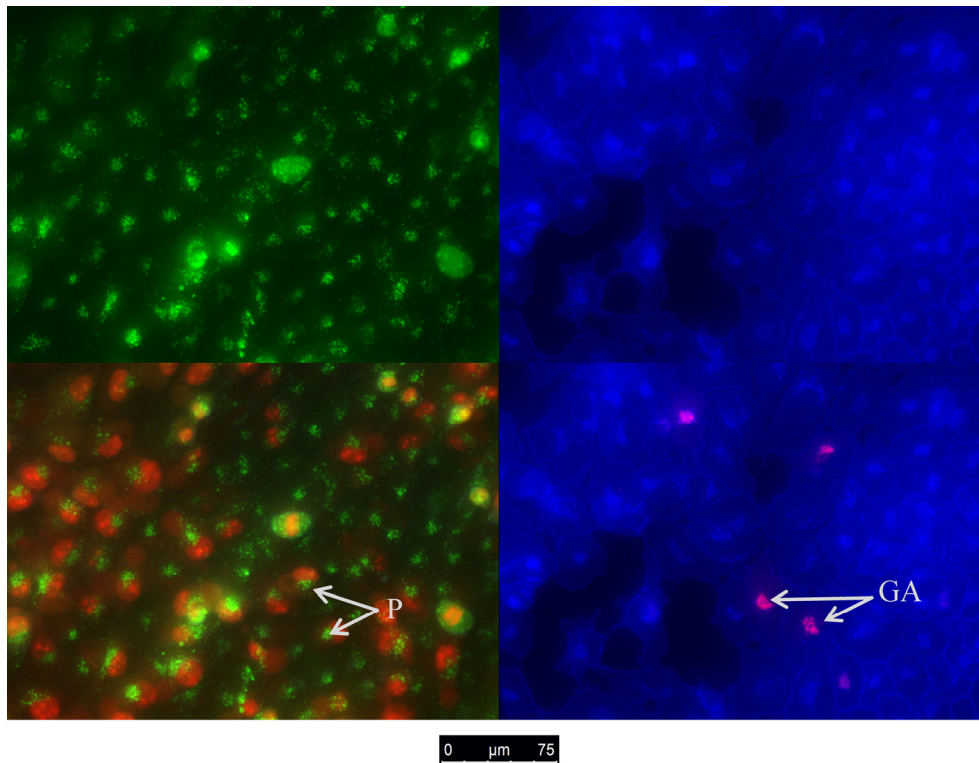


Figure 23: Localization of (5-6)-FAM-R-DIM-P-LF11-322 to Golgi in A375. Melanoma cells were incubated for two hours with 10 μM fluorescently labeled R-DIM-P-LF11-322 (P; green) (left side, bottom image shows overlay with PI). Overlay of Golgi (GA) and cholesterol staining (blue; right side top image) reveals co-localization (pink) (right column, bottom image). Golgi and peptide show localization next to the nucleus, suggesting co-localization.

The following study was therefore intended to clarify the different effects of the peptides on the organelles involved in apoptosis or necrosis.

3.3.1 Effect of peptides on plasma membranes and cholesterol distribution

The first interaction partner of the cationic peptides is the negatively charged PS exposed on the outer leaflet of the plasma membrane of cancer cells. To study possible differences in the effect of R-DIM-P-LF11-322 and DIM-LF11-318 on the morphology of the plasma membrane and plasma membrane cholesterol, melanoma cells were incubated for 30 minutes up to two hours with the peptides with subsequent cholesterol staining. In absence of the peptide, cholesterol was found homogeneously distributed all over the plasma membrane as well as intracellularly, presumably in the Golgi as indicated by arrows (see Figure 24, 1st row and Figure 12). Addition of the specific peptide R-DIM-P-LF11-322 did neither change the cholesterol distribution in the plasma membrane nor inside the cell after 30 minutes, while the non-specific DIM-LF11-318 led to a significant disappearance of the intracellular cholesterol located to the Golgi. Furthermore, upon 30 minutes DIM-LF11-318 incubation, the plasma membrane did not show the homogeneous cholesterol distribution anymore. Cholesterol was located in punctual domains (arrows).

After two hours of R-DIM-P-LF11-322 incubation the intracellular cholesterol of the Golgi also started to dissolve. It seemed that cholesterol got transported to the plasma membrane. The plasma membrane itself showed punctual cholesterol domains similar to the effect of DIM-LF11-318. When A375 were incubated for two hours with DIM-LF11-318 the effect of disappearance of intracellular cholesterol and the formation of punctual domains in the plasma membrane were further enhanced. The bright field picture revealed that the cells were severely damaged showing lysed fragments (blebs) in presence of the non-specific peptide DIM-LF11-318 (arrows right side, bottom). In contrast, cells treated for two hours with R-DIM-P-LF11-322 still showed intact cell membrane morphology (Figure 24, 4th row). This indicates that the specific peptide interacts more slowly, but similarly regarding its effect on the cholesterol distribution. Though different effect on the morphology of the plasma membrane of the cancer cells was seen compared to the non-specific peptide. This is consistent with published data by Riedl et al. [44], who reported that R-DIM-P-LF11-322 leads to apoptosis after 4 to 8 hours, whereas DIM-LF11-318 rapidly leads to necrosis of cancer cells and lysis of the plasma membrane. Summarized, besides DIM-LF11-318, also R-DIM-P-LF11-322 shows induction of cholesterol domains in the plasma membrane and consumption or transport of intracellular cholesterol, however, only DIM-LF11-318 induces visible lyses of the plasma membrane. The effects might indicate different stress responses of the cells to the presence of the peptides.

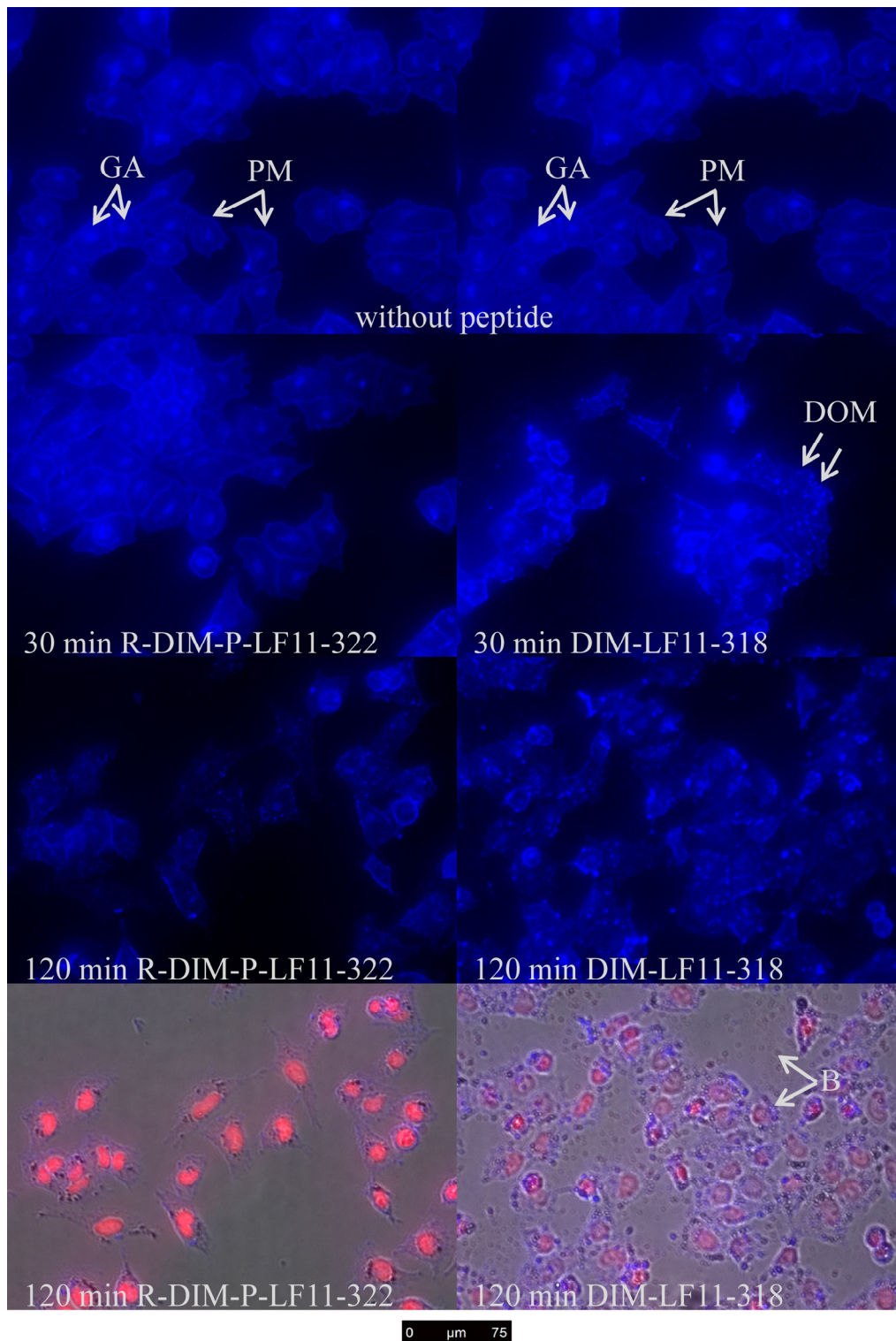


Figure 24: Changes in morphology of plasma membrane and cholesterol distribution of A375 upon peptide addition. Cholesterol stained (filipin, blue) melanoma cells (A375) in absence of peptide (1st row), after 30 minutes of peptide incubation (2nd row: left R-DIM-P-LF11-322; right DIM-LF11-318) and after two hours peptide incubation (3rd row: left R-DIM-P-LF11-322; right DIM-LF11-318). The bottom row shows the overlay images (bright field, filipin and PI) of A375 after two hours peptide incubation (left R-DIM-P-LF11-322; right DIM-LF11-318). DIM-LF11-318 leads to a stronger effect (lysis after two hours) compared to R-DIM-P-LF11-322. Peptide concentration was 10 μM . Arrows indicate the plasma membrane (PM), Golgi apparatus (GA) as well as domains (DOM) and blebs (B).

3.3.2 Effect of peptides on mitochondria

First steps of apoptosis are often characterized by mitochondrial swelling followed by cytochrome C release. In melanoma cells apoptosis is in many cases blocked due to a mutation of Apaf1, though it is reported to be induced as response upon cellular stress or to anti-cancer drugs [66]. To determine if R-DIM-P-LF11-322 or DIM-LF11-318 induce any morphological changes of mitochondria melanoma cells (A375) were incubated for 30 minutes up to two hours with the peptides followed by mitochondrial staining. Figure 25 (left, without peptide) shows normal mitochondrial staining (red) spanning the nucleus. However, upon incubation with R-DIM-P-LF11-322, mitochondria started to swell (middle 30 min, right 120 min) indicating induction of apoptosis in the melanoma cells. Upon longer R-DIM-P-LF11-322 incubation, some cells also showed blue stained nuclei, indicating beginning of cell death. While there was hardly any nucleus stained in presence of R-DIM-P-LF11-322, after 30 minutes of DIM-LF11-318 incubation (Figure 26) almost all A375 cells showed blue nuclei confirming the faster killing by this peptide. The images of Figure 26 show that upon DIM-LF11-318 incubation the cells shrank and also the mitochondria got kind of compressed and not swollen. The bright field images (Figure 26, 2nd row) again confirm lysis of the cells upon DIM-LF11-318 incubation. Interestingly, cells which were not nucleus stained showed swollen mitochondria and were not lysed. This would indicate apoptosis induction in some of the cells, however this was only a minor event and might be a concentration effect. The results are in confirmation with published data of Riedl et al. [44] who reported, that R-DIM-P-LF11-322 leads to cell death by apoptosis and DIM-LF11-318 mainly by necrosis.

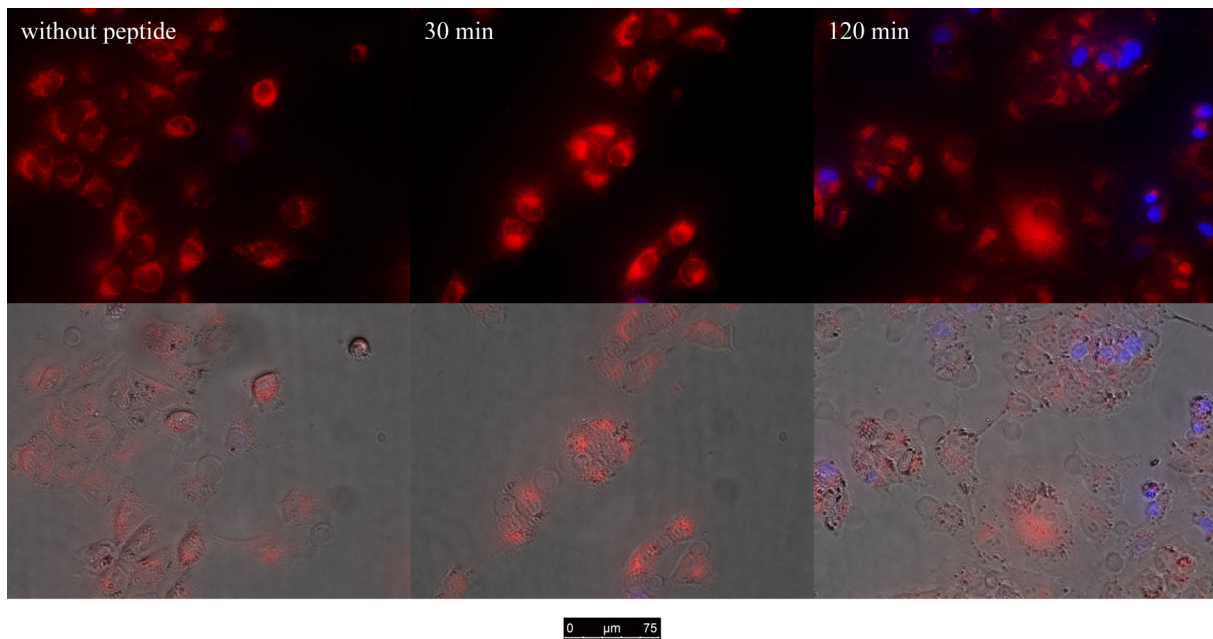


Figure 25: Changes in mitochondria of A375 upon R-DIM-P-LF11-322 incubation. Overlay images of melanoma cells (A375) with stained mitochondria (red, MitoTracker[®] Deep Red) and nucleus staining (blue, Hoechst 33342) (top row) as well as together with bright field (bottom row). Left represents A375 with stained mitochondria in absence of peptide, the middle shows A375 which were incubated for 30 minutes with peptide with starting of mitochondrial swelling. The right side shows cells which were incubated for two hours with the peptide. Peptide concentration was 10 μ M.

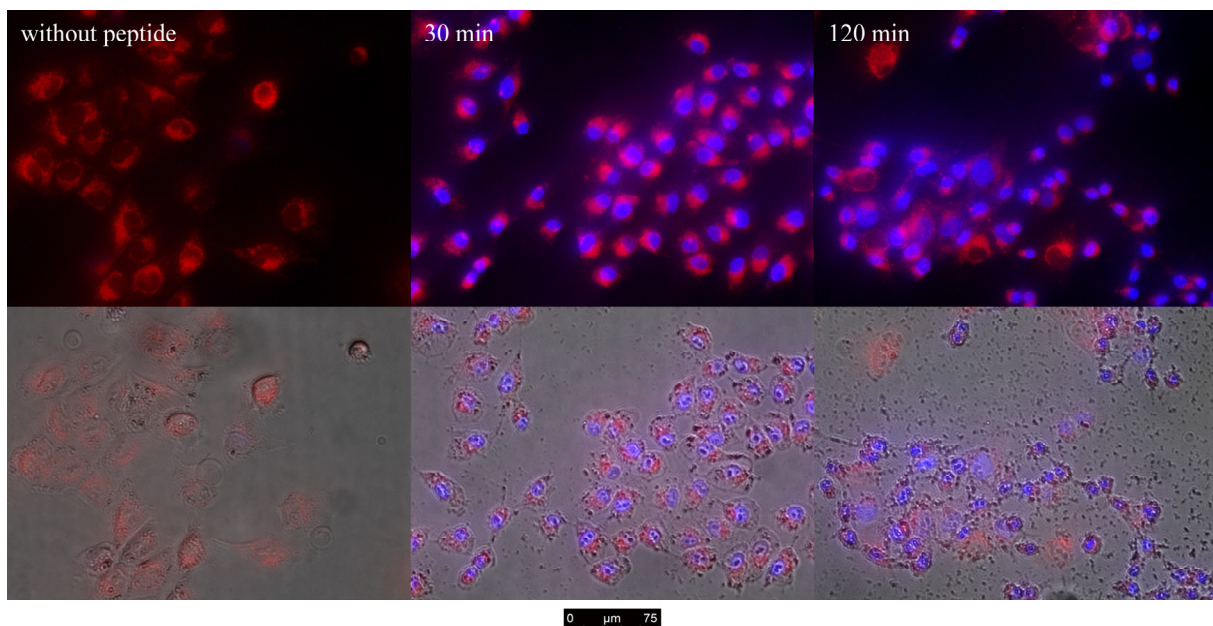


Figure 26: Changes in mitochondria of A375 upon DIM-LF11-318 incubation. Overlay images of melanoma cells (A375) with stained mitochondria (red, MitoTracker[®] Deep Red) and nucleus staining (blue, Hoechst 33342) (top row) as well as together with bright field (bottom row). Left represents A375 with stained mitochondria in absence of peptide, the middle shows A375 which were incubated for 30 minutes with the peptide. The right side shows cells which were incubated for two hours with the peptide. Peptide concentration was 10 μ M.

3.3.3 Effects of peptides on Golgi apparatus

To study potential differences of effects of peptides on the Golgi morphology, melanoma cells were incubated for 30 minutes up to two hours with R-DIM-P-LF11-322 and DIM-LF11-318, respectively. Figure 27 (right) shows normal Golgi staining (red) in stacks at one side of the nucleus in the absence of peptide of melanoma cells. Images in the middle and at the right show that upon R-DIM-P-LF11-322 incubation the Golgi did not show any significant morphological changes. Only the amount of blue nuclei stained cells increased with the time of peptide incubation indicating partial start of cell death at longer peptide incubation periods. The bright field shows that there was no membrane lysis upon peptide addition. On the contrary membrane lysis as well as shrinking of the cells already occurs after 30 minutes of DIM-LF11-318 incubation (Figure 28, bright field). Nevertheless, also upon DIM-LF11-318 incubation no significant morphological changes of the Golgi were seen (see Figure 28, fluorescence channel). All cells were blue nuclei stained substantiating that DIM-LF11-318 has stronger effects on the cells.

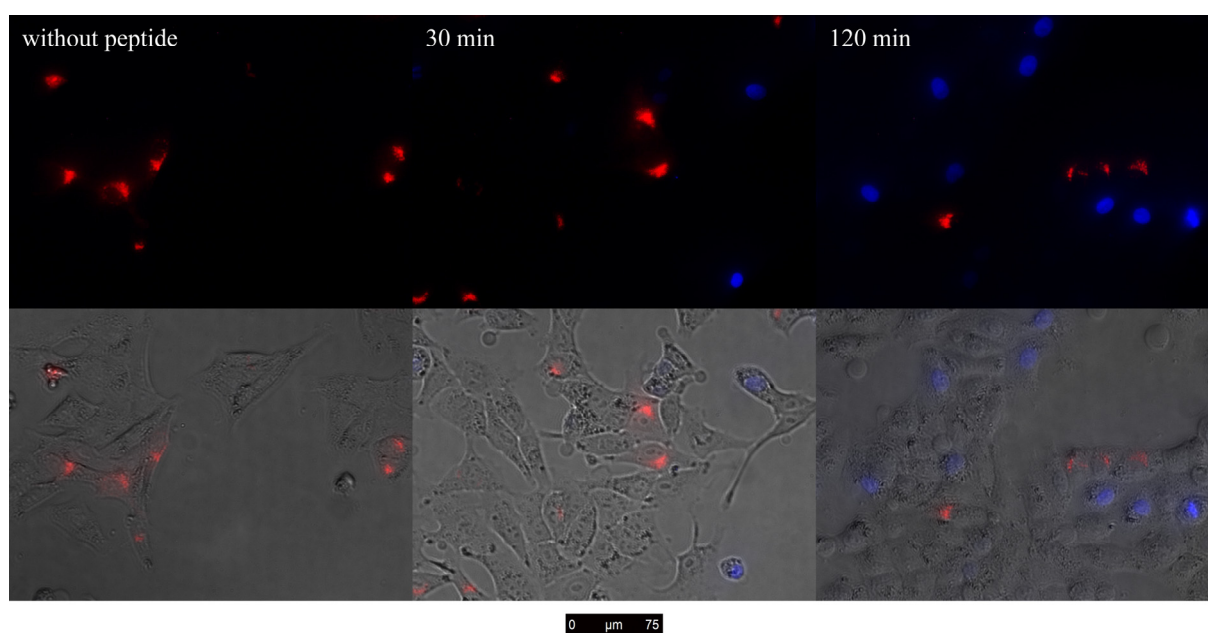


Figure 27: Changes in morphology of Golgi of A375 upon R-DIM-P-LF11-322 incubation. Overlay images of melanoma cells (A375) with stained Golgi (red, CellLight® Golgi-RFP BacMam 2.0) and nucleus staining (blue, Hoechst 33342) (top row) as well as together with bright field (bottom row). Left represents A375 in absence of peptide, the middle shows A375 which were incubated for 30 minutes with the peptide. The right side shows cells which were incubated for two hours with the peptide. Peptide concentration was 10 μ M.

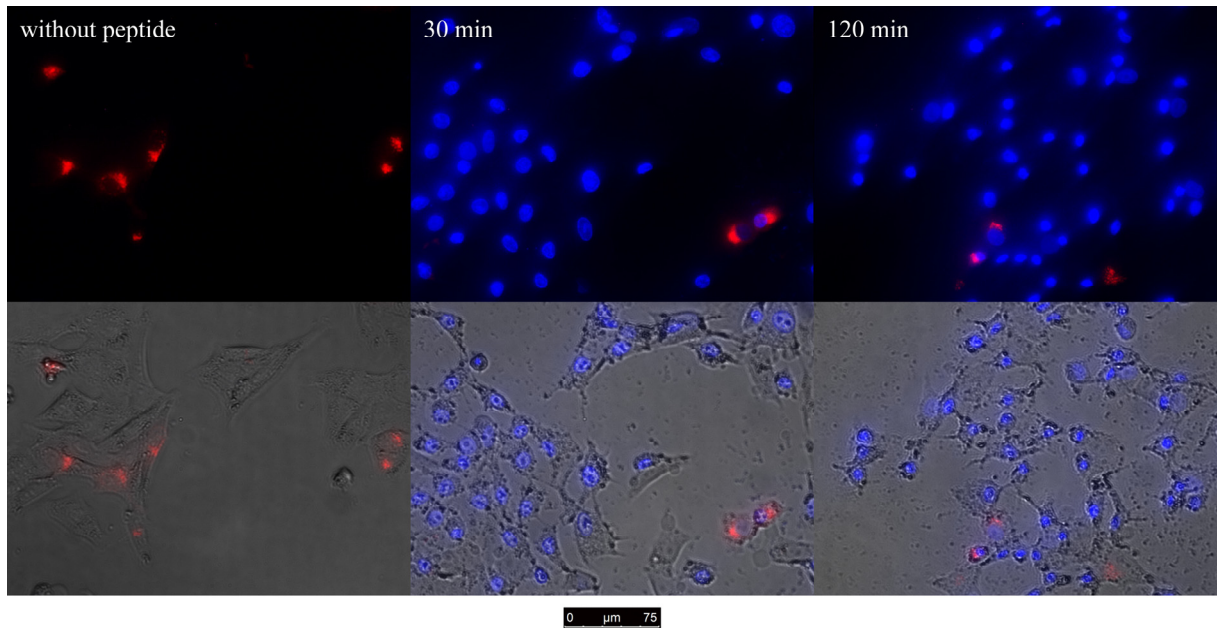


Figure 28: Changes in morphology of Golgi of A375 upon DIM-LF11-318 incubation. Overlay images of melanoma cells (A375) with stained Golgi (red, CellLight® Golgi-RFP BacMam 2.0) and nucleus staining (blue, Hoechst 33342) (top row) as well as together with bright field (bottom row). Left represents A375 in absence of peptide, the middle shows A375 which were incubated for 30 minutes with the peptide. The right side shows cells which were incubated for two hours with the peptide. Peptide concentration was 10 μM .

3.4 Summary of Results

For a better overview characteristics of R-DIM-P-LF11-322 and DIM-LF11-318 as well as their activities on model systems and results of *in vitro* studies are condensed in Table 8.

Table 8: Summary of R-DIM-P-LF11-322 and DIM-LF11-318 characteristics / activities on model system as well as in *in vitro* analyzes

	R-DIM-P-LF11-322		DIM-LF11-318	
Sequence	PFWRIRIRR-P-RRIRIRWFP-NH ₂		FWQRRIRRWRR-FWQRRIRRWRR-NH ₂	
Net charge	+ 9		+ 13	
Structure	β-sheet		α-helix	
Model system studies				
Bilayer-perturbation (DSC)				
<i>Non cancer mimic</i>	-		-	
<i>Cancer mimic</i>	+++		++++	
<i>Cancer mimic + Chol</i>	++		+++++	
Penetration-depth (Tryptophan Quenching)				
<i>Non cancer mimic</i>	-		-	
<i>Cancer mimic</i>	++		++*	
<i>Cancer mimic + Chol</i>	++		*	
Lateral changes in lipid distribution (GUVs)				
<i>DPPS mixtures</i>	++		++	
<i>POPS mixtures</i>	+++		+++	
<i>Size changes</i>	Smaller upon peptide addition			
<i>Presence of cholesterol</i>	Increasing amounts of cholesterol led to decreasing effects of peptides			
Electrostatic & hydrophobic interaction (Zeta potential)				
<i>Non cancer mimic</i>	-		-	
<i>Cancer mimic</i>	++		+++	
<i>Cancer mimic + Chol</i>	+		+++	
<i>In vitro</i> studies with A375				
Chol depletion	Activity decreasing effect		No effect on activity	
Morphological changes	30 min	120 min	30 min	120 min
<i>Golgi Apparatus</i>	No morphological changes		No morphological changes	
<i>Mitochondrion</i>	Swelling	Swelling	No swelling	No swelling
<i>Chol / Plasma membrane</i>	~	Chol redistribution / domains	Chol redistribution / domains	Chol redistribution / domains + lysis

Chol is Cholesterol; (*) emission spectra with more than one maximum, method not suitable for strong perturbing and destructive peptides; (+) peptide effect, (++) stronger peptide effect etc.; (-) no peptide effect; (~) no influence

4. Discussion

It was reported that cancer cells specifically expose the negatively charged lipid phosphatidylserine (PS) in the outer leaflet of the plasma membrane [13,15–17]. In 2014, Riedl et al. [42] revealed that human lactoferricin (hLFcin) derivatives target the negatively charged PS. They found that one derivative, R-DIM-P-LF11-322, interacts specifically with cancer cells, whereas another LFcin derivative DIM-LF11-318 also harms non-cancer cells [44].

Thus, the aim of this study was to reveal differences in mode of action and specificity of these two LFcin derivatives using model system studies as well as *in vitro* experiments, whereby a focus was on a cancer with poor prognosis, the malignant melanoma. This should help to further optimize the peptides with the purpose to design a new, specific and potent therapy against this cancer type. Since cancer cells specifically expose PS on the outer leaflet, cancer mimicking model systems composed of PS alone or mixed with PC were used. Healthy cell mimics were composed of PC. Furthermore, cholesterol was added to the cancer and non-cancer model systems to determine if it influences the effectivity, mode of action or specificity of the peptides, since cholesterol is present in high amounts in cancer as well as in non-cancer cell plasma membranes. In that respect, it was reported that cholesterol reduces the effectiveness of magainin a host defense peptide of *Xenopus laevis* on erythrocytes, and was therefore thought to probably have a protective function in the host against its own defense peptides [35]. Besides the amount also the distribution of cholesterol was shown to be altered in plasma membranes of cancer cells [18,55].

In cancer model systems where PS was present, R-DIM-P-LF11-322 showed electrostatic interactions (zeta potential) as well as perturbation of the liposomes (DSC) and penetration (tryptophan quenching) of the peptide. Model studies with PS/PC mixtures revealed a specific interaction of R-DIM-P-LF11-322 with the cancer marker PS. DIM-LF11-318, however, developed a much stronger effect against cancer model systems, since DSC results showed stronger perturbation of the cancer mimic and in presence of PS/PC mixtures effects on both components, PS and PC. Furthermore, zeta potential measurements in presence of DIM-LF11-318 showed hydrophobic besides electrostatic interactions. Addition of cholesterol to PC/PS model systems in DSC and zeta potential measurements revealed a decrease in the efficacy of R-DIM-P-LF11-322 against the cancer mimics, however, still indicating a specific interaction with PS. In contrast cholesterol in DSC measurements with DIM-LF11-318 even increased the effect of the peptide. In these model systems DIM-LF11-318 was again shown to interact not only with PS but also with PC, an effect even enhanced through presence of

cholesterol. Also GUV experiments revealed that the peptides preferentially interact with PS, whereas the interaction with the fluid POPS was stronger than with gel phase DPPS, confirming the preferential interaction of both peptides with the target PS. Size measurements for both peptides revealed that upon peptide addition the size of the particles increases, suggesting cross linking by the peptides. Zeta potential experiments showed that the first interaction of R-DIM-P-LF11-322 with the target membrane is via electrostatic interactions, whereas increasing amounts of cholesterol seemed to lead again to a decrease in electrostatic interactions between the lipid model system and the peptide. On the contrary, DIM-LF11-318 seems to interact via electrostatic as well as hydrophobic forces, whereas increasing amounts of cholesterol had no influence on zeta potential. Those hydrophobic besides electrostatic interactions may also be a hint for a characteristic mode of action of the non-specific DIM-LF11-318. These data are further in perfect correlation with zeta potential studies of the two peptides with cancer and non-cancer cells, proving the main interaction of the peptides with lipids [44]. The interaction of DIM-LF11-318 with the cancer target PS, but also with PC present in healthy cells, that is even enhanced in the presence of cholesterol, is already a hint for the interactions that can cause the non-specificity of this peptide. The interaction of the cancer specific R-DIM-P-LF11-322, however, seems to be exclusively triggered by the presence of PS.

No effects according bilayer perturbation (DSC), electrostatic (zeta potential) or hydrophobic interactions (zeta potential, tryptophan quenching) were seen for non-cancer mimics (pure DPPC) for R-DIM-P-LF11-322. This is in agreement with its non-toxicity for healthy cells and studies performed by Riedl et al. [44] showing that R-DIM-P-LF11-322 only affects model systems when PS is present. However, it is of interest why DIM-LF11-318 did not show any effects on healthy cell mimicking model systems either, although it leads to cell death of normal human dermal fibroblasts. Riedl et al. [44] reported that DIM-LF11-318 can penetrate POPC bilayers without causing membrane perturbation (comparable to function of cell penetrating peptides [67,68]) by measuring the effect of the quencher acryl amide enclosed in POPC liposomes on DIM-LF11-318, when entering the liposome. Killing of healthy cells by DIM-LF11-318 was thus suggested to occur by cell death induction from the inside of the plasma membrane rather than from the outside [44]. Nevertheless, model studies revealed that DIM-LF11-318 had an influence on DPPC when DPPS was present. Further on, in the presence of higher ratios of cholesterol in PC models besides penetration also membrane perturbation was seen to occur (recent data, not shown). Surprisingly, it was observed in the model studies that the presence of cholesterol had a different effect on the two

peptides. R-DIM-P-LF11-322 was decreased in its activity, whereas DIM-LF11-318 was not affected in some studies or even enhanced in its membrane interaction. An effect of cholesterol decreasing the activity of certain host defense peptides has already been described in 1995 by Matsuzaki et al. [35]. They reported that upon cholesterol depletion of erythrocytes, the effect of the cancer specific peptide magainin (frog skin) increases, indicating that cholesterol is able to reduce activity of the peptides. This may be a way for cells to protect themselves against lytic peptides. Interestingly, they also found that the non-specific peptide melittin (bee) is not influenced by cholesterol depletion, and exhibits the same effects independent of cholesterol content in erythrocytes. This is in nice correlation with our results showing a decreasing effect of cholesterol on the specific peptide R-DIM-P-LF11-322 and no decreasing effect on the non-specific peptide DIM-LF11-318. Two explanations have been discussed so far. First, cholesterol is responsible for stiffening the membrane and therefore decreasing the lytic activity of the peptides [53]. Second, in 1999 Matsuzaki et al. [29] also suggested another reason for an activity decreasing effect of cholesterol, which may occur by prevention of the formations of a membrane active secondary structure of the peptide when binding to an acidic phospholipid bilayer. By formation of a hydrogen bond between the hydroxyl group of cholesterol and the peptide molecule it might inhibit intramolecular hydrogen bond formation within the peptide which is needed for its effectivity. In contrast, the non-specific melittin already has a well-defined structure in aqueous solution and therefore already has the appropriate structure for harming the cells. This may be the reason why cholesterol has an effect on R-DIM-P-LF11-322 even though the peptide activity is not completely reduced when cholesterol is present, since the peptide remains effective against cancer membranes. It has been reported that the β -sheet structure of the peptide only emerges in presence of an anionic hydrophobic environment [44]. Therefore, cholesterol may prevent the secondary structure formation of the specific peptide to a certain extent, consequently decreasing its effectiveness. DIM-LF11-318, however, was shown to develop an α -helical structure in presence of the cancer and the non-cancer mimic and acts very fast [44]. Thus, the fast and non-specific formation of its active structure might not be disturbed by cholesterol. For a schematic depiction see Figure 29. That cholesterol has an activity decreasing effect on R-DIM-P-LF11-322 but not on DIM-LF11-318 was also confirmed *in vitro* with melanoma cells (A375) treated with a cholesterol depletion agent. While cholesterol depletion led to an increase of the killing effectivity of R-DIM-P-LF11-322, no influence was seen for DIM-LF11-318. One explanation for the activity of R-DIM-P-LF11-322 being influenced by cholesterol as discussed above might be that

cholesterol increases the stiffness of eukaryotic plasma membranes in general. Upon cholesterol depletion the membrane gets less stiff and can therefore be more easily permeabilized or penetrated. A reduced disrupting effect in presence of cholesterol was also described for other AMPs as gramicidin S [69], MSI variants [70] or laticin 2a [71].

The plasma membrane of mammalian cells is reported to comprise certain microdomains with increased levels of protein receptors and lipids as PC, SM and cholesterol termed lipid rafts. Rietveld et al. [72] assigned these lipid rafts in model membranes to an immiscibility of ordered (L_o phase) and disordered (L_d or L_α phase) liquid phases. For cancer cells changes in these microdomains have been discussed, thus Li et al. [55] stated that some cancer types like breast or prostate cancer exhibit elevated levels of cholesterol-enriched lipid rafts, whereas the rest of the membrane contains less cholesterol. Presumably the missing cholesterol increases the fluidity of these regions. Addition of AMP derived anti-cancer peptides may better reach the target PS and the decreased stiffness may lead to easier incorporation of the peptides in further consequence [18]. Since non-cancer membranes have a higher content of cholesterol in non-raft regions and therefore are more rigid and they lack anionic lipids in the outer leaflet of the membrane, specific anti-cancer peptides may not harm them [18]. This leads to the assumption that the stiffness of healthy cell membranes is a major reason why the cells are protected against specific host defense peptides while it has no influence on non-specific peptides. To study a possible impact of naturally occurring domains, some experiments were performed with mimics showing an inhomogeneous distribution of lipids. Interestingly, both peptides within this study acted independently, no matter if domains were present or not, a promising result assuring activity of peptides even in natural membranes *in vitro* and *in vivo*. One difference in the interaction of the two peptides was that DIM-LF11-318 even acted better in the presence of domains, explaining the stronger and probably also in part the non-specific effect of the peptide *in vitro*. Further, studies of GUVs revealed that upon peptide addition a dramatic change in the lipid distribution and fluidity/disorder of domains occurred. Bright spots indicated regions where on the one hand the target PS and on the other hand the peptide was localized. This is conform with reports of Epanand et al. [73] that arginine rich peptides (like LF11-322; there named PR-9) induce segregation of anionic and zwitterionic lipids. This clustering of lipids generates defects between peptide poor and peptide rich domains which may lead to membrane permeabilization and secondary effects as changes of protein activity [31,73]. Phase separation was also shown in DSC studies with R-DIM-P-LF11-322 when added to DPPS liposomes which is in agreement with DSC measurements by Riedl et al. [42,44]. Changes in the lipid (cholesterol) distribution were further seen when

A375 cells were incubated with the peptide. The addition of the non-specific DIM-LF11-318 rapidly resulted in a strong change in cholesterol distribution in the plasma membrane. As well, the intracellular cholesterol in the Golgi started to disappear which indicated strong cellular stress. The same phenomena were observed with R-DIM-P-LF11-322, though appearing more slowly. This slower interaction of the specific peptide is also consistent with published data by Riedl et al. [44].

Such differences in killing velocity can often be related to different killing mechanism, slow specific killing mechanism with formation of apoptotic blebs following induction of apoptosis and fast often non-specific membrane lysis of the plasma membrane by necrosis [18]. Accordingly, Riedl et al. have reported [44] that the cancer specific R-DIM-P-LF11-322 triggers apoptosis while the non-specific DIM-LF11-318 leads to necrosis of cancer cells and cell death of non-cancer cells. Apoptosis demands entrance into the cancer cells through the plasma membrane and further interaction with an intracellular target like mitochondria or Golgi, whereas the plasma membrane is known to be mainly important for necrotic interactions. In all cases, negatively charged lipids are present and might be responsible for the peptide interaction. Since one hallmark of cancer is the circumvention of apoptosis [74], anti-cancer treatment, which would lead to apoptosis, is favorable. In addition, the controlled cell death via apoptosis does not lead to inflammation because phagocytic cells eliminate the dying cells very fast, no cellular components are released in the environment and no cytokine production by engulfing macrophages occurs [75,76]. Within this study, influences of the peptides on the target organelles playing a major role within these killing mechanisms, the plasma membrane, the mitochondria and the Golgi apparatus were intended to bring further clarification.

Interestingly, localization studies revealed that the fluorescently labeled R-DIM-P-LF11-322 mainly localizes to the Golgi. R-DIM-P-LF11-322 may enter the cell in a manner analogous to the so called sinking raft model where the peptide localizes at the membrane surface. Only in the presence of exposed PS and at a certain point it sinks into the bilayer [77] and then localizes to the Golgi by interaction with negatively charged lipids, as PS or phosphatidylinositol (PI) (see Figure 29). The localization to Golgi was to some extent surprising, since it was assumed that the specific peptide localizes to mitochondria, the main starting spot of apoptosis [39]. However, such localization of potential anti-cancer drugs to Golgi has also been reported before, e.g., for the Shiga-Toxin B subunit [78]. Further, it was reported that the Golgi upon stress sensing can activate pro-survival mechanisms as well as suicide programs if stress results in irreparable damage [64,79]. This may be due to the

activation of caspase-2 which is besides other regions also located in the Golgi. Caspase-2 cleaves golgin160 which was reported to be an early event of apoptosis [80,81]. Another way for activation of apoptosis by the Golgi was reported to be the conversion of ceramide into the ganglioside GD3 by GD3 synthase. GD3 is then transported to the mitochondrion provoking mitochondrial membrane permeability [82,83] which then leads to induction of the intrinsic pathway of apoptosis via cytochrome C efflux. Furthermore, another link between Golgi and apoptosis is suggested to be the transport of death receptors (like Fas or TNF-receptor 1) upon stress signaling to the plasma membrane as death receptors are localized under non-stress conditions in the Golgi [79,81,84]. This may be the reason why intracellular cholesterol of the Golgi was seen to disappear upon peptide incubation, since the transport of the death receptors occurs via vesicle transport where cholesterol would be located in the vesicle membrane. Therefore, morphological changes of the Golgi [85], mitochondria [86,87] or the plasma membrane upon peptide addition were studied within this work. Though R-DIM-P-LF11-322 localizes to the Golgi, no morphological changes of the organelle were seen, whereas mitochondria started to swell when the peptide was present. The swelling of the mitochondria of the cells upon peptide addition is a sign for ongoing apoptosis which is in accordance with Riedl et al. [44] who reported that upon incubation with R-DIM-P-LF11-322 the caspase-3 and -7 activities increase. The missing of morphological changes of the Golgi may be due to the fact that disassembly of the Golgi requires more time (last time point for our experiment was two hours) or that activation of caspase-2 or conversion of ceramide into ganglioside in Golgi can act as a signal for apoptosis without ongoing distortion of the organelle. A further explanation might also be supported by the observation that localization of the fluorescence labeled peptide seemed to be hindered in cells carrying the used Golgi-staining. Probably morphological changes of the Golgi cannot be observed in the case of a peptide localizing to the Golgi, due to a potential similar target of the peptide and the Golgi staining. DIM-LF11-318, which is known to act rapidly by membrane lysis, showed neither morphological changes in the Golgi nor swelling of the mitochondria. The organelles rather shrunk due to a shrinking of the whole cell after lysis of the membrane. Only the plasma membrane was shown to get massively distorted. The results confirmed once more that DIM-LF11-318 leads to necrosis rather than apoptosis which is in agreement with Riedl et al. [44] (see Figure 29).

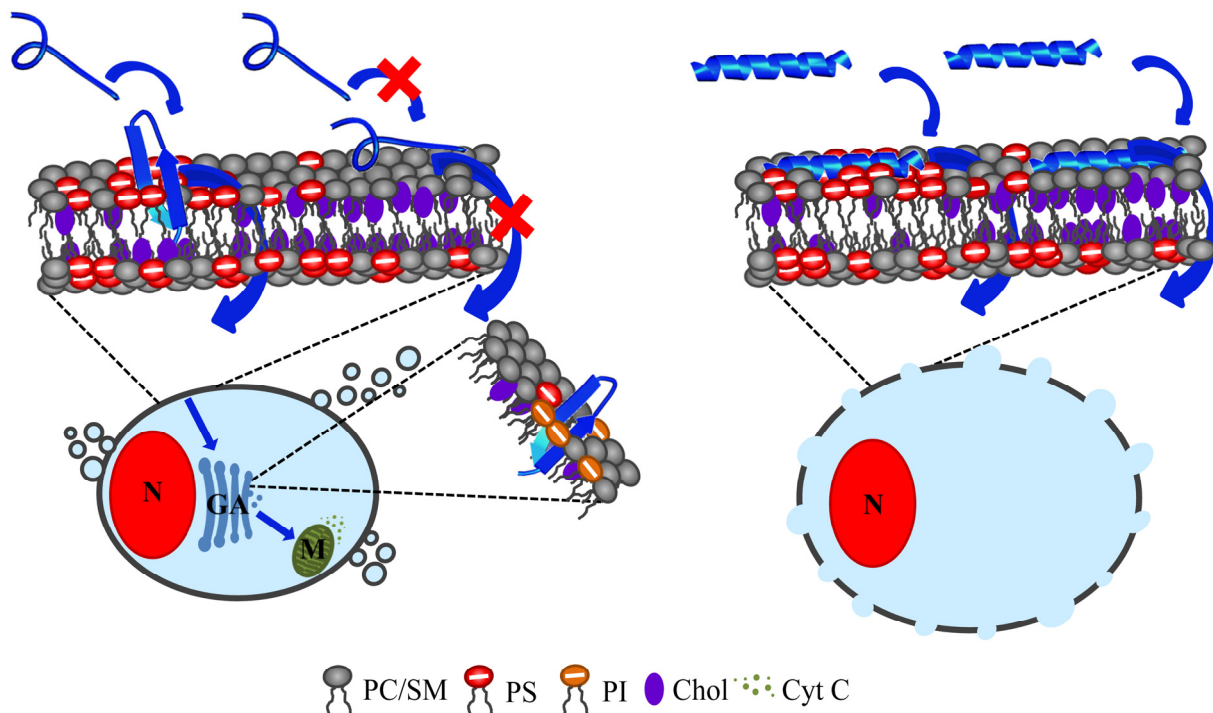


Figure 29: Predicted modes of action of R-DIM-P-LF11-322 and DIM-LF11-318 on cancer cells. Cancer cells specifically expose the negatively charged phosphatidylserine (PS, red) in the outer leaflet of the plasma membrane [17]. Cholesterol (Chol, purple) is particularly localized with phosphatidylcholine and sphingomyelin (PC and SM, gray) in rafts [55]. Both peptides result in changes in the lipid distribution, leading to defect borderlines and thereby to primary and secondary harming effects. **Left:** R-DIM-P-LF11-322 (blue) forms its membrane active structure (β -sheet) only in presence of PS, whereas cholesterol has a disturbing effect on R-DIM-P-LF11-322, presumably by disturbing the formation of the membrane active secondary structure. After interaction with the target membrane and after the peptide entered the cell, the intracellular target of the peptide seems to be the Golgi apparatus (GA; green represents phosphatidylinositol (PI)) located next to the nucleus (N) and leads to apoptosis via different ways (see text), e.g., by inducing loss of membrane potential of mitochondria (M) which leads to cytochrome C (Cyt C) efflux. **Right:** DIM-LF11-318 (blue) forms its membrane active structure (α -helix) in presence of both, PS and PC, independently of cholesterol. DIM-LF11-318 is thought to harm the cell directly at the plasma membrane leading to necrosis. Modified from Riedl et al. [44].

Within this work it was shown that the cancer specific peptide R-DIM-P-LF11-322 and the non-specific DIM-LF11-318 alter the lipid distribution and fluidity of cancer cell membranes, which may lead to changes of the permeability of the plasma membrane and to secondary effects like loss of function of membrane proteins or release of stress signals. More importantly we could prove that R-DIM-P-LF11-322 specifically interacts with PS exposed in the outer leaflet of cancer cell plasma membranes. It is less effective when cholesterol is present but still leads to specific death of the cancer cells. By contrast, the non-specific DIM-LF11-318 preferentially interacts with PS but can also interact with neutral lipids like PC. The non-specific peptide is unaffected by cholesterol. One conceivable reason may be that cholesterol prevents the formation of the membrane active structure. This different ability of lipid discrimination and sensibility to cholesterol might already indicate one crucial feature for a cancer specific peptide such as R-DIM-P-LF11-322. Furthermore, it was shown that R-DIM-P-LF11-322 specifically enters the cancer cell through the plasma membrane via PS and

then localizes to the Golgi, thereby constituting a stress signal which leads to swelling of mitochondria and further induction of apoptosis (in confirmation with Riedl et al. [44]). In contrast, DIM-LF11-318 seems to interact non-specifically with PS and PC on the plasma membrane, where it immediately leads to membrane lysis with no need of an intracellular target. In conclusion the results reveal that both peptides kill melanoma cells, however, the different mode and site of interaction decide on their specificity.

5. References

- [1] PDQ Adult Treatment Editorial Board. (Ed.), Melanoma Treatment (PDQ®): Health Professional Version, PDQ Cancer Information Summaries [Internet], Bethesda (MD), 2016.
- [2] C. Garbe, Zunehmende Häufigkeit des malignen Melanoms, *Der Hautarzt* 51 (2000) 518.
- [3] H. Davies, G.R. Bignell, C. Cox, P. Stephens, S. Edkins, S. Clegg, J. Teague, H. Woffendin, M.J. Garnett, W. Bottomley, N. Davis, E. Dicks, R. Ewing, Y. Floyd, K. Gray, S. Hall, R. Hawes, J. Hughes, V. Kosmidou, A. Menzies, C. Mould, A. Parker, C. Stevens, S. Watt, S. Hooper, R. Wilson, H. Jayatilake, B.A. Gusterson, C. Cooper, J. Shipley, D. Hargrave, K. Pritchard-Jones, N. Maitland, G. Chenevix-Trench, G.J. Riggins, D.D. Bigner, G. Palmieri, A. Cossu, A. Flanagan, A. Nicholson, J.W.C. Ho, S.Y. Leung, S.T. Yuen, B.L. Weber, H.F. Seigler, T.L. Darrow, H. Paterson, R. Marais, C.J. Marshall, R. Wooster, M.R. Stratton, P.A. Futreal, Mutations of the BRAF gene in human cancer, *Nature* 417 (2002) 949–954.
- [4] V. Gray-Schopfer, C. Wellbrock, R. Marais, Melanoma biology and new targeted therapy, *Nature* 445 (2007) 851–857.
- [5] M.S. Soengas, P. Capodieci, D. Polsky, J. Mora, M. Esteller, X. Opitz-Araya, R. McCombie, J.G. Herman, W.L. Gerald, Y.A. Lazebnik, C. Cordon-Cardó, S.W. Lowe, Inactivation of the apoptosis effector Apaf-1 in malignant melanoma, *Nature* 409 (2001) 207–211.
- [6] A. Anichini, R. Mortarini, M. Sensi, M. Zanon, APAF-1 signaling in human melanoma, *Cancer letters* 238 (2006) 168–179.
- [7] P.B. Chapman, L.H. Einhorn, M.L. Meyers, S. Saxman, A.N. Destro, K.S. Panageas, C.B. Begg, S.S. Agarwala, L.M. Schuchter, M.S. Ernstoff, A.N. Houghton, J.M. Kirkwood, Phase III multicenter randomized trial of the Dartmouth regimen versus dacarbazine in patients with metastatic melanoma, *Journal of clinical oncology : official journal of the American Society of Clinical Oncology* 17 (1999) 2745–2751.
- [8] E. Maverakis, L.A. Cornelius, G.M. Bowen, T. Phan, F.B. Patel, S. Fitzmaurice, Y. He, B. Burrall, C. Duong, A.M. Kloxin, H. Sultani, R. Wilken, S.R. Martinez, F. Patel, Metastatic melanoma - a review of current and future treatment options, *Acta dermato-venereologica* 95 (2015) 516–524.
- [9] D.J. Shah, R.S. Dronca, Latest advances in chemotherapeutic, targeted, and immune approaches in the treatment of metastatic melanoma, *Mayo Clinic proceedings* 89 (2014) 504–519.
- [10] E.M. Bevers, P. Comfurius, R.F. Zwaal, Regulatory mechanisms in maintenance and modulation of transmembrane lipid asymmetry: pathophysiological implications, *Lupus* 5 (1996) 480–487.
- [11] R.F.A. Zwaal, P. Comfurius, E.M. Bevers, Surface exposure of phosphatidylserine in pathological cells, *Cellular and molecular life sciences : CMLS* 62 (2005) 971–988.
- [12] M. Seigneuret, P.F. Devaux, ATP-dependent asymmetric distribution of spin-labeled phospholipids in the erythrocyte membrane: relation to shape changes, *Proceedings of the National Academy of Sciences of the United States of America* 81 (1984) 3751–3755.
- [13] T. Utsugi, A.J. Schroit, J. Connor, C.D. Bucana, I.J. Fidler, Elevated expression of phosphatidylserine in the outer membrane leaflet of human tumor cells and recognition by activated human blood monocytes, *Cancer research* 51 (1991) 3062–3066.

- [14] R.F. Zwaal, A.J. Schroit, Pathophysiologic implications of membrane phospholipid asymmetry in blood cells, *Blood* 89 (1997) 1121–1132.
- [15] S. Ran, B. Gao, S. Duffy, L. Watkins, N. Rote, P.E. Thorpe, Infarction of solid Hodgkin's tumors in mice by antibody-directed targeting of tissue factor to tumor vasculature, *Cancer research* 58 (1998) 4646–4653.
- [16] S. Ran, A. Downes, P.E. Thorpe, Increased exposure of anionic phospholipids on the surface of tumor blood vessels, *Cancer research* 62 (2002) 6132–6140.
- [17] S. Riedl, B. Rinner, M. Asslaber, H. Schaidler, S. Walzer, A. Novak, K. Lohner, D. Zwegytick, In search of a novel target - phosphatidylserine exposed by non-apoptotic tumor cells and metastases of malignancies with poor treatment efficacy, *Biochimica et biophysica acta* 1808 (2011) 2638–2645.
- [18] S. Riedl, D. Zwegytick, K. Lohner, Membrane-active host defense peptides--challenges and perspectives for the development of novel anticancer drugs, *Chemistry and physics of lipids* 164 (2011) 766–781.
- [19] M. Zasloff, Antimicrobial peptides of multicellular organisms, *Nature* 415 (2002) 389–395.
- [20] R.E. Hancock, R. Lehrer, Cationic peptides. A new source of antibiotics, *Trends in Biotechnology* 16 (1998) 82–88.
- [21] Z. Wang, G. Wang, APD: the Antimicrobial Peptide Database, *Nucleic acids research* 32 (2004) D590-2.
- [22] G. Wang, X. Li, Z. Wang, APD2: the updated antimicrobial peptide database and its application in peptide design, *Nucleic acids research* 37 (2009) D933-7.
- [23] G. Wang, X. Li, Z. Wang, APD3: the antimicrobial peptide database as a tool for research and education, *Nucleic acids research* 44 (2016) D1087-93.
- [24] J.-P.S. Powers, R.E.W. Hancock, The relationship between peptide structure and antibacterial activity, *Peptides* 24 (2003) 1681–1691.
- [25] J. Gesell, M. Zasloff, S.J. Opella, Two-dimensional ¹H NMR experiments show that the 23-residue magainin antibiotic peptide is an alpha-helix in dodecylphosphocholine micelles, sodium dodecylsulfate micelles, and trifluoroethanol/water solution, *Journal of Biomolecular NMR* 9 (1997) 127–135.
- [26] A. Laederach, A.H. Andreotti, D.B. Fulton, Solution and Micelle-Bound Structures of Tachyplesin I and Its Active Aromatic Linear Derivatives †,‡, *Biochemistry* 41 (2002) 12359–12368.
- [27] A. Rozek, C.L. Friedrich, R.E.W. Hancock, Structure of the Bovine Antimicrobial Peptide Indolicidin Bound to Dodecylphosphocholine and Sodium Dodecyl Sulfate Micelles †,‡, *Biochemistry* 39 (2000) 15765–15774.
- [28] N. Mandard, P. Sodano, H. Labbe, J.M. Bonmatin, P. Bulet, C. Hetru, M. Ptak, F. Vovelle, Solution structure of thanatin, a potent bactericidal and fungicidal insect peptide, determined from proton two-dimensional nuclear magnetic resonance data, *European journal of biochemistry / FEBS* 256 (1998) 404–410.
- [29] K. Matsuzaki, Why and how are peptide–lipid interactions utilized for self-defense? Magainins and tachyplesins as archetypes, *Biochimica et Biophysica Acta (BBA) - Biomembranes* 1462 (1999) 1–10.
- [30] K. Lohner, S.E. Blondelle, Molecular mechanisms of membrane perturbation by antimicrobial peptides and the use of biophysical studies in the design of novel peptide antibiotics, *Combinatorial chemistry & high throughput screening* 8 (2005) 241–256.

- [31] K. Lohner, New strategies for novel antibiotics: peptides targeting bacterial cell membranes, *General physiology and biophysics* 28 (2009) 105–116.
- [32] B. Bechinger, K. Lohner, Detergent-like actions of linear amphipathic cationic antimicrobial peptides, *Biochimica et biophysica acta* 1758 (2006) 1529–1539.
- [33] W.C. Wimley, K. Hristova, Antimicrobial peptides: successes, challenges and unanswered questions, *The Journal of membrane biology* 239 (2011) 27–34.
- [34] Y. Shai, Mode of action of membrane active antimicrobial peptides, *Biopolymers* 66 (2002) 236–248.
- [35] K. Matsuzaki, K. Sugishita, N. Fujii, K. Miyajima, Molecular basis for membrane selectivity of an antimicrobial peptide, magainin 2, *Biochemistry* 34 (1995) 3423–3429.
- [36] D. Zweytick, G. Deutsch, J. Andra, S.E. Blondelle, E. Vollmer, R. Jerala, K. Lohner, Studies on Lactoferricin-derived Escherichia coli Membrane-active Peptides Reveal Differences in the Mechanism of N-Acylated Versus Nonacylated Peptides, *Journal of Biological Chemistry* 286 (2011) 21266–21276.
- [37] E. Staudegger, E.J. Prenner, M. Kriechbaum, G. Degovics, R.N. Lewis, R.N. McElhaney, K. Lohner, X-ray studies on the interaction of the antimicrobial peptide gramicidin S with microbial lipid extracts: evidence for cubic phase formation, *Biochimica et biophysica acta* 1468 (2000) 213–230.
- [38] D. Gaspar, A.S. Veiga, Castanho, Miguel A R B, From antimicrobial to anticancer peptides. A review, *Frontiers in microbiology* 4 (2013) 294.
- [39] N. Papo, Y. Shai, Host defense peptides as new weapons in cancer treatment, *Cellular and molecular life sciences : CMLS* 62 (2005) 784–790.
- [40] J.L. Gifford, H.N. Hunter, H.J. Vogel, Lactoferricin: a lactoferrin-derived peptide with antimicrobial, antiviral, antitumor and immunological properties, *Cellular and molecular life sciences : CMLS* 62 (2005) 2588–2598.
- [41] D. Zweytick, G. Pabst, P.M. Abuja, A. Jilek, S.E. Blondelle, J. Andrä, R. Jerala, D. Monreal, G. Martinez de Tejada, K. Lohner, Influence of N-acylation of a peptide derived from human lactoferricin on membrane selectivity, *Biochimica et biophysica acta* 1758 (2006) 1426–1435.
- [42] S. Riedl, B. Rinner, H. Schaidler, K. Lohner, D. Zweytick, Killing of melanoma cells and their metastases by human lactoferricin derivatives requires interaction with the cancer marker phosphatidylserine, *Biometals : an international journal on the role of metal ions in biology, biochemistry, and medicine* 27 (2014) 981–997.
- [43] N. Yang, M.B. Strøm, S.M. Mekonnen, J.S. Svendsen, O. Rekdal, The effects of shortening lactoferrin derived peptides against tumour cells, bacteria and normal human cells, *Journal of peptide science : an official publication of the European Peptide Society* 10 (2004) 37–46.
- [44] S. Riedl, R. Leber, B. Rinner, H. Schaidler, K. Lohner, D. Zweytick, Human lactoferricin derived di-peptides deploying loop structures induce apoptosis specifically in cancer cells through targeting membranous phosphatidylserine, *Biochimica et biophysica acta* 1848 (2015) 2918–2931.
- [45] J. Maupetit, P. Derreumaux, P. Tuffery, PEP-FOLD: an online resource for de novo peptide structure prediction, *Nucleic acids research* 37 (2009) W498-503.
- [46] J. Maupetit, P. Derreumaux, P. Tufféry, A fast method for large-scale de novo peptide and miniprotein structure prediction, *Journal of computational chemistry* 31 (2010) 726–738.

- [47] Y. Shen, J. Maupetit, P. Derreumaux, P. Tufféry, Improved PEP-FOLD Approach for Peptide and Mini-protein Structure Prediction, *Journal of chemical theory and computation* 10 (2014) 4745–4758.
- [48] P. Thévenet, Y. Shen, J. Maupetit, F. Guyon, P. Derreumaux, P. Tufféry, PEP-FOLD: an updated de novo structure prediction server for both linear and disulfide bonded cyclic peptides, *Nucleic acids research* 40 (2012) W288-93.
- [49] G. van Meer, D.R. Voelker, G.W. Feigenson, Membrane lipids: where they are and how they behave, *Nature reviews. Molecular cell biology* 9 (2008) 112–124.
- [50] E. Ikonen, Cellular cholesterol trafficking and compartmentalization, *Nat Rev Mol Cell Biol* 9 (2008) 125–138.
- [51] K. Simons, W.L.C. Vaz, Model systems, lipid rafts, and cell membranes, *Annual review of biophysics and biomolecular structure* 33 (2004) 269–295.
- [52] A. Ramamoorthy, D.-K. Lee, T. Narasimhaswamy, R.P. Nanga, Cholesterol reduces pardaxin's dynamics—a barrel-stave mechanism of membrane disruption investigated by solid-state NMR, *Biochimica et Biophysica Acta (BBA) - Biomembranes* 1798 (2010) 223–227.
- [53] A.J. McHenry, M.F. Sciacca, J.R. Brender, A. Ramamoorthy, Does cholesterol suppress the antimicrobial peptide induced disruption of lipid raft containing membranes?, *Biochimica et Biophysica Acta (BBA) - Biomembranes* 1818 (2012) 3019–3024.
- [54] J.R. Brender, A.J. McHenry, A. Ramamoorthy, Does Cholesterol Play a Role in the Bacterial Selectivity of Antimicrobial Peptides?, *Front. Immun.* 3 (2012).
- [55] Y.C. Li, M.J. Park, S.-K. Ye, C.-W. Kim, Y.-N. Kim, Elevated Levels of Cholesterol-Rich Lipid Rafts in Cancer Cells Are Correlated with Apoptosis Sensitivity Induced by Cholesterol-Depleting Agents, *The American Journal of Pathology* 168 (2006) 1107–1118.
- [56] R.N. McElhaney, The use of differential scanning calorimetry and differential thermal analysis in studies of model and biological membranes, *Chemistry and physics of lipids* 30 (1982) 229–259.
- [57] T. Tao, J. Cho, Fluorescence lifetime quenching studies on the accessibilities of actin sulfhydryl sites, *Biochemistry* 18 (1979) 2759–2765.
- [58] M.R. Eftink, C.A. Ghiron, Dynamics of a protein matrix revealed by fluorescence quenching, *Proceedings of the National Academy of Sciences of the United States of America* 72 (1975) 3290–3294.
- [59] M.R. Eftink, C.A. Ghiron, Exposure of tryptophanyl residues in proteins. Quantitative determination by fluorescence quenching studies, *Biochemistry* 15 (1976) 672–680.
- [60] M.I. Angelova, S. Soléau, P. Méléard, F. Faucon, P. Bothorel, Preparation of giant vesicles by external AC electric fields. Kinetics and applications, in: C. Helm, M. Lösche, H. Möhwald (Eds.), *Progress in Colloid & Polymer Science, Trends in Colloid and Interface Science VI*, Steinkopff, Darmstadt, 1992, pp. 127–131.
- [61] G. van Meer, de Kroon, Anton I P M, Lipid map of the mammalian cell, *Journal of cell science* 124 (2011) 5–8.
- [62] S.Y. Dejgaard, K. Dejgaard, J.F. Presley, Cell Staining: Fluorescent Labelling of the Golgi Apparatus, in: John Wiley & Sons Ltd (Ed.), *eLS*, John Wiley & Sons, Ltd, Chichester, UK, 2001, pp. 1–5.
- [63] T.P. McMullen, R.N. Lewis, R.N. McElhaney, Differential scanning calorimetric study of the effect of cholesterol on the thermotropic phase behavior of a homologous series of linear saturated phosphatidylcholines, *Biochemistry* 32 (1993) 516–522.

- [64] S.W. Hicks, C.E. Machamer, Golgi structure in stress sensing and apoptosis, *Biochimica et biophysica acta* 1744 (2005) 406–414.
- [65] C. Wang, R.J. Youle, The role of mitochondria in apoptosis*, *Annual review of genetics* 43 (2009) 95–118.
- [66] I. Herr, K.M. Debatin, Cellular stress response and apoptosis in cancer therapy, *Blood* 98 (2001) 2603–2614.
- [67] J.S. Mader, D.W. Hoskin, Cationic antimicrobial peptides as novel cytotoxic agents for cancer treatment, *Expert opinion on investigational drugs* 15 (2006) 933–946.
- [68] M. Zorko, U. Langel, Cell-penetrating peptides: mechanism and kinetics of cargo delivery, *Advanced drug delivery reviews* 57 (2005) 529–545.
- [69] E.J. Prenner, R.N. Lewis, M. Jelokhani-Niaraki, R.S. Hodges, R.N. McElhaney, Cholesterol attenuates the interaction of the antimicrobial peptide gramicidin S with phospholipid bilayer membranes, *Biochimica et biophysica acta* 1510 (2001) 83–92.
- [70] D.-K. Lee, A. Bhunia, S.A. Kotler, A. Ramamoorthy, Detergent-type membrane fragmentation by MSI-78, MSI-367, MSI-594, and MSI-843 antimicrobial peptides and inhibition by cholesterol: a solid-state nuclear magnetic resonance study, *Biochemistry* 54 (2015) 1897–1907.
- [71] A. Won, A. Ruscito, A. Ianoul, Imaging the membrane lytic activity of bioactive peptide latarcin 2a, *Biochimica et biophysica acta* 1818 (2012) 3072–3080.
- [72] A. Rietveld, K. Simons, The differential miscibility of lipids as the basis for the formation of functional membrane rafts, *Biochimica et Biophysica Acta (BBA) - Reviews on Biomembranes* 1376 (1998) 467–479.
- [73] R.M. Epand, R.F. Epand, C.J. Arnusch, B. Papahadjopoulos-Sternberg, G. Wang, Y. Shai, Lipid clustering by three homologous arginine-rich antimicrobial peptides is insensitive to amino acid arrangement and induced secondary structure, *Biochimica et biophysica acta* 1798 (2010) 1272–1280.
- [74] D. Hanahan, R.A. Weinberg, The hallmarks of cancer, *Cell* 100 (2000) 57–70.
- [75] J. Savill, V. Fadok, Corpse clearance defines the meaning of cell death, *Nature* 407 (2000) 784–788.
- [76] K. Kurosaka, M. Takahashi, N. Watanabe, Y. Kobayashi, Silent cleanup of very early apoptotic cells by macrophages, *Journal of immunology (Baltimore, Md. : 1950)* 171 (2003) 4672–4679.
- [77] A. Pokorny, T.H. Birkbeck, P.F.F. Almeida, Mechanism and kinetics of delta-lysin interaction with phospholipid vesicles, *Biochemistry* 41 (2002) 11044–11056.
- [78] M. Maak, U. Nitsche, L. Keller, P. Wolf, M. Sarr, M. Thiebaud, R. Rosenberg, R. Langer, J. Kleeff, H. Friess, L. Johannes, K.-P. Janssen, Tumor-specific targeting of pancreatic cancer with Shiga toxin B-subunit, *Molecular cancer therapeutics* 10 (2011) 1918–1928.
- [79] R.S. Maag, S.W. Hicks, C.E. Machamer, Death from within: apoptosis and the secretory pathway, *Current opinion in cell biology* 15 (2003) 456–461.
- [80] M. Mancini, C.E. Machamer, S. Roy, D.W. Nicholson, N.A. Thornberry, L.A. Casciola-Rosen, A. Rosen, Caspase-2 is localized at the Golgi complex and cleaves golgin-160 during apoptosis, *The Journal of cell biology* 149 (2000) 603–612.
- [81] D. Wlodkowic, J. Skommer, D. McGuinness, C. Hillier, Z. Darzynkiewicz, ER-Golgi network--a future target for anti-cancer therapy, *Leukemia research* 33 (2009) 1440–1447.

- [82] F. Malisan, R. Testi, GD3 ganglioside and apoptosis, *Biochimica et biophysica acta* 1585 (2002) 179–187.
- [83] M.R. Rippo, F. Malisan, L. Ravagnan, B. Tomassini, I. Condo, P. Costantini, S.A. Susin, A. Rufini, M. Todaro, G. Kroemer, R. Testi, GD3 ganglioside directly targets mitochondria in a bcl-2-controlled fashion, *FASEB journal : official publication of the Federation of American Societies for Experimental Biology* 14 (2000) 2047–2054.
- [84] K.F. Ferri, G. Kroemer, Organelle-specific initiation of cell death pathways, *Nature cell biology* 3 (2001) E255-63.
- [85] Z. Jiang, Z. Hu, L. Zeng, W. Lu, H. Zhang, T. Li, H. Xiao, The role of the Golgi apparatus in oxidative stress: is this organelle less significant than mitochondria?, *Free radical biology & medicine* 50 (2011) 907–917.
- [86] D.R. Green, G. Kroemer, The pathophysiology of mitochondrial cell death, *Science* (New York, N.Y.) 305 (2004) 626–629.
- [87] M.G. Bottone, G. Santin, F. Aredia, G. Bernocchi, C. Pellicciari, A.I. Scovassi, Morphological Features of Organelles during Apoptosis: An Overview, *Cells* 2 (2013) 294–305.